ORF3c is expressed in SARS-CoV-2-infected cells and inhibits innate sensing by targeting MAVS

Dissertation

der Mathematisch-Naturwissenschaftlichen Fakultät
der Eberhard Karls Universität Tübingen
zur Erlangung des Grades eines
Doktors der Naturwissenschaften
(Dr. rer. nat.)

vorgelegt von
Martin Müller
aus Erfurt

Tübingen
2024

Gedruckt mit Genehmigung der Mathematisch-Naturwissenschaftlichen Fakultät der Eberhard Karls Universität Tübingen.

Tag der mündlichen Qualifikation:	08.04.2024
Dekan:	Prof. Dr. Thilo Stehle
1. Berichterstatter/-in:	Prof. Dr. Daniel Sauter
2. Berichterstatter/-in:	Prof. Dr. Thorsten Stafforst

"If you can't be a good example, you'll have to be a horrible warning."

Contents

Abbreviations

A	adenine
Å	Angström
ACE2	angiotensin-converting enzyme 2
AF	AlexaFluor
ANOVA	analysis of variance
ab	antibody
BAC	bacterial artificial chromosome
BiFC	bimolecular fluorescence complementation
BFP	blue fluorescent protein
bp	base pair
BSA	bovine serum albumin
C	cytosine
$CaCl_2$	calcium chloride
CARD	caspase activation and recruitment domain
Cat#	catalogue number
cDNA	complementary DNA
CO_2	carbon dioxide
CoV	coronavirus
COVID-19	coronavirus disease 2019
CPE	cytopathic effect
CPER	circular polymerase extension reaction
ctrl	control
DAPI	4',6-Diamidine-2'-phenylindole
DBD	DNA binding domain
DMEM	Dulbecco's Modified Eagle Medium
DMSO	dimethylsulfoxide
DMV	double membrane vesicles
DNA	deoxyribonucleic acid
dNTP	deoxynucleosidetriphosphate

DPBS	Dulbecco's Phosphate-Buffered Saline
dpi	days post infection
dpt	days post transfection
ds	double stranded
E. coli	*Escherichia coli*
EDTA	ethylenediaminetetraacetic acid
eGFP	enhanced green fluorescent protein
e.g.	for example
ER	endoplasmatic reticulum
EtBr	ethidiumbromide
FACS	fluorescence activated cell sorting
FCS	fetal calf serum
fwd	forward
g	gramme(s))
g	centrifugal force
GAPDH	glyceraldehyde 3-phosphate dehydrogenase
gDNA	genomic DNA
GFP	green fluorescent protein
G	guanine
h	hour(s))
HBS	HEPES buffered saline
HEK	human embryonic kidney
HLA	human leukocyte antigen
HPLC	high-performance liquid chromatography
hpt	hours post transfection
IBV	infectious bronchitis virus
IFN-β	interferon-β
IFN-γ	interferon-γ
IKK	Iκkinase
IRES	internal ribosome entry site

IRF3	interferon regulatory factor 3
ISG	interferon-stimulated gene
iso	isotype control
kb	kilobase(s)
kDa	kilo Dalton
l	litre(s)
lacZ	β-galactosidase
LIPS	luciferase immuno precipitation system assay
LTR	long terminal repeat
M	molarity (mol/l)
MAVS	mitochondrial antiviral-signaling protein
MDA5	melanoma differentiation-associated protein 5
MERS	middle east respiratory syndrome
MFI	mean fluorescence intensity
mg	milligramme(s)
MHC	major histocompatibility complex
min	minute(s)
ml	millilitre(s)
mM	millimol(s)
mock	uninfected control
mRNA	messenger RNA
NCDV	Nebraska Calf Diarrhea Virus
nef	negative regulatory factor
NF-κB	nuclear factor kappa-light-chain-enhancer of activated B-cells
ng	nanogramme(s)
NPC	nuclear pore complex
Nsp	non-structural protein
nt	nucleotide(s)
ORF	open reading frame
OSU	Ohio State University

pAb	polyclonal antibody
PAMP	pathogen-associated molecular pattern
PBS	phosphate-buffered saline
PCR	polymerase chain reaction
PFA	paraformaldehyde
pIRF3	phospho-IRF3
pp1a/b	poly-peptide 1a/b
PRR	pattern recognition receptor
pTAL	TATA-like promoter
PVDF	polyvinylidene fluoride
qPCR	quantitative polymerase chain reaction
RddRp	RNA-dependent RNA polymerase
rev	reverse
RhiLu1	*Rhinolophus alcyone* lung
RIG-I	retinoic acid-inducible gene I
RLU	relative light units
RNA	ribonucleic acid
RPMI	Roswell Park Memorial Institute Medium
rpm	revolutions per minute
RT	reverse transcriptase
RTC	replication and transcription complex
s	second/s
SARS	Severe acute respiratory syndrome
SD	standard deviation
SDS	sodium dodecyl sulfate
sec	secondary
SEM	standard error of the mean
SeV	Sendai virus
sgRNA	sub-genomic RNA
ss	single stranded

TAE	Tris-acetate-EDTA
TBK1	TANK-binding kinase 1
TCID50	tissue culture infectious dose 50
TCR	T-cell receptor
TLR	Toll-like receptor
TMPRSS2	transmembrane protease serine 2
TRS-B	transcription regulatory sequence - body
TRS-L	transcription regulatory sequence - leader
U	unit
U	uracil
UTR	untranslated region
UV	ultra-violet
V	volt(s)
v/v	volume to volume ratio
WHO	world health organization
w/v	weight to volume ratio
wt	wild-type
YFP	yellow fluorescent protein
µg	microgramme(s)
µl	microlitre(s)
°C	degree Celsius

1 Introduction

1.1 Coronaviruses

Discovery

In 1966, the group of David Tyrell was working on an unknown 'common cold' virus his group had isolated in 1961 and which initially proved to be impossible to propagate by standard methods. Around the same time in Chicago, Dorothy Hamre and John Procknow isolated another novel common cold virus from medical students, labeled 229E [1]. To identify the causative agent, Tyrell sent samples of both isolates to June Almeida at the St Thomas's Hospital Medical School in London. At the time, Almeida was a pioneer in electron microscopy and with her extensive knowledge was able to to detect viral particles in both specimens in clear images. Surprisingly, the particles showed striking similarities with infectious bronchitis virus (IBV), a virus she had previously worked on and detected in chicken and mice. However, the previous studies describing the novel virus were rejected at the time because the reviewers thought the images were of poor quality and simply showing Influenza virus particles. This time, however, the evidence was irrefutable [2]. Because of the halo-like formations surrounding their exterior, they were named 'Coronaviruses' and categorized as a novel family in 1968 (Fig. 1A) [3], [4], [5].

Classification

The *Coronaviridae* family belongs to the suborder *Cornidovirinae* under the order *Nidovirales* and is divided into three sub-families, namely *Orthocornavirinae*, *Letovirinae*, *Pitovirinae* (Fig. 1B). *Orthocornavirinae* are further divided into four genera: Alpha, Beta, Gamma and Deltacoronavirus [6]. Both, alpha- and betacoronaviruses exclusively infect mammalian species, including humans, and originate from bats [7], [8]. Gamma- and deltacoronaviruses, in contrast, have their reservoirs in birds [7]. One characteristic of all genera of coronaviruses is their ability to infect a wide range of different species [9], [10], [11], [12]. While the virus adapts to its host to efficiently

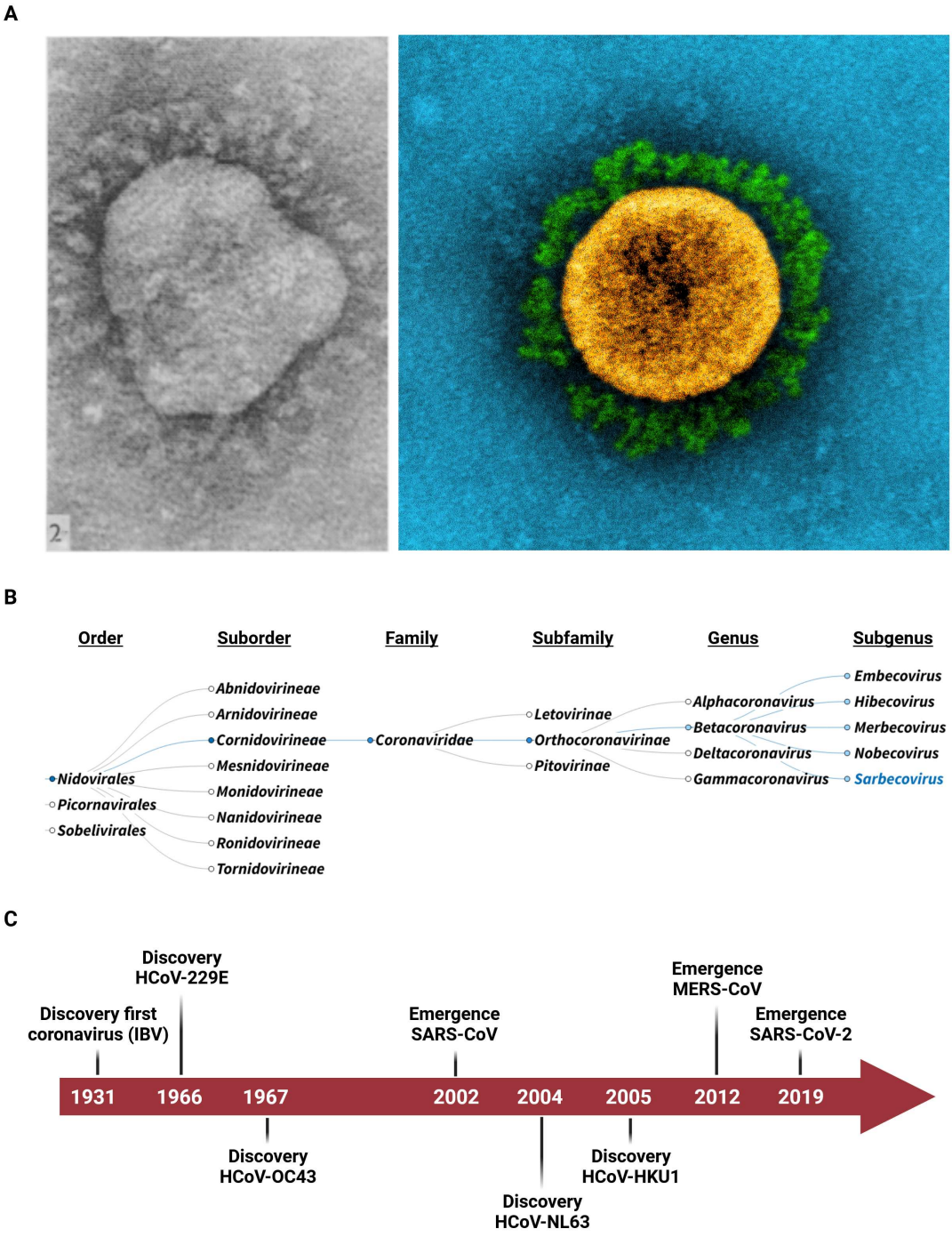

Figure 1: History of coronaviruses

(A) Early electron microscopy image of an HCoV-E229 particle, "surrounded by a distinct 200 Å long fringe" (1967) [3] (left). False-colour transmission electron micrograph of a B.1.1.7 variant coronavirus. The surface protein Spike (green) surrounds the genome containing virus particle (yellow) (right) NIAID.
(B) Taxonomy of the *Coronaviridae* family. As of 2022, all viruses in the subgenus *Sarbecovirus* (blue) belong to the species *Severe acute respiratory syndrome-related coronavirus* ICTV.
(C) Timeline of discovery and emergence of coronaviruses known to infect humans. HCoV-NL63 and HCoV-229E belong to the genus alphacoronavirus, while HCoV-HKU1, HCoV-OC43, SARS-CoV, MERS-CoV and SARS-CoV-2 are betacoronaviruses. Created with BioRender.com.

replicate, it may indirectly adapt to species with a phylogenetically related immune system. Combined with the close spatial proximity between humans and other host species that can be infected by Coronaviruses, this has formed the crucible for past and current epidemics and pandemics (Fig. 1C). The first such event that was well documented began in 2002 in Guangdong (China) and was caused by a Betacoronavirus, the severe acute respiratory syndrome coronavirus (SARS-CoV). The first infected individuals likely contracted the virus from masked palm civets on wet markets [13], [14]. However, mounting evidence suggests that these animals were only an intermediate host and that the virus originated from horseshoe bats [15], [16]. Infected individuals showed clinical symptoms similar to other infections of the lower respiratory tract, and the overall mortality rate is estimated to be 15% [17]. The last documented cases occurred in 2004, and transmission of the virus has not been detected since [14].

The next spillover event was detected in Jeddah (Saudi Arabia) in 2012 and caused by the Middle East respiratory syndrome–related coronavirus (MERS-CoV), another betacoronavirus phylogenetically distinct from SARS-CoV. Here, the virus crossed the species barrier from bats to humans via dromedary camels as an intermediate host [18]. In contrast to SARS-CoV, cases are still being reported, but are mostly limited to the Arabian Peninsula. While transmissibility between humans is limited, infection with the virus is associated with a high mortality rate (35%) [19], [20].

1.2 SARS-CoV-2

In December 2019, several hospitals in Hubei province (China) reported cases of pneumonia of unknown origin [21], [22]. By early January, the causative agent had been identified as a novel betacoronavirus, and increasing numbers of infections were reported throughout all of China. On the 30th of January, the WHO declared the coronavirus outbreak a public health emergency of international concern, with the novel virus officially termed SARS-CoV-2 and the resulting disease COVID-19. Over the course of the following months, infections spread across the globe with thousands of cases reported daily, prompting the WHO to declare COVID-19 a pandemic. The time

since has been marked by nation-wide lockdowns, mass testing and a race to find an effective vaccine against the virus [23], [21]. Phylogenetic analysis shows that SARS-CoV-2 shares a higher degree of genome sequence identity with SARS-CoV (79%) than with MERS-CoV (50%) [24], [21]. However, some genomic variations clearly define SARS-CoV-2 as a distinct virus species, such as the truncation or complete absence of certain genes [25], [26]. The exact origin of the virus has also remained enigmatic to this day. However, due to its close sequence homology with SARS-like CoVs, such as bat-SL-CoVZXC21 (87%) and BANAL-20-52 (97%) [27], SARS-CoV-2 has been suggested to have emerged from a bat-borne virus [28].

Transmission and entry

SARS-CoV-2 is transmitted through droplets, which are exhaled or coughed out by an infected individual. Once the virus reaches the respiratory tract, it attaches to its target cells, primarely ciliated epithelial cells in nasal mucosa and type II alveolar pneumocytes in lung alveoli [29], [30]. The surface of the virus is covered by a homo-trimeric fusion protein, Spike, which gives it its halo-like appearance. Initially, the viral Spike protein interacts with its target receptor, angiotensin converting enzyme 2 (ACE2), which is expressed by cells of the respiratory tract, but is also found on cells of the small intestine, testis, kidney, heart muscle, colon and thyroid gland [31]. Receptor engagement initiates conformational changes within the receptor binding domain (RBD) of Spike and permits its activation by the serine protease TMPRSS2 on the cell surface. This event in turn triggers the fusion between the viral and cellular membrane, creating a fusion pore through which the virus genome is released into the cytoplasm [32], [33].

Genome

The genome of SARS-CoV-2 consists of one continuous, single-stranded RNA of 29.9 kb, making it one of the largest viral RNA genomes currently known. It contains 14 open reading frames (ORFs) and codes for at least 25 different proteins. These can be

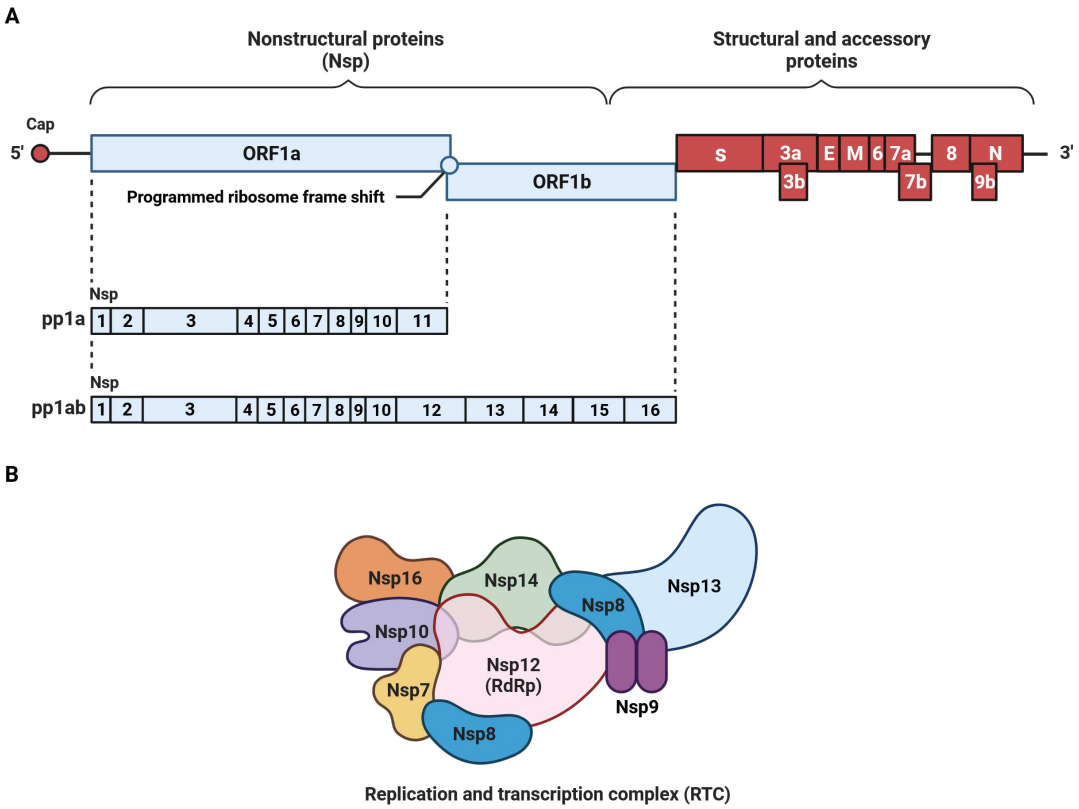

Figure 2: SARS-CoV-2 genome organization

(A) The first two-thirds of the SARS-CoV-2 genome encode sixteen non-structural proteins (Nsp) within open reading frames 1a (ORF1a) and ORF1b. Nsp1-11 are encoded by polyprotein 1a (pp1a). Nsp12-16 are expressed from pp1b after extension of pp1a through a programmed ribosomal frameshift. Structural proteins Spike (S), Envelope (E), Matrix (M), Nucleocapsid (N) as well as accessory proteins are encoded downstream of ORF1b. Sequences for ORF3b, 7b and 9b are embedded within other ORFs and expressed by leaky scanning. ORFs are not drawn to scale. Adapted from "Genome Organization of SARS-CoV", by BioRender.com (2024). Retrieved from https://app.biorender.com/biorender-templates

(B) Simplified model of the viral replication and transcription complex (RTC). Replication and transcription are driven primarily by the enzymes Nsp12 (RNA-dependent RNA polymerase), Nsp13, Nsp14 and Nsp16. Adapted from "Model of Putative Coronavirus Replisome", by BioRender.com (2024). Retrieved from https://app.biorender.com/biorender-templates

divided into 16 non-structural proteins (Nsps) which occupy the first two thirds of the genome and form the replication and transcription machinery. Located towards the 3' end of the genome are the 4 structural proteins Spike (S), envelope (E), membrane (M) and nucleocapsid (N), forming the viral particle and enabling attachment to the target cell receptor. Finally, there are at least 7 additional ORFs spread between the structural proteins (ORF3a, ORF3b, ORF6, ORF7a, ORF7b, ORF8 and ORF9b) (Fig. 2A). These accessory genes code for proteins which assist in viral replication and/or suppress the immune response [34], [35]

Replication

CoV entry into the cell marks the beginning of viral transcription and translation and is tightly regulated in space and time. The translation of ORF1a and ORF1b from viral genomic RNA leads to the generation of two large polypeptides: pp1a & pp1b [36]. An interesting mechanism found in coronaviruses is a -1 programmed ribosomal frameshift which occurs in a short spacer region between ORF1a and ORF1b, making pp1ab in essence an extension of pp1a. Both are then further processed by proteolytic cleavage by two cysteine proteases that are located within Nsp3 and Nsp5 to release Nsp1-11 (pp1a) and Nsp1-10 & 12-16 (pp1b). Nsp1 is one of the first proteins to be produced and immediately targets the translation machinery to initiate a host shutoff [37]. Nsp2-16 form the viral replication and transcription complex (RTC) and carry out the main function of RNA synthesis, modification and proofreading (Fig. 2B). Nsp2-11 fulfils a supporting role by modifying membrane structures, acting as co-factors and facilitating immune evasion [38], [39]. The first step of viral replication is the transcription of the positive sense RNA genome into full length, negative sense copies by the Nsp12 RNA-dependent RNA polymerase (RdRp) (Fig. 3A). These copies in turn act as templates for the generation of new, full length, positive sense RNA genomes. The accumulating positive sense genome copies are used for the translation of additional Nsps, RTCs or are packaged into new virions [34].

Discontinuous transcription

Most viruses rely on the translation machinery of their host cell. Specifically, RNA viruses have to adapt to the 5′ dependency of eukaryotic translation initiation, which follows the dogma of one mRNA being translated into one protein. To express all proteins encoded in its genome, SARS-CoV-2 produces sub-genomic RNAs (sgRNA) in addition to the full length copies during negative strand synthesis (see Replication). Reading from the 3′ end of the genomic RNA template, the RTC encounters transcription regulatory body elements (TRS-B) found upstream of many ORFs (3B, top).

RNA synthesis is interrupted at these elements and the RTC re-initiates at a leader sequence (TRS-L) 5′-ACGAAC-3′ found roughly 70 nucleotides downstream of the 5′ start of the template (Fig. 3A). This process of 'discontinuous RNA synthesis' [40] leads to the generation of nine canonical sgRNAs of different lengths, which serve as templates for positive sense sgRNA synthesis and subsequent viral protein translation of Spike, E, M, N, as well as ORF3a, ORF6, ORF7a and ORF8 (Fig. 3B, bottom). While this process accounts for approximately 90 % of sgRNAs in SARS-CoV-2, some sgRNAs are generated by TRS-L-independent and/or out of frame fusion resulting in at least 41 additional sub-genomic templates for viral protein translation [41]. These mechanisms greatly enhance the coding capacity of SARS-CoV-2 but do not exhaust all options for the virus to express additional proteins [42], [43].

Non-canonical translation

Ribosomes scan triplets of nucleotides to insert the corresponding amino acid into a growing chain (Fig. 4A). This results in three possible (overlapping) reading frames within the canonical sequence of nucleotides. During the initiation of translation in SARS-CoV-2, the ribosome subunit S40 binds near the 5′ end of an sgRNA and begins scanning for a start codon (AUG). In some cases, however, ribosomes do not initiate translation at the first AUG they encounter and continue scanning further in the 3′ direction. This 'leaky scanning' allows initiation to occur at a downstream AUG codons and can lead to the expression of N-terminally truncated isoforms of the protein (Fig. 4B left). Moreover, initiation can also occur at an out of frame AUG and allow expression of an unrelated protein with entirely different functions, while conserving the overall genome size (Fig. 4B right). Many viruses have utilized these additional reading frames to encode for accessory proteins. For example, the genomic sequence of Influenza A virus PB1 encodes an accessory protein, PB1-F2, in its +1 reading frame [44]. Similarly, Rotavirus gene segment 11 codes for Nsp5 and an additional protein (Nsp6) of unknown function [45]. Interestingly, this mechanism of nested coding sequences can also be found in coronaviruses. The genomic sequence of the bovine coronavirus N protein for example encodes an additional protein, I, in

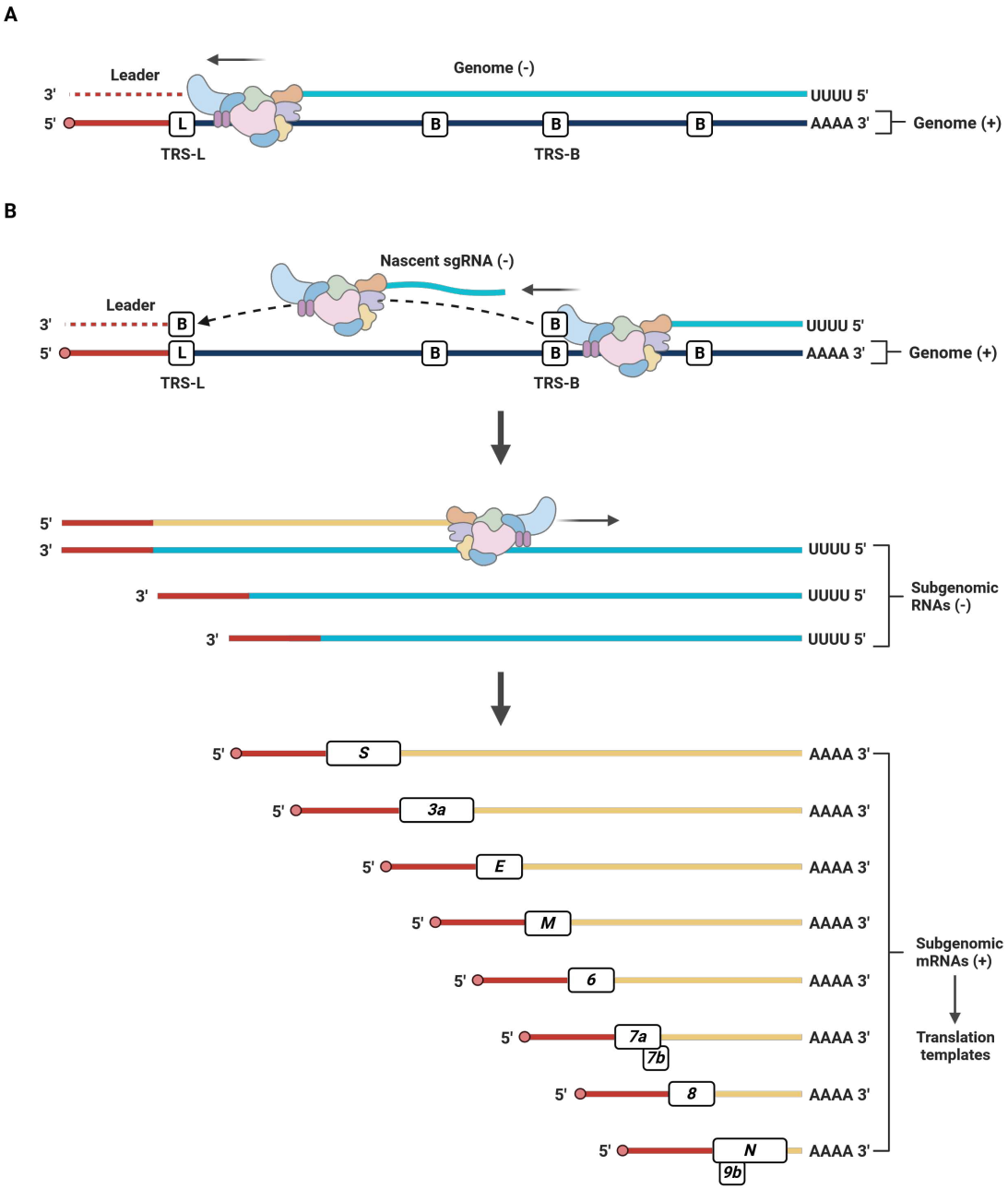

Figure 3: SARS-CoV-2 replication and discontinuous transcription

(A) The RdRp complex initiates transcription at the 3′ end of the positive-sense genome (dark blue). If the TRC skips every transcription regulatory sequences body (TRS-B), full length (-)RNAs are generated (light blue) which serve as templates for (+)genome synthesis.

(B) Upon reaching a (TRS-B), the RdRp complex may discontinue transcription and "jump" to the TRS Leader sequence (TRS-L) located towards the 5′ end of the genome. Transcription is resumed on the new template, and the leader sequence (red) is copied to complete the negative-strand sgRNA (light blue). The presence of different TRS-B throughout the genome allows for the generation of nine sgRNA. The negative-strand RNAs serve as templates for the synthesis of genome-length positive-strand RNAs or sgmRNAs (yellow). Adapted from "Discontinuous Transcription", by BioRender.com (2024). Retrieved from https://app.biorender.com/biorender-templates

its +1 reading frame [46]. Not surprisingly, this pattern of overlapping genes is also utilized by SARS-CoV-2 to encode additional accessory proteins in a single sgRNA molecule. For example, ORF3b [47], ORF3c [43], ORF7b and ORF9b [42] have been suggested to be expressed from bicistronic sgRNAs by means of leaky scanning. Interestingly, some of these ORFs, including ORF7b and ORF9b, have already been described and characterized in SARS-CoV where they appear to play an immune modulatory or virion-associated role [48], [49].

1.3 ORF3c

The current knowledge on accessory proteins in SARS-CoV-2 is limited. Although a plethora of studies has focused on the coronavirus genome, to this day there is no consensus on the exact number of accessory proteins expressed by SARS-CoV-2 [42], [43]. Moreover, cryptic open reading frames which overlap with classical ORFs have received even less attention.

The ORF3a gene, for example, harbors additional overlapping reading frames, which

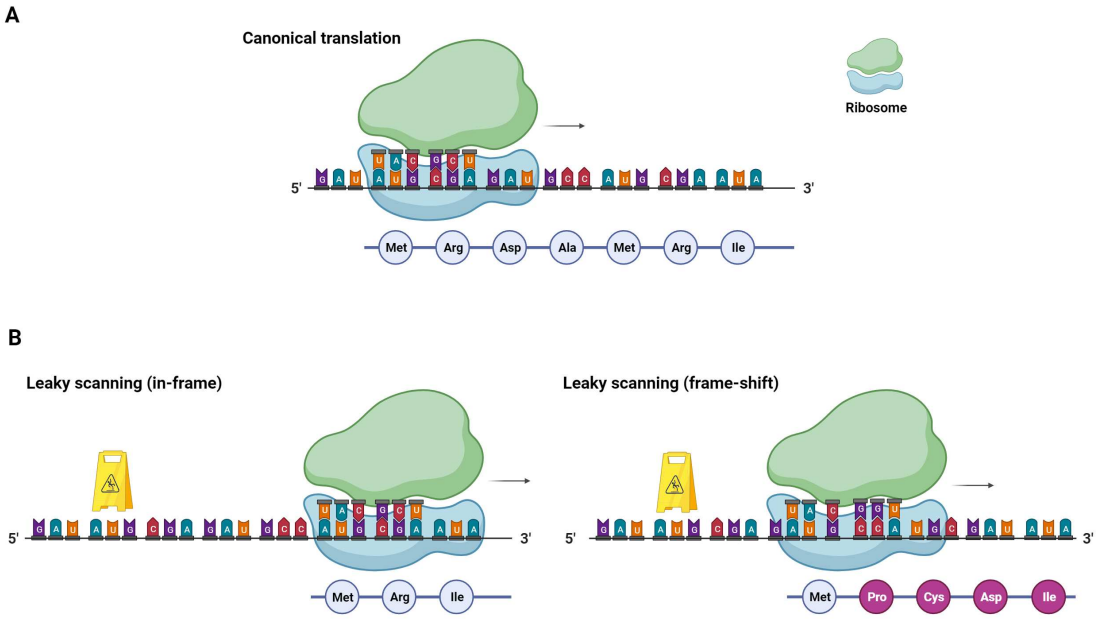

Figure 4: Non-canonical translation mechanisms in SARS-CoV-2
(A) To initiate translation, ribosomes scan the (viral) RNA template for the start codon AUG. Upon initiation, the ribosome assembles a nascent amino acid chain correspondend to the nucleotide triplet code downstream of the start codon.
(B) Ribosomes can fail to initiate translation at the first AUG they encounter and continue scanning the template for an AUG triplet (leaky scanning). Initiation at a downstream AUG within the same frame leads to the synthesis of an N-terminally truncated amino acid chain (left). Initiation at an out of frame AUG results in the synthesis of a different amino acid chain of individual composition and length (right) Created with BioRender.com.

may potentially code for small peptides (Fig. 5A). One example is the aforementioned ORF3b protein, which has been shown to act as an IFN inhibitor [47]. In 2020, ORF3c was identified independently by different groups as an accessory protein of SARS-CoV-2. While initially receiving different names (e.g. ORF3c [51], [42]; ORF3h [52]; 3a.iORF1 [42] and ORF3b [53]), a community consensus decided to designate the protein ORF3c, based on its homologue in SARS-CoV [54]. The sequence for ORF3c is embedded in the +1 reading frame of the ORF3a sgRNA and is likely the product of leaky scanning. *In silico* analyses have shown that the start codon of ORF3c (AUG) contains an upstream A at the -3 position, resulting in a strong initiation context, while the upstream AUG of ORF3a contains an intermediate context initiation site (Fig. 5B) [55], [50]. Together, this allows a proportion of ribosomes loaded onto ORF3a sgRNA to translate *ORF3c* by leaky scanning [51]. Interestingly, although ORF3c is also present in SARS-CoV, no studies have been conducted to investigate its expression or function during infection. *In silico* analyses have predicted the presence of a transmembrane domain within its C-terminal region and a potential function as a viroporin [52]. The combination of conserved sequence and presence in different Sarbecoviruses suggests not only the expression during infection but also a

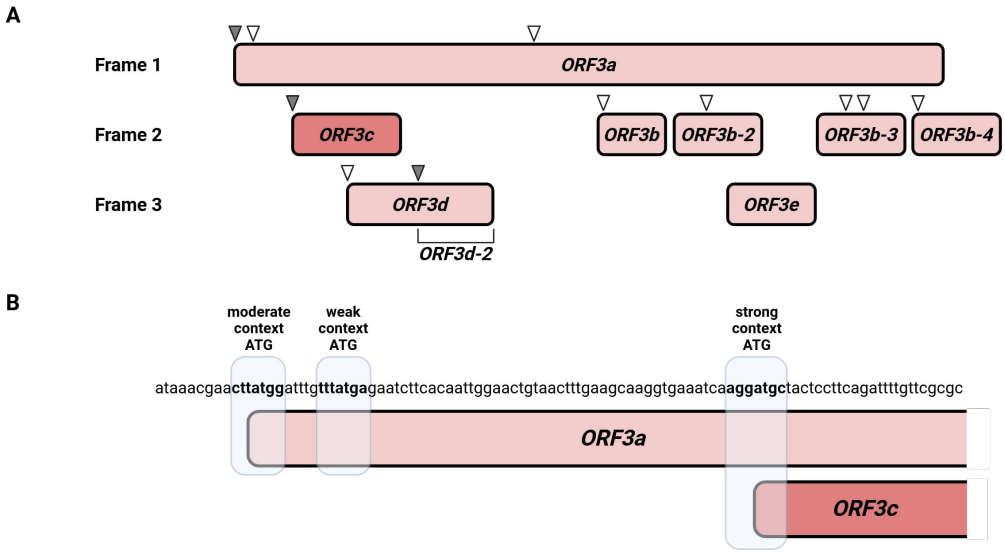

Figure 5: Cryptic open reading frames in *ORF3a*
(A) Location of cryptic open reading frames within *ORF3a*. Empty triangles indicate internal ATG codons. Experimentally confirmed translation initiation sites are highlighted by gray triangles [42].
(B) Initiation context of the *ORF3c* start codon and upstream ATG codons in *ORF3a*. Predictions were performed using Predict TIS [50]. Created with BioRender.com.

functional importance of ORF3c in the viral replication cycle. While accessory proteins in general are not essential for viral replication, they do increase viral fitness. At the center of this thesis stands the question whether or not ORF3c is a functional protein expressed during viral infection.

1.4 Immune Response

The entry of the virus into the cell sets the stage for a battle over the translational machinery, amino acids and host factors necessary for viral replication. For SARS-CoV-2, winning ensures evolutionary success and means certain demise of the cell. In response, cells have evolved a remarkable network of signaling cascades, receptors and warning mechanisms to promote an antiviral state within and around them. The effective spread of SARS-CoV-2 in and between hosts is therefore inadvertently tied to the ability of the host immune system to detect and/or neutralize the virus.

Interferon signaling

Cells express different pattern recognition receptors (PRRs) to detect RNA species, which are usually not found in the cytosol unless a virus is replicating. The viral RNA acts as a pathogen-associated molecular pattern (PAMP) and a warning signal to the cell [56]. Host RNAs, such as mRNA, are distinguished from these PAMPs by specific modifications such as capping structures or methylation and therefore usually do not lead to unwanted immune activation [57]. The activation of PRRs induces signaling cascades that culminate in the production of, amongst others, type-I interferons (IFN-I), a crucial first step in the innate immune response. Initial detection of SARS-CoV-2 replication is mediated by retinoic acid-inducible gene (RIG)-like receptors, dominantly RIG-I and melanoma differentiation-associated gene 5 (MDA5) [58]. Although structurally similar, both receptors are activated by different RNA species. RIG-I is sensitive to the 5′ modifications of RNA molecules and recognizes missing 2′-O-methylation, base pairing adjacent to the 5′ end and

un-capped 5′-triphosphates [57]. The molecular mechanisms that lead to MDA5 activation are less well understood, but include the secondary structure and length of RNA. While RIG-I is activated by short RNA species (< 500 bp), MDA5 recognizes longer dsRNA [59], [60], [61]. Once bound to their target RNA, both receptors form homo-oligomers and undergo conformational changes to expose and multimerize two N-terminal Caspase recruitment domains (CARD). These complexes subsequently interact with the mitochondrial antiviral-signaling protein (MAVS) through direct CARD-CARD interactions. MAVS is an essential adapter protein and works as a signal distributor and amplifier of the innate immune response. Upon activation, MAVS aggregates at the surface of mitochondria and forms protein filaments, which in turn activate additional MAVS proteins [62]. Subsequently, MAVS activates TANK-binding kinase 1 (TBK1) by phosphorylation. Lastly, phosphorylation of the TBK1 target substrate interferon regulatory factor 3 (IRF3) leads to the formation of homodimers and its nuclear translocation. IRF3 acts as a key transcription factor in antiviral signaling and binds to promoter elements of antiviral genes, most importantly type I interferons and leads to their induction. Interferons are secreted by the cell and act in an auto- and paracrine manner by binding to members of the IFNα receptor family [63]. The resulting activation of the Jak-STAT signaling pathway leads to the induction of interferon-stimulated genes (ISGs) and translation of proteins that suppress viral replication, improve sensing and signaling or prolong the antiviral immune response [64]. While the main entry route of SARS-CoV-2 is mediated by Spike-ACE2 receptor interaction, the virus can also be taken up via clathrin-mediated endocytotis [65]. SARS-CoV-2 is capable of escaping the harsh environment of the endosome by Spike activation through Cathepsin L and Cathepsin B. However, many virions get degraded and their raw materials serve as ligands for endosomal PRRs such as Toll-like receptor 3 (TLR3). TLR3 signaling also culminates in the activation of IRF3 (via TBK1), and there is extensive complementation and cross-talk between TLR and RIG-I/MDA5 signaling [32].

1.5 Immune evasion

The mechanisms that cells have evolved to detect, suppress and eradicate viruses have forced the latter to adapt to ensure their replication and spread. Not surprisingly, SARS-CoV-2 does not rely on one single strategy to avoid detection, and each step of the viral replication cycle utilizes different viral proteins to safeguard these processes. Proteomic analyses have identified a wide range of viral proteins involved in the immune modulation of the host such as N, M, Nsp1, Nsp3, Nsp11, Nsp12, Nsp13, Nsp14, Nsp15, ORF3, ORF6, ORF8, ORF7b and ORF9b [66], [67], [68]. The mechanisms by which these proteins assist SARS-CoV-2 immune evasion include: inhibiting recognition, targeting PRR signaling and blocking nuclear translocation of immunity-related transcription factors (Fig. 6, left). Together with the induction of a host-translational shutoff and specific targeting of IFN signaling, these effects lead to a delayed and reduced immune response [69]. Importantly, even short delays in PAMP recognition at the early steps of infection can lead to significant advantages in viral replication efficiency later on. Thus, many of the immune modulatory proteins in SARS-CoV-2 target PRRs such as RIG-I, MDA5 and their downstream signaling pathways. The following section will highlight some but not all viral proteins that influence PAMP recognition and anti-viral signaling in the infected cell.

Avoiding recognition

Immediately after entry into the target cell, the coronaviral RNA needs to be modified with a cap structure to allow proper translation initiation. This process is facilitated by four sequential reactions involving Nsp12 [70], Nsp13 [71], Nsp14 [72] and Nsp16 [73] as catalysts, as well as Nsp10 as a co-factor (Fig. 6, upper box) [74]. By disguising viral RNA as host mRNA, this capping step also hides its presence from intracellular sensors and prevents an early immune response. Subsequent continuous viral RNA replication is marked by the accumulation of newly synthesized genomic and sub-genomic RNAs. However, both of these products use negative-strand intermediates as templates, which allows for the formation of dsRNAs by sequence

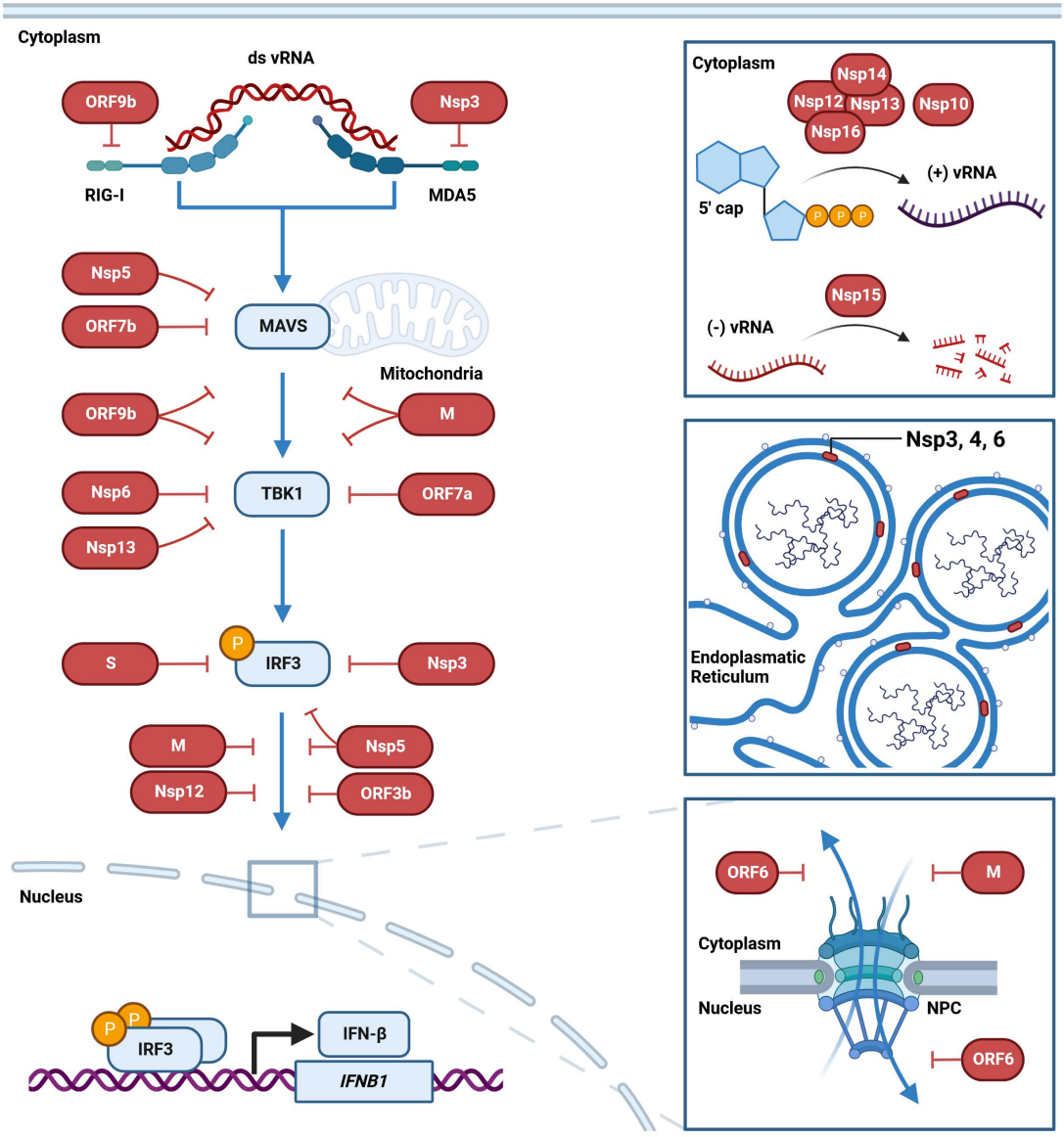

Figure 6: Immune evasion mechanisms of SARS-CoV-2

(Left) Viral replication leads to the generation of pathogen-associated molecular patterns which can be recognized by pattern recognition receptors RIG-I and MDA5. Upon detection of double-stranded or uncapped RNA, these receptors induce the aggregation and activation of mitochondrial antiviral signaling protein (MAVS). Subsequent activation of TANK-binding kinase 1 (TBK1) leads to the phosphorylation (yellow) and dimerization of the interferon regulatory factor 3 (IRF3). Translocation of IRF3 into the nucleus culminates in the induction of interferon-β (IFN-β). Finally, IFN-β secretion acts in an auto- and paracrine manner to establish an antiviral state in the cell. Each step of the signaling pathway is targeted by different SARS-CoV-2 proteins (red).
(top box) SARS-CoV-2 caps its single-stranded RNA genome to prevent PRR recognition. Nsp15 degrades (-)vRNA to prevent formation of dsRNA intermediates.
(middle box) Nsp3, 4 and 6 assemble double membrane vesicles (DMV) to compartmentalise viral replication.
(lower box) SARS-CoV-2 ORF6 and M interfere with proteins of the nuclear import (ORF6 and M) and export (ORF6) machinery to slow down the immune response.
Created with BioRender.com.

complementarity. These dsRNA species in turn are potent PAMPs for RIG-I and MDA5. SARS-CoV-2 avoids accumulation of dsRNAs by virtue of Nsp15, which acts as an endonuclease and degrades negative-strand RNAs (Fig. 6, upper box) [75]. In

parallel, SARS-CoV-2 forms double membrane vesicles (DMVs) on the endoplasmatic reticulum (ER), established mainly by Nsp3, 4 and 6 [76], [77]. These 'replication organelles' allow accumulation of RNA species that are important for viral replication but would act as PAMPs for innate sensors within the cytosol (Fig. 6, middle box).

Inhibiting PRR signaling

Once replication is in full effect, detection of accumulating RNA species becomes inevitable. As laid out earlier, recognition by PRRs and their downstream signaling involves multiple proteins, many of which have been identified to be targeted by SARS-CoV-2 (Fig. 6 right). For example, ORF9b has been shown to bind to RIG-I to prevent its interaction with MAVS [78]. Similarly, Nsp3 has been suggested to prevent ISG15-mediated activation of MDA5 [79]. As detection and antiviral signaling cannot be fully prevented, downstream signaling factors are also targeted by viral proteins. The MAVS protein acts as a central node for different PRR pathways and is therefore a valuable target for viral interference. Not surprisingly, at least ORF7b, ORF9b, Nsp5 and M have been shown to disrupt MAVS activity via various mechanisms including its direct ubiquitination and proteasome-mediated degradation [80], [81], [82], [83]. TBK1 is a direct substrate of MAVS and another important host factor targeted by SARS-CoV-2. Specifically, ORF9b, Nsp6 and Nsp13 directly bind to TBK1 and prevent its activation while ORF7a and M have been shown to reduce overall TBK1 protein levels, resulting in diminished signaling strength and reduced IRF3 activation [84], [78], [85]. Lastly, SARS-CoV-2 Spike, Nsp3 and Nsp5 both target IRF3 directly by inducing its degradation [86], [87], [88].

Blocking nuclear translocation

Since SARS-CoV-2 replication takes place in the cytoplasm, the virus does not rely on the nuclear import or export machinery of the cell. This makes the nuclear pore complex (NPC) a vulnerable target (Fig. 6, lower Box). For example, ORF6 outcompetes cellular RNA for binding to nuclear translocation complexes and makes

it inaccessible for host transcription factors [89], [90]. This disrupts cellular defence mechanisms in two ways. First, cellular mRNAs are constrained to the nucleus and cannot be translated to exert their antiviral functions. Second, transcription factors such as IRF3 are limited in their access to the nucleus and cannot induce their target ISGs. Similarly, ORF3b, M, Nsp5 and Nsp12 have been shown to suppress the IFN response by retaining IRF3 in the cytoplasm, preventing its function as a transcription factor [47], [91]. [92], [93].

Together, SARS-CoV-2 uses a wide range of its proteins to target different steps in antiviral signaling. While accessory proteins play a central role in these evasion mechanisms, not all of them have been functionally analysed yet.

1.6 Scientific aims

SARS-CoV-2 has probably been studied in more detail than any other virus before. While the joint efforts of the scientific community have led to a better understanding of the virus and the development of novel vaccines, they also highlighted the many aspects of the virus that are still unknown. For example, there is no consensus on the viral proteome and the exact number of proteins and peptides expressed by SARS-CoV-2. This is especially true for the 3' end of the viral genome, which encodes many of its accessory proteins. These are expressed from subgenomic mRNAs and fulfil a supporting role in the viral replication cycle. SARS-CoV-2, like many other viruses, enhances its coding capacity by making use of all three reading frames to code for proteins. These nested sequences can be translated by non-canonical translation mechanisms such as leaky scanning and give rise to functional proteins. While many of these ORFs are also found in closely related coronaviruses, their expression or function is often only predicted and seldom verified experimentally. This is surprising, given that they have often been identified as important contributors to immune evasion and frequently involve novel strategies and cellular targets. One interesting example is ORF3c, which is predicted to be expressed by leaky scanning from the sgRNA of *ORF3a*. Although its sequence can also be found in SARS-CoV, the combined knowledge about the protein has been largely limited to *in silico* predictions.

The aim of this thesis was to verify the expression of ORF3c during viral infection. Subsequently, the role of ORF3c as an immune modulator during the viral replication cycle and its cellular targets were to be identified. Finally, the mechanisms, by which ORF3c exerts its function was investigated and its contribution to viral fitness evaluated. In summary, this thesis aimed at getting better insights into the function and mechanism of the enigmatic SARS-CoV-2 accessory protein ORF3c. The knowledge gained here highlights the importance of overlapping reading frames as sources of viral peptides and contributes to our understanding of the immune evasion mechanisms employed by this virus.

2 Material

2.1 Cell culture

2.1.1 Cell lines

Table 1: Cell lines

Cell line	Description
HEK293T	Human embryonic kidney (HEK) cell line isolated from a female fetus (1973) transformed with the human adenovirus type 5 and stably expressing the simian virus 40 large T antigen (RRID:CVCL_0063; obtained from the ATCC #CRL-3216)
CaLu-3	Human lung cancer cell line isolated from pleura effusion from lung adenocarcinoma in a 25-year-old male (RRID:CVCL_0609; obtained from ATCC #HTB-55)
CaCo-2	Immortalized human epithelia-like colorectal adenocarcinoma cell line from a 72-year-old male (RRID:CVCL_0025; obtained from ATCC #HTB-37)
VeroE6	Epithelia-like cell line isolated from African green monkey (*Cercopithecus aethiops*) (RRID:CVCL_0574; obtained from ATCC #CRL-1586)
VeroE6 TMPRSS2	Epithelia-like cell line isolated from African green monkey (*Cercopithecus aethiops*), constitutively expressing the serine protease TMPRSS2 under selection of geneticin (RRID:CVCL_YQ49; kindly provided by K. Sato)

RhiLu1 hACE2	Clonaly immortalized embryonal lung cell line from a pregnant female *Rhinolophus alcyone* bat, stabily expressing human ACE2 (RRID:CVCL_RX22; kindly provided by M. Müller [94])

2.1.2 Bacteria strains

Table 2: Bacteria

Bacteria Strain	**Background**
E. coli XL-2 Blue	endA1 supE44 thi-1 hsdR17 recA1 gyrA96 relA1 lac [F´proAB lacI^{q}ZΔM15 Tn10 (Tet^{r}) Amy Cam^{r}] (Agilent Technologies)

2.1.3 Medium

Table 3: Media

Medium	**Composition**
DMEM	Dulbecco's Modified Eagle Medium High Glucose (Thermo Fisher Scientific) containing 2 mM L-glutamine, 100 µg/ml streptomycin, 100 U/ml penicillin and 10% (v/v) heat inactivated fetal bovine serum (FBS)

LB-medium	Lysogeny broth (LB) medium containing 10 g/l bacto-tryptone, 5 g/l bacto yeast extract, 10 g/l NaCl in distilled water, supplemented with ampicillin (100 mg/l) or kanamycin (50 mg/l)
LB-agar	LB-medium containing 16 g/l bacto agar and ampicillin (100 mg/l) or kanamycin (50 mg/l)
S.O.C.-medium	Super optimal broth with catabolite repression containing 2% Tryptone, 0.5% yeast extract, 10 mM NaCl, 2.5 mM KCl, 10 mM $MgCl_2$, 10 mM $MgSO_4$ and 20 mM glucose (Thermo Fisher Scientific)

2.2 Oligonucleotides

Table 4: TaqMan qPCR Primer Probes

Target	**Species**	Dye	Manufacturer (Cat #)
GAPDH	Human	VIC-MGB	Thermo Fisher Scientific (Hs02786624_g1)
IFNB1	Human	FAM	Thermo Fisher Scientific (Hs01077958_s1)

Table 5: Sequencing primers

Name	Sequence 5′ - 3′
pCG Seq. fwd	GGAGACGCCATCCACGCTGTTTTGACCTCC
pCG Seq. rev (-IRES)	CTGAAAACTTTGCCCCCTCCATATAACATGAATTT TAC
pCG Seq. rev (+IRES)	CATTGCCAAAAGACGGCAATATGGTGG
Gaus3 CMV fwd	GGAGGTCTATATAAGCAG
pRen2 Luc fwd	CCAAAAATGTTTATTGAATCGG
pCAGGS fwd	GACGGCTGCCTTCG

Table 6: Mutagenesis primers

Name	Sequence 5′ - 3′
ORF3c M1T fwd	GAAATCAAGGACGCTACTCCTTC
ORF3c M1T rev	GAAGGAGTAGCGTCCTTGATTTC
ORF3c Q5* fwd	GCTACTCCTTTAGATTTTGTTCG
ORF3c Q5* rev	CGAACAAAATCTAAAGGAGTAGC
ORF3a R6* fwd	GGATTTGTTTATGTGAATCTTCAC
ORF3a R6* rev	GTGAAGATTCACATAAACAAATCC
ORF3(any)-HA rev	TTACGCGTTTAAGCGTAATCTGGAACATC GTATGGGTACAAAGGCACGCTAGTAG
Wuhan Orf3 SDM Q57H fwd	CTGTTTTTCATAGCGCTTCC

Wuhan Orf3 SDM Q57H rev	GGAAGCGCTATGAAAAACAG
Wuhan Orf3c SDM Q57H rev	TTACGCGTTTATGATTTTGGAAGCGCTATG
Wuhan Orf3c-HA SDM Q57H rev	TTACGCGTTTAAGCGTAATCTGGAACATC GTATGGGTATGATTTTGGAAGCGCTATG
Orf3c Q5* fwd	CTCCTTTAGATTTTGTTCCGCGCTAC
Orf3c Q5* rev	CGCGAACAAAATCTAAAGGAGTAGC
Tor2 SDM A9M L11Q fwd	GATTTTGTTCATGCTACAGCAACG
Tor2 SDM A9M L11Q rev	CGTTGCTGTAGCATGAACAAAATC
Tor2 XbaI V6I SDM fwd	CTTCTAGAGCCACCATGCTACTCCTTCAG GTATTGTTC
SL SDM P39Q S41- fwd	TTTCAAAGCGCTTCAAAAATACCCATAC GATGTTCCAGATT
SL SDM P39Q S41- rev	CATCGTATGGGTATTTTTGAAGCGCTTTG AAAAAC
SL XbaI fwd	AATCTAGAGCCACCATGCTACTCCTTC
MAVS ΔCARD fwd HindIII	TTAAGCTTGGCTGTGAGCTAGTTGATCTC G
MAVS ΔCARD rev XbaI	AATCTAGACTAGTGCAGACGCCGCCGGT ACAG
ORF3c L2A L3A fwd	AATCTAGAATGGCAGCCCTTCAGATTTTG
ORF3c L4A Q5A fwd	AATCTAGAATGCTACTCGCTGCGATTTTG TTCG
ORF3c I6A L7A fwd	AATCTAGAATGCTACTCCTTCAGGCTGCG TTCGC

ORF3c F8A fwd	AATCTAGAATGCTACTCCTTCAGATTTTG GCCGCG
ORF3c L10A L11A fwd	ATTTTGTTCGCGGCAGCGCAACGATAC
ORF3c L10A L11A rev	TCGGTATCGTTGCGCTGCCGCGAACAA
ORF3c Q12A R13A fwd	TTCGCGCTACTGGCAGCATACCGATAC
ORF3c Q12A R13A rev	CTTGTATCGGTATGCTGCCAGTAGCGC
ORF3c Y14A R15A fwd	CTACTGCAACGAGCCGCATACAAGCCT
ORF3c Y14A R15A rev	GTGAGGCTTGTATGCGGCTCGTTGCAG
ORF3c Y16A K17A fwd	CAACGATACCGAGCCGCGCCTCACTCC
ORF3c Y16A K17A rev	AAGGGAGTGAGGCGCGGCTCGGTATCG
ORF3c P18A H19A fwd	TACCGATACAAGGCTGCCTCCCTTTCG
ORF3c P18A H19A rev	ATCCGAAAGGGAGGCAGCCTTGTATCG
ORF3c S20A L21A fwd	TACAAGCCTCACGCCGCTTCGGATGGC
ORF3c S20A L21A rev	TAAGCCATCCGAAGCGGCGTGAGGCTT
ORF3c S22A D23A fwd	CCTCACTCCCTTGCGGCTGGCTTATTG
ORF3c S22A D23A rev	CAACAATAAGCCAGCCGCAAGGGAGTG
ORF3c G24A L25A fwd	TCCCTTTCGGATGCCGCATTGTTGGCG
ORF3c G24A L25A rev	CAACGCCAACAATGCGGCATCCGAAAG
ORF3c L26A L27A fwd	TCGGATGGCTTAGCGGCGGCGTTGCAC
ORF3c L26A L27A rev	GAAGTGCAACGCCGCCGCTAAGCCATC
ORF3c L29A H30A fwd	TTATTGTTGGCGGCGGCCTTCTTGCTG
ORF3c L29A H30A rev	AAACAGCAAGAAGGCCGCCGCCAACAA

ORF3c F31A L32A fwd	TTGGCGTTGCACGCCGCGCTGTTTTTC
ORF3c F31A L32A rev	TCTGAAAAACAGCGCGGCGTGCAACGC
ORF3c L33A F34A fwd	TTGCACTTCTTGGCGGCTTTCAGAGCG
ORF3c L33A F34A rev	AAGCGCTCTGAAAGCCGCCAAGAAGTG
ORF3c F35A R36A fwd	TTCTTGCTGTTTGCCGCAGCGCTTCCA
ORF3c F35A R36A rev	TTTTGGAAGCGCTGCGGCAAACAGCAA
ORF3c L38A P39A fwd	TTTTTCAGAGCGGCTGCAAAATCATAC
ORF3c L38A P39A rev	TGGGTATGATTTTGCAGCCGCTCTGAA
ORF3c K40A S41A fwd	AGAGCGCTTCCAGCAGCATACCCATAC
ORF3c K40A S41A rev	ATCGTATGGGTATGCTGCTGGAAGCGC
ORF3a fwd	AATCTAGAGCCACCATGGATTTGTTTATG AGAATCTTCAC
ORF3a rev	TTACGCGTTTACAAAGGCACGCTAGTAG
ORF3c fwd	AATCTAGAGCCACCATGCTACTCCTTCAG ATTTTG
Orf3d fwd	AATCTAGAGCCACCATGGCTTATTGTTGG CG
Orf3d-2 fwd	AATCTAGAGCCACCATGGCAACTAGCAC TCTCC
ORF3b-fwd	AATCTAGAGCCACCATGATGCCAACTATT TTC
ORF3b-2 fwd	AATCTAGAGCCACCATGGCACAACAAGT CC

ORF3b-3 fwd	AATCTAGAGCCACCATGTTACCTTCTTCATCTAC
ORF3b-4 fwd	AATCTAGAGCCACCATGATGAACCGACGACG
ORF3e fwd	AATCTAGAGCCACCATGGGAATCTGGAGTAAAAG
pRen2 Orf3d wt fwd	AAGAATTCATGCTACTCCTTCAGATTTTG
pRen2 Orf3d wt rev	AACTCGAGTTATGATTTTGGAAGCGCTC
pRen2 Orf3c* fwd	AAGAATTCATGGCAACTAGCACTCTCC
mut3c-fwd	CAATTGGAACTGTAACTTTGAAGCAAGGTGAAATCAAGGACGCTACTCCTTCAGATTTGAGGATGACGACGATAAGTAGGG
mut3c-rev	GTATCGTTGCAGTAGCGCGAACAAAATCTGAAGGAGTAGCGTCCTTGATTTCACCTTGCTCAACCAATTAACCAATTCTGATTAG

Table 7: CPER fragments primers

Name	**Sequence 5′ - 3′**
Linker/F1-F	CTATATAAGCAGAGCTCGTTTAGTGAACCGTATTAAAGGTTTATACCTTCCCAGGTAAC
F1/F2-R	CAGATTCAACTTGCATGGCATTGTTAGTAGCCTTATTTAAGGCTCCTGC

F1/F2-F	GCAGGAGCCTTAAATAAGGCTACTAACAATGCCATGCAAGTTGAATCTG
F2/F3-R	GGTAGGATTTTCCACTACTTCTTCAGAGACTGGTTTTAGATCTTCGCAGGC
F2/F3-F	GCCTGCGAAGATCTAAAACCAGTCTCTGAAGAAGTAGTGGAAAATCCTACC
F3/F4-R	GGTGCACAGCGCAGCTTCTTCAAAAGTACTAAAGG
F3/F4-F	CACCACTAATTCAACCTATTGGTGCTTTGGACATATCAGCATCTATAGTAGCTGGTGG
F4/F5-R	GTTTAAAAACGATTGTGCATCAGCTGACTG
F4/F5-F	CACAGTCTGTACCGTCTGCGGTATGTGGAAAGGTTATGGCTGTAGTTGTGATC
F5/F6-R	GCGGTGTGTACATAGCCTCATAAAACTCAGGTTCCCAATACCTTGAAGTG
F5/F6-F	CACTTCAAGGTATTGGGAACCTGAGTTTTATGAGGCTATGTACACACCGC
F6/F7-R	CATACAAACTGCCACCATCACAACCAGGCAAGTTAAGGTTAGATAGCACTCTAG
F6/F7-F	CTAGAGTGCTATCTAACCTTAACTTGCCTGGTTGTGATGGTGGCAGTTTGTATG
F7/F8-R	CTAGAGACTAGTGGCAATAAAACAAGAAAAACAAACATTGTTCGTTTAGTTGTTAAC
F7/F8-F	GTTAACAACTAAACGAACAATGTTTGTTTTTCTTGTTTTATTGCCACTAGTCTCTAG

F8/F9+10-R	GCAGCAGGATCCACAAGAACAACAGCCCTTGAGACAA CTACAGCAACTGG
F8/F9+10-F	CCAGTTGCTGTAGTTGTCTCAAGGGCTGTTGTTCTTGTG GATCCTGCTGC
F9+10/Linker-R	GGAGATGCCATGCCGACCCTTTTTTTTTTTTTTTTTTTT TTTGTCATTCTCCTAAG
F9+10/Linker-F	CTTAGGAGAATGACAAAAAAAAAAAAAAAAAAAAAA AAAGGGTCGGCATGGCATCTCC
Linker/F1-R	GTTACCTGGGAAGGTATAAACCTTTAATACGGTTCACTA AACGAGCTCTGCTTATATAG

2.3 Expression plasmids

Table 8: Expression plasmids

Vector	**Description**
pCG_HIV-1 M NL4-3 *nef* 3* (Δ)IRES eGFP	Expression vector based on the human cytomegalovirus (CMV) immediate early promoter containing an *ampR* gene. Unique XbaI and MluI restriction sites were used to insert the open reading frame (ORF) of HIV-1 NL4-3 *nef* with premature stop codons. The unique BamHI restriction site was used to insert or remove (Δ) an internal ribosome entry site (IRES) and the sequence for green fluoressent protein (GFP).

pCAGGS_IAV NS1 A/Puerto Rico/8/34 (H1N1 PR8) N-3x-HA-tag	kindly provided by Kei Sato [47]
IFN-β promoter firefly luciferase reporter	kindly provided by Michael Gale Jr [95]
pTAL-*Gaussia* luciferase reporter	kindly provided by Bernd Baumann
pNF-κB(3x) firefly luciferase reporter	kindly provided by Bernd Baumann
IFN-β promoter (ΔNF-κB binding sites) firefly luciferase reeporter	kindly provided by Frank Kirchhoff [96]
pcDNA5-fl-Ha-RIG-I	kindly provided by Konstantin MJ Sparrer
pEF-Bos-RIG-I 1-211-flag	kindly provided by Konstantin MJ Sparrer
pcDNA5-fl-Ha-MDA5	kindly provided by Konstantin MJ Sparrer
pCMV3-3xFLAG-TBK1	kindly provided by Konstantin MJ Sparrer
peYFP_IRES_NSP1 (NCDV)	kindly provided by Michele Hardy [97]
peYFP_IRES_NSP1 (OSU)	kindly provided by Michele Hardy [97]
p(N)FLAG-CMV2 MAVS	kindly provided by Konstantin MJ Sparrer
pRen2	kindly provided by Peter D Burbelo [98]
pRen2-N	kindly provided by Peter D Burbelo [98]
pBeloSCoV2-dORF6-YFP	kindly provided by Prof. Armin Ensser
pBeloSCoV2-dORF6-YFP-ORF3c	kindly provided by Prof. Armin Ensser
pEGFP-C1_IRF3 wt	kindly provided by Prof. Takashi Irie

pEGFP-C1_IRF3 5D	kindly provided by Prof. Takashi Irie
DsRed2-Mito-7	kindly provided by Michael Davidson
pCAGGS-ynMAVS	kindly provided by Prof. Adolfo G Sastre [99]
pCAGGS-ycMAVS	kindly provided by Prof. Adolfo G Sastre [99]
pCAGGS-ynCARD	kindly provided by Prof. Adolfo G Sastre [99]
pCAGGS-ycCARD	kindly provided by Prof. Adolfo G Sastre [99]
pCAGGS-RIG-Iyn	kindly provided by Prof. Adolfo G Sastre [99]
pCAGGS-ycRIG-I	kindly provided by Prof. Adolfo G Sastre [99]
pCAGGS-ynRIG-I	kindly provided by Prof. Adolfo G Sastre [99]
pCSII-sars-cov-2 F1	kindly provided by Prof. Takasuke Fukuhara
pCSII-sars-cov-2 F2	kindly provided by Prof. Takasuke Fukuhara
pCSII-sars-cov-2 F3	kindly provided by Prof. Takasuke Fukuhara
pCSII-sars-cov-2 F4	kindly provided by Prof. Takasuke Fukuhara
pCSII-sars-cov-2 F5	kindly provided by Prof. Takasuke Fukuhara
pCSII-sars-cov-2 F6	kindly provided by Prof. Takasuke Fukuhara
pCSII-sars-cov-2 F7	kindly provided by Prof. Takasuke Fukuhara
pCSII-sars-cov-2 F9F10	kindly provided by Prof. Takasuke Fukuhara
pCSII-sars-cov-2 F9-10-sfGFP	kindly provided by Prof. Takasuke Fukuhara
pMW118-sars-cov2-CMV Linker	kindly provided by Prof. Takasuke Fukuhara

2.4 Kits

Table 9: Kits

Kit	Manufacturer (Cat #)
Lipofectamine2000	Invitrogen (11668019)
TransIT-LT1	MirusBio (2300)
Restriction enzymes	New England Biolabs
PrimeSTAR GXL DNA polymerase	TaKaRa Bio (R050A)
TURBO DNase	Thermo Fisher Scientific (AM2238)
Q5 Site-Directed Mutagenesis Kit	New England Biolabs (E0554S)
Monarch® DNA Gel Extraction Kit	New England Biolabs (T1020L)
Luna Universal Probe qPCR Master Mix	New England Biolabs (M3004X)
DNA-free DNA Removal Kit	Invitrogen (AM1906)
Phusion High-Fidelity DNA Polymerase	Thermo Fisher Scientific (F530L)
DNA Ligation Kit Ver.2.1	TaKaRa Bio (6022)
PrimeScript RT Reagent Kit	TaKaRa Bio (RR037A)
Quik Change II XL Site Directed Mutagenesis Kit	Agilent Technologies (200523)

Fix & Perm Kit 1000 (CE)	Nordic-MUbio (NMB-GAS-002-1-CE/IVD)
Wizard Plus Midipreps DNA Purification System	Promega (A7640)
Luciferase Assay System	Promega (E1501)
Wizard(R) Plus DNA Purification System	Promega (A7640)
RNeasy Plus Mini Kit	Qiagen (74136)

2.5 Buffer

Table 10: Buffers

Method	**Buffer**	**Composition**
LIPS	Buffer A	50 mM Tris base, 100 mM NaCl, 5 mM $MgCl_2$, 1 % Triton X-100 (pH 7.5)
	Lysis Buffer	50 mM Tris base, 100 mM NaCl, 5 mM $MgCl_2$, 1 % Triton X-100, 50 % glycerol and protease inhibitors (pH 7.5)
Flow Cytometry	FACS Buffer	1 % (v/v) FBS in PBS
	Clean Solution	BD Bioscience
	Flow Solution	
	Shutdown Solution	

Calcium-phosphate transfection	10x HBS	8.18 % NaCl (w/v), 5.94 % HEPES (w/v) and 0.25 % Na_2HPO_2 (w/v) in distilled water. For a 2x HBS preparation, the 10x stock solution was diluted with distilled water (final pH 7.12) and sterilized by filtration.
	2 M $CaCl_2$	2 M $CaCl_2$ was prepared in distilled water and sterilized by filtration.
Western Blot	Lysis Buffer	150 mM NaCl, 50 mM HEPES, 5 mM EDTA, 0.1 % Nonidet P-40 (v/v), 0.5 mM Na_3VO_4, 0.5 mM NaF in distilled water (pH 7.5); add one cOmplete ULTRA protease inhibitor cocktail tablet per 10 ml buffer
	Running Buffer	1x NuPAGE MES SDS Running Buffer in distilled water
	Transfer Buffer	47.9 mM Tris base, 38.6 mM glycine, 1.3 mM SDS, 20 % methanol (v/v) in distilled water (pH 8.3)
	Blocking Buffer	5 % skimmed milk powder (w/v) in PBS or 5 % BSA (w/v) in TBS-T
	Staining Buffer	1 % skimmed milk powder (w/v) in PBS or 1 % BSA (w/v) in TBS-T
	Wash Buffer	0.2 % Tween 20 (v/v) in PBS or TBS
	5x PBS	140 mM NaCl, 8.1 mM Na_2HPO_4, 2.7 mM KCL, 1.5 mM KH_2PO_4 in distilled water (pH 7)

General	10x TBS	200 mM Tris base, 1500 mM NaCl in distilled water (pH 7.6)
	50x TAE	2 M Tris-HCl, 1 M acetic acid, 0.1 M EDTA in distilled water (pH 8.3)

2.6 Antibodies

Table 11: Primary antibodies

Target	Host	Final concentration	Manufacturer (Cat #)
HA	rabbit	1 µg/ml	Sigma (SAB4300603)
HA	mouse	1 µg/ml	Sigma (H3663)
Flag	rabbit	1 µg/ml	Sigma (SAB4301135)
Flag	mouse	1 µg/ml	Sigma (F1804)
IRF3	rabbit	1 µg/ml	Cell Signaling (11904S)
pIRF3 (Ser386)	rabbit	2 µg/ml	Cell Signaling (37829)
RIG-I	rabbit	1 µg/ml	Cell Signaling (3743)
MDA5	rabbit	1 µg/ml	Cell Signaling (5321)
MAVS	rabbit	1 µg/ml	Cell Signaling (3993)
TBK1	rabbit	1 µg/ml	Cell Signaling (38066)
GAPDH	rat	1 µg/ml	Biolegend (607902)
SeV	rabbit	2 µg/ml	MBL (PD029)

Table 12: Secondary antibodies

Target	Host	Conjugate	Dilution	Manufacturer (Cat #)
mouse	goat	680RD	1:20.000	LI-COR (926-680-70)
rabbit	goat	680RD	1:20.000	LI-COR (925-68071)
rat	goat	680RD	1:20.000	LI-COR (926-68076)
mouse	goat	800RD	1:20.000	LI-COR (926-32210)
rabbit	goat	800RD	1:20.000	LI-COR (926-32211)
rat	goat	800RD	1:20.000	LI-COR (926-32219)
mouse	goat	AF488	1:500	Invitrogen (A11001)
rabbit	goat	AF488	1:500	Invitrogen (A11008)
mouse	goat	AF555	1:500	Invitrogen (A21422)
rabbit	goat	AF555	1:500	Thermo Fisher (A-21428)

2.7 Reagents

Table 13: Reagents

Reagent	Manufacturer
Agarose	Sigma-Aldrich
Ampicillin	Ratiopharm
Bacto agar	BD Bioscience

Bacto tryptone	BD Bioscience
Bacto yeast extract	BD Bioscience
BlueStar Plus Prestained Protein Marker	Nippon Genetics Europe
Calcium chloride dihydrate ($CaCl_2 \cdot 2H_2O$)	Sigma-Aldrich
Coelenterazine	PJK Biotech
Complete ULTRA protease inhibitor tablets, Mini EDTA-free	Roche
Dimethyl sulfoxide (DMSO)	Merck Chemicals GmbH
Di-sodium hydrogen phosphate dihydrate ($Na_2HPO_2 \cdot 2H_2O$)	Merck Chemicals GmbH
Disodium phosphate (Na_2HPO_4)	AppliChem GmbH
dNTPs	Thermo Fisher Scientific
Doxycycline hyclate	Sigma-Aldrich
Dulbecco's phosphate-buffered saline (DPBS)	Thermo Fisher Scientific
Ethanol	PanReac AppliChem
Ethidium bromide	AppliChem GmbH
Ethylendiaminetetraacetate (EDTA)	Sigma-Aldrich
Fetal bovine serum (FBS)	Thermo Fisher Scientific
HEPES-buffered saline	Sigma-Aldrich
HPLC water	Thermo Fisher Scientific
Isopropanol	Pharma SAV
Kanamycin	Thermo Fisher Scientific

L-glutamine	Pan-Biotech
Luciferase Assay System	Promega
Luciferase Cell Culture Lysis 5x Reagent	Promega
Methanol	Merck Chemicals GmbH
M-PER Mammalian Protein Extraction Reagent	Thermo Fisher Scientific
Nonidet P-40 (NP40)	Thermo Fisher Scientific
NuPAGE MES SDS Running Buffer (20x)	Thermo Fisher Scientific
Paraformaldehyde (PFA)	Merck Chemicals GmbH
Penicillin-Streptomycin	Pan-Biotech
Poly-L-Lysine	Sigma-Aldrich
Potassium chloride (KCl)	AppliChem GmbH
Potassium dihydrogen phosphate (KH_2PO_4)	AppliChem GmbH
Protein Loading Buffer (4x)	LI-COR
Restriction endonucleases	New England BioLabs
RNase A	Qiagen
Roti Load DNA (with glycerol)	Carl Roth
S.O.C. medium	Thermo Fisher Scientific
Sodium chloride (NaCl)	Merck Chemicals GmbH
Sodium dodecyl sulfate (SDS)	Carl Roth
Sodium fluoride (NaF)	Sigma-Aldrich
Sodium orthovanadate (Na_3VO_4)	Sigma-Aldrich

Skimmed milk powder, blotting grade	Sigma-Aldrich
IRDye® 800CW Streptavidin	LI-COR
Tris-HCl	Sigma-Aldrich
Tris base	Sigma-Aldrich
Triton X-100	Sigma-Aldrich
Trypsin/EDTA	Pan-Biotech
Tween-20	Sigma-Aldrich
1 Kb Plus DNA Ladder	Thermo Fisher Scientific
β-mercaptoethanol	Sigma-Aldrich
FBS Ultra Low Endotoxin, < 1 EU/ml, 500 ml	Bio & Sell

2.8 Consumables

Table 14: Consumables

Product	**Manufacturer**
Cell culture dish (6-, 12-, 24, 48-, 96-well)	Sarstedt
Cell Culture Flasks (25, 75, 175 cm^2)	Cell Star
Cryo tubes	Sarstedt
Falcon (15 & 50 ml)	Cell Star
Filter tips (10 µl)	Biozym
Filter tips (200 & 1000 µl)	greiner BIO-ONE

Reaction tubes (1.5 ml, 2 ml)	greiner BIO-ONE
Reaction tubes (0.25 ml)	Sarstedt AG & Co. KG
Serological pipettes (5 ml, 10 ml, 25 ml, 50 ml)	Sarstedt AG & Co. KG
Le Sac autoclavable	Sarstedt AG & Co. KG
LightCycler 480 Multiwell Plate 96, white	Roche
LightCycler 480 Sealing Foil	Roche
Nunc white polystyrene 96-well Microwell plates	Thermo Fisher Scientific
NuPAGE Novex 4-12 % Bis-Tris Gels	Thermo Fisher Scientific
Classic protect nitril gloves	Abena
Whatman chromatography paper 2 mm CHR	GE Healthcare
RNAse away	MBP Molecular Bio Products
Immobilon-FL Transfer Membrane	Merck Millipore
Round Gel loading tips	Santa Cruz Biotechnology Inc.
Reagent reservoir	Thermo Fisher Scientific

2.9 Equipment

Table 15: Equipment

Product	Type	Manufacturer
Centrifuges	5417R, 5810R 5430R	Eppendorf
	Rotina 48R	Hettich
Electrophoresis Chamber	Mini-Sub GT cell	Bio-Rad Laboratories
Flow Cytometer	MACS Quant VYB	Miltenyi Biotech
Gel Documentation System	Intas GelDoc	Intas
Water Bath	WB27	Memmert
Incubator	Heracell	Heraceus instruments
	CB_E6	BINDER™
Light Microscope	Axiovert 200	Zeiss
Laminar Flow Hood	HERAsafe	Heraeus Instruments
UV Hood	DNA/RNA UV-Cleaner UVC/T-M-AR	Toepfer Labsystems
Western Blot imager	Odyssey Fc	LI-COR
Multimode Reader	TriStar² S LB 942	Berthold Technologies
pH meter	WTW Inolab pH level 2	VWR
Pipette	P10L, P200L, P1000L, F20L	Gilson
Pipetting aid	pipetus®	Hirschmann

Multichannel Pipette	Research Plus 10-100 µl, 30-300 µl	Eppendorf
Power supplies	PowerPac 200, 300, Basic	Bio-Rad Laboratories
LightCycler	480 II	Roche
Scales	GJ & 770	Kern
Semi-Dry Transfer Cell	Trans-Blot® SD	Bio-Rad Laboratories
Sonicater	SONOPULS	BANDELIN
Spectrophotometer	NanoDrop 2000	Thermo Fisher Scientific
ThermoMixer	F1.5	Eppendorf
Thermal Cycler	PTC-200	MJ Research
Tube Roller Mixer	uniROLLER 6 easy	LLG Labware
Vortexer	REAX top & Vortex Genie 2	Heidolph
Western Blot Chamber	Mini Gel Tank	Invitrogen
Western Blot Chamber	SureLock™ Tandem	Invitrogen

2.10 Software

Table 16: Software

Software	**Provider**
Benchling	Benchling, Inc.
CorelDRAW 24.1.0.360	Corel Corporation 2022

FloLogic 8.3	Inivai Technologies Pty. LTd.
Gel doc software v.0.2.14	Initas
GraphPad Prism 9.4.1	GraphPad Software
Image Studio Lite Ver. 5.2	LI-COR Biosciences GmbH
LaTeX	The LaTeX Project
LightCycler 480 SW 1.5.1	Roche
Microsoft Office Professional Plus 2019	Microsoft Corporation
PEP-FOLD 3	RPBS [100]
TIS predictor	Roos Laboratory [50]
TMHMM-2.0	DTU Health Tech [101]

3 Methods

3.1 Eukaryotic cell culture and transfection

3.1.1 Cell lines

HEK293T, HEK293T C34, CaCo-2, VeroE6 and VeroE6/TMPRSS2 cells were cultured in Dulbecco's Modified Eagle Medium (DMEM) containing 2 mM L-glutamine, 100 mg/ml streptomycin, 100 U/ml penicillin and 10% (v/v) heat-inactivated fetal bovine serum (FBS). Calu-3 cells were cultured in DMEM supplemented with 2 mM L-glutamine, 100 mg/ml streptomycin, 100 U/ml penicillin and 20% (v/v) FBS. RhiLu1 hACE2 cells were cultured in DMEM supplemented with 2 mM L-glutamine, 100 mg/ml streptomycin, 100 U/ml penicillin and 10% (v/v) endotoxin-free FBS. Cells were cultured in an Incubator at 37°C, 90% relative humidity and 5% CO_2. Upon confluence (80% for HEK293T, HEK293T C34, CaCo-2, RhiLu1 hACE2, VeroE6 and VeroE6/TMPRSS2 and 90% for Calu-3), cells were split 1:10. For this purpose, the medium was removed, and the cells were washed with PBS. To detach cells, 2 ml trypsin (0,05%) was added and the cells were incubated for 1-5 min at 37°C. The cells were then resuspended in 8 ml medium, and either 1 ml of the cell suspension was filled up with medium for further cultivation or the cell number was determined in a Neubauer counting chamber for downstream experiments. Cell lines were tested regularly for mycoplasma contamination.

3.1.2 Calcium phosphate transfection

HEK293T cells were transfected using a standard calcium phosphate method. For co-immunoprecipitation, western blot, LIPS assay and flow cytometry, a 6-well format was used. Cells were seeded at $3x10^5$/ml in 2 ml supplemented DMEM one day prior to transfection. To perform qPCR, $2.4x10^5$ cells/ml in 500µl supplemented DMEM were seeded in a 24-well format. Luciferase assays were performed in a 96-well format, seeding cells at $2x10^5$/ml in 100 µl supplemented DMEM. Prior to transfection in this format, wells were coated with poly-L-lysine at 37°C for 1 h and afterwards washed twice with PBS. After 24 h, culture medium was replaced, and cells were

transfected at confluence above 70%. Up to 5 µg DNA was mixed with 13 µl $CaCl_2$ and filled up to 100 µl with HPLC water. One sample containing no DNA served as a negative control (Mock). 100 µl 2x HEPES-buffered saline (HBS) was added dropwise to each sample and resuspended. Cells were transfected by adding a total of 10% culture volume of the transfection mix to each well. For co-immunoprecipitation and luciferase assays, cells were transfected in technical triplicates. After incubation for 6 h, the medium was replaced with fresh supplemented DMEM. Cells were processed after an additional 24 h incubation period for downstream analysis.

3.2 Virological methods

3.2.1 Virus stock production

To generate virus stocks, VeroE6/TMPRSS2 cells were seeded at $5x10^5$/ml in 10 ml complete medium in a T75 flask one day prior to infection. After 24 h, the cells were infected with 10 µl virus stock added to the cells without replacing the medium and incubated for 1 h at 37°C. Next, the medium was changed to supplemented medium containing 2% FBS (infection medium), and the cells were incubated for an additional 24 h. After two days, cells showed a clear cytopathic effect (CPE), and virus containing supernatants were harvested and centrifuged at 5942 g for 4 min to remove any cell debris. Virus titers were determined by TCID50, and aliquots were stored at -80°C.

3.2.2 Tissue culture infectious dose 50 (TCID50)

To determine the infectivity of virus stocks, the TCID50/ml method was used. VeroE6/TMPRSS2 cells were seeded at $1x10^5$/ml in 100 µl supplemented DMEM into a 96-well plate one day prior to infection (titration plate). On the next day, a dilution series of the virus stock was set up in a separate 96-well plate in sextuplicates ranging from 10^{-1} to 10^{-7} (dilution plate). Then, 10 µl of the dilutions were transferred to the infection plate yielding a final dilution series of 10^{-2} to 10^{-8}. The last row of the plate was left without virus and served as a negative control. The plate was then

incubated at 37°C for 5 days. The cells were checked under a microscope for CPE and the TCID50/ml was calculated using the Reed–Muench method [102].

3.2.3 Replication kinetics

For replication kinetics of BAC-derived SARS-CoV-2 ΔORF6-YFP and SARS-CoV-2 ΔORF6-YFP ΔORF3c, CaCo-2 cells (1x10^5/ml), CaLu-3 cells (2x10^5/ml) or RhiLu1 hACE2 cells (5x10^5/ml) were seeded in 100 µl supplemented DMEM into a 96-well plate one day prior to infection. Cells were infected in triplicates at an MOI of 0.1 (CaCo-2 & CaLu-3) or 0.001 & 0.1 (RhiLu1 hACE2) for 1 h at 37°C. After exchanging the medium with fresh culture medium, the plates were placed in an Incucyte plate reader. Plates were incubated for up to four days, and four images per well were taken every 4 h. The 'Basic Analysis Mode' was used to quantify virus growth as green area normalized to phase area. Supernatants and cells were harvested at 72 h post infection to determine cytokine levels by Cytokine Array and RT-qPCR, respectively.

3.3 Molecular biology techniques

3.3.1 Luciferase reporter assay

Reporter constructs expressing firefly luciferase under the control of the interferon-β promoter, a mutant thereof lacking all NF-κB binding sites (IFN-β ΔNF-κB) and an NF-κB promoter (5x NF-κB binding sites) were used to examine the effect of ORF3c variants on different steps of the interferon signaling cascade. HEK293T cells were transfected in triplicates with a combination of: (1) firefly luciferase reporter construct (100 ng), (2) a pTAL-*Gaussia* luciferase expression construct for normalization (5 ng), (3) individual constructs expressing RIG-I-CARD-Flag , Flag-HA-MDA5, Flag-MAVS or IRF3 5D serving as a stimulus of the interferon pathway (5 ng), as well as (4) increasing amounts of different ORF3c-HA expression constructs (12.5 - 100 ng). DNA amounts were adjusted across all conditions by addition of an empty vector control (pCG_HIV-1 M NL4-3 *nef* stop ΔIRES-eGFP) to a total of 210 ng/well. One day post

transfection, 40 µl cell culture supernatant containing secreted *Gaussia* luciferase was transferred into a Nunc white polystyrene 96-well microwell plate. Luciferase activity was measured after addition of 50 µl coelenterazine (PJK Biotech) to each well on a TriStar² S LB 942 Multimode Reader (Berthold Technologies) for 0.1 s and a read height of 1 mm. Since the *Gaussia* luciferase gene is under the control of a minimal promoter, which is not responsive to any of the stimuli, its expression can be used for normalization. The cells were lysed in 40 µl 1x Luciferase Cell Culture Lysis Reagent (Promega) for 5 min at room temperature under constant shaking. Subsequently, 30 µl of the cell lysate was transferred to a Nunc white polystyrene 96-well microwell plate, 50 µl Luciferase Assay System (Promega) was added, and firefly luciferase signal was measured with the same settings as for *Gaussia* luciferase activity. For data analysis, the firefly luciferase signal was normalized to the respective *Gaussia* luciferase control of the same well.

3.3.2 Flow Cytometry

HEK293T cells were transfected with increasing amounts of an expression plasmid for ORF3c-HA co-expressing eGFP via an IRES to determine the effect on endogenous IRF3 levels. Transfection with expression plasmids for NSP1 from the rotaviruses NCDV (reduces IRF3 expression) or OSU (inactive against IRF3) (both co-expressing YFP) served as positive and negative controls, respectively [97]. To quantify IRF3 protein levels, cells were permeabilized using the FIX & PERM kit (Nordic-MUbio) according to the manufacturer's instructions. In detail, one day post transfection, cells were transferred into FACS tubes and washed once with 1 ml FACS buffer. The cells were then fixed in 50 µl solution A for 1 h at 4°C. Afterwards, cells were washed again with 1 ml FACS buffer and incubated for another hour in 50 µl permeabilization solution B containing the primary antibody against endogenous IRF3 (Cell Signaling, Cat# 11904S). The cells were washed once again in 1 ml FACS buffer followed by staining with a secondary AlexaFluor 555 antibody (Invitrogen, Cat# A-21422) in 50 µl FACS buffer for an additional hour. Finally, samples were washed in 1 ml and resuspended in 120 µl FACS buffer before measurement on a MACS Quant VYB (Miltenyi Biotec). Data analysis was performed using FlowLogic V.8

(Inivai). The isotype control signal was subtracted from all samples as unspecific background. Afterwards, the mean fluorescence intensity (MFI) of GFP positive cells was normalized to the MFI of GFP negative cells for each sample. Relative protein expression compared to mock-transfected cells or cells transfected with ORF3c was calculated to monitor changes in IRF3 expression.

3.3.3 Bimolecular fluorescence complementation (BiFC) Assay

To study the effect of ORF3c on the interaction between RIG-I and MAVS, a BiFC assay was performed essentially as previously described [99]. In brief, HEK293T cells were transfected with a combination of expression plasmids encoding YFP amino acids 1 to 154 (yn) or 155 to the C-terminus (yc) conjugated to the N-terminus of MAVS or RIG-I, respectively. Cells were additionally transfected with an expression plasmid encoding different variants of ORF3c-HA or an empty vector control, as well as an expression plasmid encoding BFP as transfection control (overall ratio: 2:2:1:0.5, respectively). After 24 h, cells were fixed using the Fix & Perm Kit 1000 (Nordic-MUbio) according to the manufacturer's instructions as described in the section Flow Cytometry. Cells transfected with yc-RIG-I or yn-MAVS only served as controls for background fluorescence and protein : protein interaction was determined as the MFI of YFP in BFP positive cells.

3.3.4 Immunofluorescence microscopy

Confocal immunofluorescence microscopy was used to determine (1) the subcellular localization of ORF3c and ORF3c R36I, (2) the localization of ORF3c in reference to mitochondria, as well as (3) the effect of ORF3c on the intracellular localization of IRF3 during infection. HEK293T cells were seeded at $6x10^5$/ml in 500 µl on 13 mm diameter glass coverslips coated with poly-L-lysine (Sigma-Aldrich) in 24-well plates. On the following day, cells were transfected with an expression plasmid for ORF3c-HA or ORF3c-HA R36I, a mitochondria-targeted red fluorescent protein (DsRed2-Mito-7) or an empty vector control (500 ng total) using Lipofectamine 2000 (Invitrogen) according to the manufacturer's instructions. One day post transfection, cells were washed once in PBS and fixed in 4% paraformaldehyde (PFA) for 20 min

at RT. To permeabilize cellular membranes, cells were incubated in PBS containing 0.5% Triton-X100 for 30 min and then washed three times in PBS. A subsequent incubation step with PBS supplemented with 5% BSA + 0.1% Tween-20 for 30 min served to block non-specific antibody binding and was followed by another washing step in PBS. The primary antibody staining against the HA-tag of ORF3c (Sigma-Aldrich, Cat# H3663) and IRF3 (Cell Signaling) was performed in PBS containing 0.1% BSA at 4°C for 2 h. After three washing steps with PBS containing 0.1% Tween-20, the secondary staining was performed in PBS using an AF488- (Invitrogen) or AF555-conjugated antibody (Thermo Fisher) against mouse (HA) and rabbit (IRF3) IgG, respectively. Nuclei were stained in parallel using 4',6-Diamidine-2'-phenylindole (DAPI; Thermo Fisher Scientific) for 2 h at 4°C. Finally, cells were washed three times in PBS containing 0.1% Tween-20 and mounted on an microscope slide using 10 µl Mowiol mounting medium. The samples were then left at 4°C overnight to allow hardening. Confocal microscopy was performed using an LSM710 (Carl Zeiss). The weighted colocalization coefficient of IRF3 with DAPI was determined as a marker for IRF3 translocation into the nucleus.

3.3.5 LIPS assay

A luciferase immunoprecipitation system (LIPS) assay was performed to check for the presence of antibodies against ORF3c and nucleocapsid (N) in sera from SARS-CoV-2 infected or convalescent patients. The assay allows for the quantification of antibodies by measuring luminescence emitted by the reporter enzyme *Renilla* luciferase (RLuc) fused to an antigen, here SARS-CoV-2 N or ORF3c, expressed by the pRen2 vector in mammalian cells. Sequences for N and ORF3c were inserted into pRen2 by standard cloning techniques using unique EcoRI and XhoI restriction sites downstream of Ruc. Generation of Ruc-N- and Ruc-ORF3c-containing cell lysates, as well as antibody screening of patient sera was performed according to the protocol of Burbelo *et al.* [98], with the following modifications: To generate lysates, HEK293T cells were transfected with individual constructs (pRen2, pRen2-N or pRen2-ORF3c). After one day, cells were washed once with PBS, pooled and harvested in 700 µl lysis buffer. The lysate was then sonicated for 3x5 s at

35% intensity (BANDELIN SONOPULS) and cleared from debris by centrifugation at 20817 g for 4 min at 4°C. Afterwards, the supernatant was transferred into a fresh 1.5 ml tube. Finally, 1 µl supernatant was diluted with 9 µl PBS in a 96-well nunc plate and 100µl 1x coelenterazine (PJK Biotech) was added to the mix followed by immediate measurement on a TriStar² S LB 942 Multimode Reader (Berthold Technologies) with an integration time of 0.1 s and a read height of 1 mm. The lysates were then stored in 50 µl aliquots at a concentration of 10^6 RLU/50 µl at -80°C. To prevent repeated freeze-thawing cycles of the serum samples, a master plate was prepared. For each sample, 90 µl Buffer A were added to a 96-well U-bottom plate and mixed with 10 µl serum on a shaker at 4°C for 2 h. The plate was sealed with Parafilm and stored for up to 1 month at 4°C. To test serum samples, 40 µl Buffer A were mixed with 10 µl of a serum samples from the master plate and 50 µl crude *Renilla* lysate (1x10^7 RLU/50 µl) in a 96-well U-bottom plate and incubated for 1 hour at room temperature. The mix was subsequently added to fresh 1.5 ml tubes containing 5 µl of a 30% A/G Magnetic Beads in PBS suspension and incubated on a shaker (400 rpm) for another hour. Samples were then placed on a magnetic rack, and the supernatant was removed after 1 min incubation. Magnetic beads were washed twice with 150 µl Buffer A followed by two washes with 150 µl PBS. Finally, samples were transferred into a 96-well opaque Nunc-plate (VWR), and 50 µl coelenterazine (PJK Biotech) was added to each condition. The samples were measured immediately on a TriStar² S LB 942 Multimode Reader (Berthold Technologies) with an integration time of 0.1 s and a read height of 1 mm.

3.3.6 RNA Isolation

RNA from cells was isolated using the RNeasy Plus Mini Kit (Qiagen) according to the manufacturer's instructions. Cells were harvested and pooled in 1.5 ml Eppendorf tubes and spun down at 500 g for 5 min. The cell pellet was then washed with ice-cold PBS, resuspended in 350 µl lysis buffer and incubated for 5 min. Afterwards, 250 µl of 96-100% ethanol was added and the lysate was transferred to an RNeasy Mini spin column and centrifuged at 8,000 g for 15 s at room temperature. The flow-through was discarded, and 700 µl buffer RLT was added to the column followed

by centrifugation at 8000 g for 15 s at room temperature. The RNA-containing flow-through was mixed with 500 µl 70% ethanol and transferred to an RNeasy MinElute spin column and centrifuged again at 8,000 g for 15 s. Finally, the flow-through was discarded and the column was centrifuged at 14,000 g for 2 min to dry the membrane. The RNA was eluted with 50 µl RNase-free water, and the concentration and purity were determined by NanoDrop (Thermo Fisher). Isolated RNA was used immediately for downstream processing or stored at -80°C.

3.3.7 gDNA digestion

To remove remnants of genomic DNA (gDNA) from isolated RNA, gDNA digestion was performed using the DNA-free DNA Removal Kit (Thermo Fisher Scientific) according to the manufacturer's instructions. Briefly, 10 µl isolated RNA was mixed with 5 µl 10x DNase I Buffer, 1 µl DNase I enzyme and filled up to a total volume of 50 µl with RNase free water. Reactions were incubated at 37°C for 30 min in a PCR cycler. Afterwards, 5 µl DNase inactivating reagent was added to each sample and incubated at room temperature for 2 min. Finally, samples were centrifuged at 10,000 g for 2 min to pellet the DNase inactivating reagent, and RNA containing supernatants were transferred to fresh tubes. RNA concentrations were determined by NanoDrop. Purified RNA was used immediately for downstream processing or stored at -80°C.

3.3.8 cDNA synthesis

To obtain equal amounts of cDNA from each sample after cDNA synthesis, RNA concentrations of all input samples were adjusted to the sample with the lowest concentration. RNA was then reverse transcribed into cDNA using the PrimeScript RT Reagent Kit (Thermo Fisher Scientific). Equal concentrations of 13 µl RNA were mixed with 4 µl 5x Prime Script Buffer, 1 µl 50 mM oligo dT primer, 1 µl random hexamers and 1 µl Prime Script reverse transcriptase (RT) enzyme mix. Reactions were incubated at 37°C for 20 min on a Thermal cycler (Thermo Fisher Scientific). The RT enzyme was inactivated by a final heating step at 85°C for 1 min. cDNA was either stored at -20°C or used immediately for quantitative PCR (qPCR).

3.3.9 qPCR

To investigate the effect of ORF3c on *IFNB1* mRNA transcript levels, qPCR was performed using the Luna Universal Primer Probe Mix (Thermo Fisher Scientific). Primer probe sets were directed against *GAPDH* and *IFNB1* (Thermo Fisher Scientific). *GAPDH* served as housekeeping gene for normalization, and all measurements were performed in technical duplicates. *IFNB1* and *GAPDH* were run in duplex reactions. For this, an 18 µl master mix, 1 µl FAM-MGB labelled *IFNB1*, 1 µl VIC-TAMRA labelled *GAPDH* primer probe, 10 µl Luna Universal Primer Probe Master Mix (Thermo Fisher Scientific) and 6 ml RNase free water was prepared in a LightCycler 480 Multiwell Plate 96. Then, cDNA was added to the respective wells, and the reactions were simultaneously mixed by centrifugation. The plate was sealed and qPCR was performed using the following protocol: An initial denaturation at 95°C for 60 s followed by denaturation at 95°C for 15 s and extension at 60°C for 30 s including the plate read. Denaturation and extension steps were performed for 40 to 45 cycles. For data analysis, *IFNB1* transcripts were quantified using the $\Delta\Delta C_t$ method and normalized to the housekeeping gene. The mean of technical duplicates was compared as copies per µl or percent of mRNA.

3.3.10 Western Blot

To analyse cellular and viral protein levels, cells were harvested and prepared for western blot analysis. Cells were washed once with cold PBS, pooled in a 1.5 ml tube and subsequently lysed in 500 µl western blot lysis buffer containing protease and phosphatase inhibitors. The cells were placed on ice for 20 min before centrifugation at 20,800 g at 4°C for 20 min to remove cell debris. The protein-containing supernatants were then transferred to fresh 1.5 ml tubes without disruption of the pellet. Next, the lysates were mixed with 22.5% 4x Protein Sample Loading Buffer and 2.5% β-mercaptoethanol and incubated at 95°C for 5 min. The lysates were either immediately used for sodium dodecyl sulfate-polyacrylamide gel electrophoresis (SDS-PAGE) or stored at -20°C. For SDS-PAGE, proteins were separated using 4-12% Nu-PAGE Novex Bis-Tris Gels and NuPAGE MES SDS Running Buffer. The

gels were run in XCell SureLock or XCell4 SureLock western blot chambers at 90 V for approximately 1 h and the BlueStar Plus Prestained Protein Marker was used as a size reference. Proteins were then blotted onto an Immobilon-FL Transfer Membrane using a Semi-Dry Transfer Cell at constant amperage for 2 h. Membranes were blocked with 5% milk powder in PBS-T for 1 h at room temperature. To stain cellular and viral proteins, antibodies directed against GAPDH (BioLegend), HA-tag (Abcam), Flag-tag, and SeV were used. Membranes were incubated with primary antibodies for 1 h at room temperature or overnight at 4°C. Infrared Dye labelled secondary antibodies were then added for 30 min at room temperature. Antibodies were diluted in PBS-T with 1% milk and 0.01% sodium azide. To ensure even blocking, washing and staining, membranes were gently rocked on a Roll- or Rock-shaker during all steps. After each antibody incubation or before detection, three sequential washing steps of the membrane were carried out using PBS containing 0.2% Tween 20 (PBS-T). To detect phosphorylated proteins, all washing steps and stainings were performed using Tris-buffered saline containing 0.2% Tween 20 (TBS-T) and BSA instead of PBS-T and milk powder. Proteins were finally detected using an infrared LI-COR Odyssey Imager, and band intensities were quantified using Image Studio Lite Version 5.2.

3.3.11 Co-immunoprecipitation

To investigate possible interactions between ORF3c or mutants thereof and proteins of the interferon signaling pathway, co-immunoprecipitation with subsequent analysis by western blotting was performed. Briefly, HEK293T cells were seeded in 6-well plates and co-transfected with expression plasmids for HA-tagged ORF3c and Flag-tagged RIG-I, MDA5, MAVS or TBK1 (ratio 4:1; 5 µg/well). One day post transfection, cells were lysed in 300 µl western blot lysis buffer and cleared by centrifugation as described above. 45 µl of the lysates was used for whole-cell lysate analysis, while the remainder was used for co-immunoprecipitation. A pre-clearing step was performed to remove unspecifically binding compounds. Protein A/G Magnetic beads (Pierce) were washed three times with 200 µl NP40 wash buffer and added to the lysates. After incubation for 1 h at 4°C, the samples were placed on a magnetic

rack. Following a 1 min incubation, the supernatants were transferred into fresh 1.5 ml Eppendorf tubes. To precipitate protein complexes, the lysates were incubated first with an anti-Flag antibody (1.5 µg/sample) for 1 h at 4°C followed by addition of 15 µl washed Protein A/G Magnetic Beads for one additional hour at 4°C. The samples were placed on a magnetic rack and the supernatant was discarded after a 1 min incubation. The beads were then washed two times with NP40 wash buffer and once with HPLC water before incubation in 80 µl 1 x Protein Sample Loading Buffer containing 10% β-mercaptoethanol at 95°C for 10 min to recover bound proteins. Finally, samples were placed on a magnetic rack for 1 min to remove the beads and the supernatant was transferred to a fresh 1.5 ml Eppendorf tube. Lysates were stored at -20°C or immediately analyzed by western blotting.

3.3.12 Cytokine Array

To detect cytokines in the supernatants of virus-infected cells, the Human Cytokine Array C5 and C16 kits (RayBiotech) were used with adjustments to the manufacturer's protocol. Specifically, instead of the provided streptavidin-conjugated HRP, a streptavidin-human IRDye 800CW (LI-COR) in PBS-T was used to incubate the membranes for 30 min at room temperature. After a final washing step, cytokines were detected using an infrared LI-COR Odyssey Imager as described in Western Blot.

3.4 Cloning

3.4.1 Polymerase chain reaction

Polymerase chain reaction (PCR) was performed using the Phusion High-Fidelity DNA Polymerase (Thermo Fisher Scientific), KOD One (Sigma) or PrimeSTAR GXL DNA polymerase (TaKaRa Bio/ Cat#R050A) according to the manufacturers' instructions. To generate different *ORF3* fragments, cDNA generated from SARS-CoV-2 RNA was used as a template to initially amplify a full length *ORF3a* fragment. This product served as a template for all subsequent PCR reactions to amplify embedded ORFs. To generate mutants of *ORF3c*, overlap-extension PCR was performed using

primers listed in table 6.

3.4.2 Restriction digestion

DNA restriction was performed using high-fidelity (HF) restriction enzymes (New England Biolabs) according to the manufacturer's protocol. Approximately 1 µg plasmid DNA was used for analytical plasmid restriction digestion and cloning procedures. Briefly, plasmid DNA was mixed with 2 µl 10x CutSmart buffer (NEB), 1 µl of the appropriate restriction enzyme and HPLC water in a total of 20 µl. Digestions were incubated at 37°C for 2 h on a Thermal cycler (Thermo Fisher Scientific) before further processing.

3.4.3 Gel electrophoresis and DNA purification

Agarose gels were prepared by dissolving 1% agarose (Sigma-Aldrich) in boiling TAE buffer under regular swirling. Ethidium bromide (0.2 µg/ml) was added to the solution to allow visualization of DNA under UV light. The gel was cast in a mold including a comb and left to harden. DNA samples were mixed with 6x loading dye (NEB) to a final concentration of 1x and loaded onto the gel. Fragments were separated in 1xTAE buffer at 90 V for approximately 45 min. DNA bands were visualized using a UV screen and if needed for further cloning procedures cut out with a scalpel and purified using the Monarch DNA Gel Extraction Kit (NEB) according to the manufacturer's instructions.

3.4.4 Ligation

To ligate digested and purified inserts into vectors, the DNA Ligation Kit Ver. 2.1 (TaKaRa Bio) was used according to the manufacturer's instructions. Typically, 0.5 µl vector were mixed with 2 µl insert (Ratio 1:4) and added to 2.5 µl Sol I. Ligations were incubated at 16°C for 1 h or overnight.

3.4.5 Transformation

The *E. coli* XL-2 blue strain was kept frozen at -80°C and was slowly thawed on ice for transformation. For each sample, 10 µl *E. coli* were placed in a 1.5 ml Eppendorf tube and gently mixed with either 5 µl ligation product or 1 µl plasmid DNA. After incubation on ice for 20 min, a heat shock was performed at 42°C for 30 sec followed by another 2 min incubation on ice. Then, 200 µl S.O.C. medium was added, and the transformed bacteria were incubated at 37°C for 1 h on a rotary shaker at 400 rpm. Finally, bacteria were plated on agar plates containing either ampicillin (100 mg/ml) or kanamycin (50 mg/ml) for resistance selection and incubated at 37°C overnight.

3.4.6 Mini & Midi preparation

In order to obtain plasmid DNA for cloning and sequencing, individual colonies were selected from agar plates and cultivated in 5 ml of LB medium containing either 100 mg/l of ampicillin or 50 mg/l of kanamycin. The bacterial cultures were incubated overnight with continuous shaking at 37°C. Subsequently, DNA extraction was performed using Qiagen's Mini DNA Preparation Buffers, following the instructions provided by the manufacturer. Concentration and purity of the isolated DNA were determined by NanoDrop.

To isolate plasmid DNA for transfection of eukaryotic cells, single colonies were picked from agar plates and grown in 150 ml LB medium supplemented with ampicillin (100 mg/l) or kanamycin (50 mg/l) as described for the Mini preparation. DNA was purified using the Wizard Plus Midiprep DNA Purification System (Promega) according to the manufacturer's instructions. Concentration and purity of the isolated DNA were determined by NanoDrop.

3.4.7 Sequencing

Plasmid DNA was sent for sequencing to Microsynth SeqLab GmbH (Göttingen). Sequencing reactions were prepared according to the service provider's instructions.

3.4.8 Generation and recovery of a recombinant SARS-CoV-2 *ORF3* mutant

Stop mutations within *ORF3c* were introduced into the bacmid pBSCoV2-ΔORF6-YFP harboring the SARS-CoV-2 backbone [103] using 2-step Red Recombination [104]. For this purpose, the KanS cassette was amplified from pEP-KanS with the primers listed in table 6. Integrity of the obtained bacterial artificial chromosomes (BAC) and presence of desired stop mutations were confirmed by restriction digestion and next generation sequencing. Recombinant SARS-CoV-2 viruses expressing eYFP instead of the viral ORF6 protein and containing mutations within *ORF3c* were recovered by transfection of HEK293T cells overexpressing the viral N protein, ACE2 receptor, and T7 RNA polymerase with BACs as described previously [103]. The obtained reporter viruses were further passaged on CaCo-2 cells and viral titers were determined by endpoint titration (see 3.2.2).

3.4.9 CPER cloning

To generate recombinant SARS-CoV-2 by circular polymerase extension reaction (CPER) [105] nine DNA fragments comprising parts of SARS-CoV-2 (WK-521, PANGO lineage A; GISAID ID: EPI ISL 408667) [106] were generated by PCR using PrimeSTAR GXL DNA polymerase (TAKARA, Cat# R050A). A linker fragment comprising hepatitis delta virus ribozyme, the bovine growth hormone poly-A signal and the cytomegalovirus promoter was also prepared by PCR. The ten obtained DNA fragments were mixed and used for CPER. *ORF3c* mutations were inserted in fragment 9/10 by site-directed overlap extension PCR with the primers listed in table 7. To produce recombinant SARS-CoV-2, Tetracycline-inducible ACE2 and TMPRSS-expressing IFNAR1-deficient HEK293 cells (table 1) were transfected with the CPER products using TransIT-LT1 (MirusBio) according to the manufacturer's protocol. One day post transfection, the culture medium was replaced with supplemented DMEM containing 2% FBS and doxycycline (1 µg/ml). 7 days post transfection, the culture medium was harvested, centrifuged and the supernatants were collected as the seed virus. To remove the CPER products (i.e., any SARS-CoV-2 DNA), 1 ml of the seed virus was treated with 2 µl TURBO DNase (Thermo Fisher

Scientific) and incubated at 37°C for 1 h. Complete removal of the CPER products (i.e., SARS-CoV-2-related DNA) from the seed virus was verified by PCR. To prepare virus stocks for infection, VeroE6/TMPRSS2 cells ($5x10^5$/ml in 10 ml in a T-75 flask) were infected with 20-50 µl of the seed virus. 1 h post infection, the culture medium was replaced with supplemented DMEM containing 2% FBS. Two to four days post infection, the culture medium was harvested and centrifuged, and the supernatants were collected. Viral titers were determined by TCID50. To verify the sequence of chimeric recombinant SARS-CoV-2, viral RNA was extracted from the virus stocks using the QIAamp viral RNA mini kit (Qiagen) and viral genomes were sequenced as described before [107].

3.5 Statistical analysis

Statistical analyses were performed using GraphPad PRISM 9.4.1. For statistical testing between two means, p values were calculated using paired or unpaired Student's t test. For comparison within one group, we used one-way analysis of variation (ANOVA) with Dunnett's multiple comparison test, and for comparison between two or more groups, we used two-way ANOVA with Sidak's multiple comparison test. Significant differences are indicated as: $* \ p \leq 0.05$; $** \ p \leq 0.01$; $*** \ p \leq 0.001$ and $**** \ p \leq 0.0001$.

4 Results

4.1 ORF3c is expressed in infected cells and suppresses interferon-β promoter activity

The genomic sequence covering SARS-CoV-2 *ORF3a* harbours additional start and stop codons across all reading-frames, thereby potentially encoding multiple peptides with unique functions. Previous studies predicted the expression of some of these cryptic ORFs by means of leaky scanning or ribosomal shunting [108], [50]. These *in silico* predictions are in agreement with ribosome profiling and HLA-II immunopeptidome studies suggesting the translation of ORF3c and ORF3d-2 in infected cells [42], [109]. To investigate the potential synthesis and activity of cryptic ORFs in ORF3a, I first tested whether they encode stable and detectable peptides. To achieve this, we cloned different cryptic *ORF3* sequences into expression plasmids. Since there is no commercially available antibody against any of the peptides, we modified the sequences to additionally express a C-terminal HA-tag. Of the designed constructs, ORF3a, ORF3c, ORF3d and ORF3d-2 were readily detectable at both concentrations tested. In contrast, ORF3b and ORF3e showed only low levels of expression, and ORF3b-2, b-3 and b-4 were not detectable at all (Fig. 7A).

Since many SARS-CoV-2 ORFs have already been identified to exert immunomodulatory functions, I tested if any of the cryptic ORF3 peptides are also capable of suppressing the immune response. Using a luciferase reporter system, I identified ORF3c as a strong suppressor of the human IFN-β promoter under stimulation with a constitutively active mutant of the RIG-I receptor (Fig. 7B). To confirm that suppression of the IFN-β promoter also results in a decrease of IFN-β expression during viral infection, I infected ORF3c transfected HEK293T cells with increasing amounts of Sendai virus, a known inducer of the interferon response [110]. Subsequent qPCR analysis revealed that *IFNB1* mRNA levels were increased dose-dependently in SeV exposed cells. Importantly, however, *IFNB1* transcription was significantly reduced in ORF3c expressing cells (Fig. 7C). Together these results hint to ORF3c as a potential novel interferon antagonist.

To investigate whether ORF3c is also expressed during natural infection, I used cir-

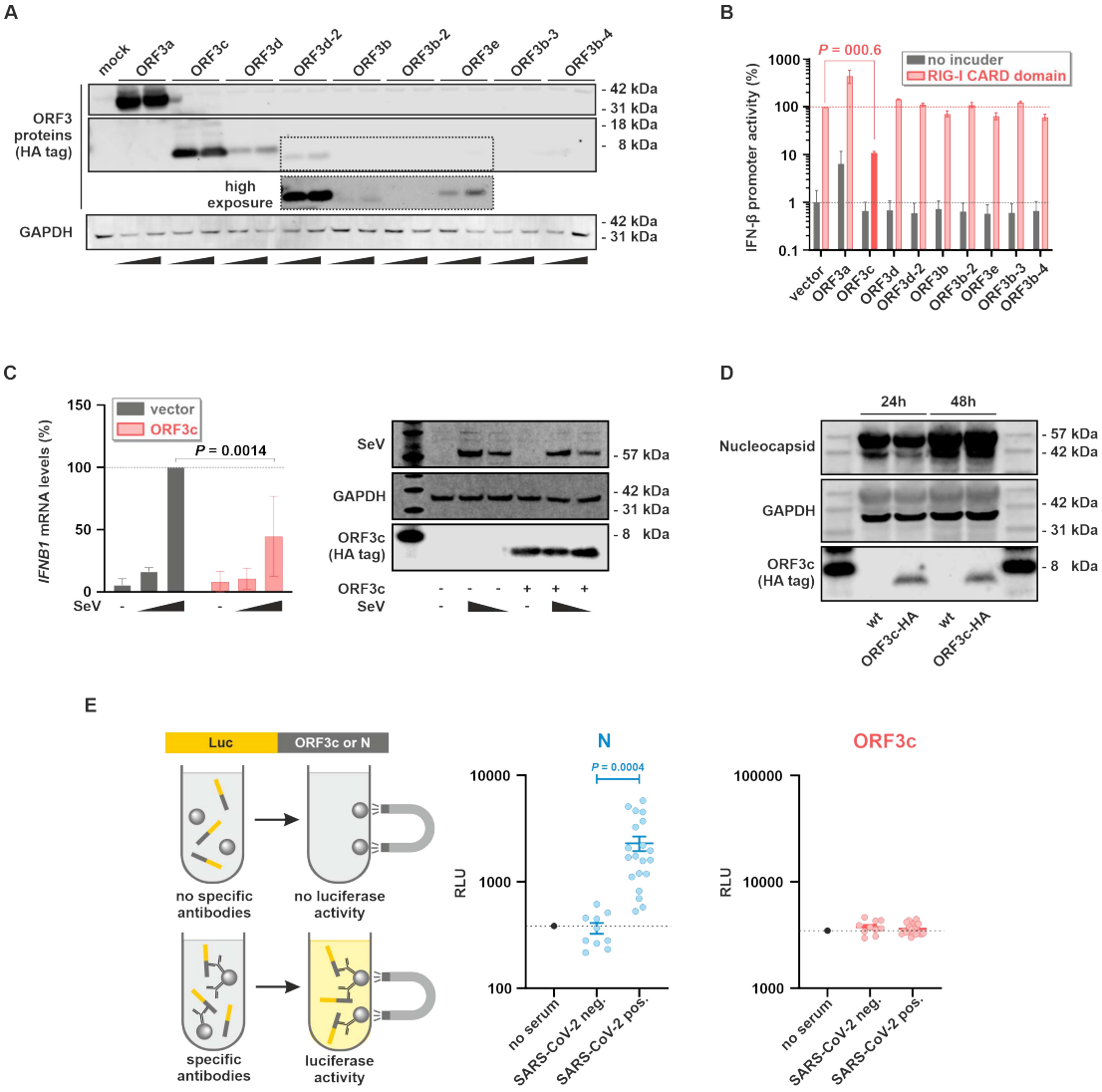

Figure 7: Expression of cryptic ORFs by SARS-CoV-2 and suppression of interferon promoter activity by ORF3c

(A) Western blot analysis of HEK293T cells transfected with two different concentrations of expression plasmids for the indicated ORF3 proteins and peptides. After 24 h, ORF3a to ORF3e were detected via C-terminal HA-tag. GAPDH served as loading control. Data are representative of two biological replicates (n = 2).
(B) HEK293T cells were co-transfected with the indicated ORF3 expression plasmids, a reporter plasmid expressing firefly luciferase under the control of the *IFNB1* promoter and a construct expressing *Gaussia* luciferase under the control of a minimal promoter. To induce immune signaling, half of the samples were additionally co-transfected with an expression plasmid for the CARD domain of RIG-I. One day post transfection, firefly luciferase activity was determined and normalized to *Gaussia* luciferase activity. Data are shown as mean and s.d. of three biological replicates (n = 3) and were analyzed by two-way ANOVA with Sidak's multiple comparison test.
(C) HEK293T cells were transfected with an expression plasmid for SARS-CoV-2 ORF3c or an empty vector control. 24 h post transfection, cells were infected with increasing amounts of Sendai virus (SeV) for an additional 8 h. Cells were lysed to perform either RNA extraction and subsequent qPCR for IFN-β (left panel) or Western blot analysis (right panel). Data are shown as mean and s.d. of three biological replicates (n = 3) and were analyzed by two-way ANOVA with Sidak's multiple comparison test.
(D) CaCo-2 cells were infected with SARS-CoV-2 wt or SARS-CoV-2 encoding HA-tagged ORF3c at an MOI of 2. 24 and 48 h post infection, cells were harvested for Western blot analysis. ORF3c expression was detected via the HA-tag. SARS-CoV-2 Nucleocapsid and GAPDH served as controls. Data are representative of two biological replicates (n = 2).
(E) HEK293T cells were transfected with expression plasmids for a viral protein of interest fused to *Renilla* luciferase. Subsequently, transfected cells were lysed and incubated with serum samples and magnetic beads. Antibodies against viral proteins of interest cross-linked the luciferase-containing proteins with beads and allowed magnet-assisted pull-down of both beads and luciferase activity (left). LIPS-mediated quantification of antibodies against SARS-CoV-2 N (left panel, n = 10) and ORF3c (right panel, n = 20) in sera from SARS-CoV-2 naïve (neg.) and convalescent (pos.) sera (RLU, relative light units) (right) is shown. Each dot represents one independent serum sample. Data are shown as mean ±SEM. Differences in antibody levels between SARS-CoV-2 naïve and convalescent sera were determined by unpaired, one-tailed student's t-test.

cular polymerase extension reaction to generate a SARS-CoV-2 variant expressing a C-terminally HA-tagged ORF3c. Although insertion of the respective nucleotides led to an artificial extension of the other reading frames as well, the rescued virus grew to high titers, similar to the wild-type virus. Western blot analysis of CaCo-2 cells infected with a wild-type or ORF3c-HA encoding virus revealed stable expression of the tagged ORF3c protein after one and two days of infection (Fig. 7D). These data demonstrate the expression of ORF3c in a natural infection setting.

A previous study was able to provide evidence of an antibody response against ORF3d-2, another cryptic peptide encoded in *ORF3a* [111]. To investigate if a similar humoral immune response is mounted against ORF3c, I tested sera of previously SARS-CoV-2 infected individuals for the presence of ORF3c-specific antibodies in an adapted luciferase immunoprecipitation system (LIPS) assay (see 3.3.5) (Fig. 7E, left). While I was able to detect robust antibody levels against SARS-CoV-2 N, I did not observe a specific response against ORF3c (Fig. 7E, right). Together, these results show that SARS-CoV-2 ORF3c is a stable peptide, capable of suppressing IFN-β induction, albeit not eliciting an antibody response. Furthermore, to the best of my knowledge, these experiments show for the first time that ORF3c is expressed during SARS-CoV-2 infection.

4.2 The interferon-suppressing effect of ORF3c is conserved across Sarbecoviruses

The persistence of a coding sequence, as well as sequence similarities across or within virus families can be an indicator for functional conservation of proteins. We performed *in silico* analyses to compare the sequences of ORF3c between different coronavirus families and genera. While ORF3c appears to be conserved within the subgenus of Sarbecoviruses, it is completely absent from phylogenetically distant coronavirus families (Fig. 8A). Interestingly, within Sarbecoviruses, we found only little changes in amino acids (aa) across viruses infecting different species. The most prominent mutation is the absence of the C-terminal 41st aa (Ser) in the SARS-CoV cluster and some viruses of the SARS-CoV-2 clade (Fig. 8B). These data indicate that ORF3c has evolved after the divergence of Sarbeco- and Hibecoviruses.

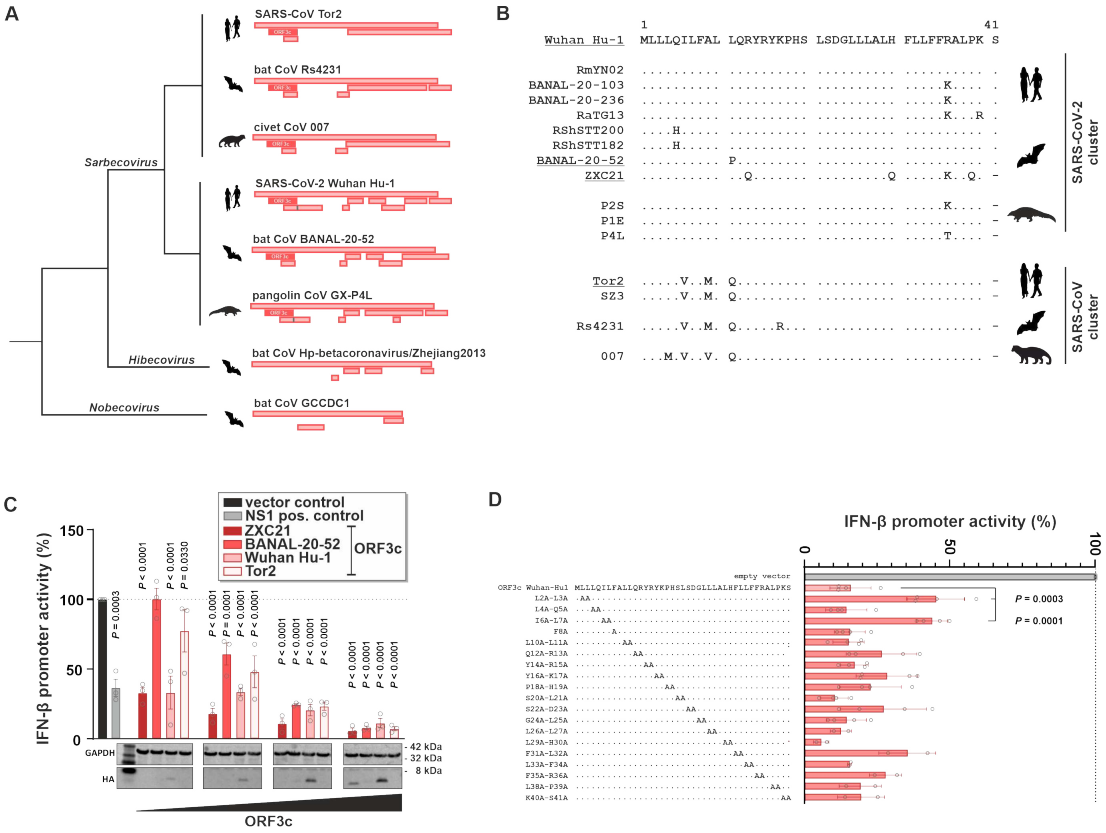

Figure 8: Sequence and activity conservation of ORF3c across Sarbecoviruses

(A) Cartoon illustrating the *ORF3* locus of randomly selected members of the Sarbeco-, Hibeco- and Nobecovirus subgenera. Open reading frames with a length of at least 30 nucleotides are indicated as rectangles. *ORF3c* is highlighted in dark red.

(B) Alignment of ORF3c amino acid sequences of the indicated viral isolates. Members of the SARS-CoV-2 cluster are shown on top, members of the SARS-CoV cluster at the bottom. For the underlined ORF3c sequences, expression plasmids were generated and analyzed for their ability to inhibit *IFNB1* promoter activation in (C).

(C) HEK293T cells were co-transfected with increasing amounts of the indicated ORF3c expression plasmids, a reporter plasmid expressing firefly luciferase under the control of the *IFNB1* promoter and a construct expressing *Gaussia* luciferase under the control of a minimal promoter. An expression plasmid for Influenza A virus non-structural protein 1 (NS1, gray) served as positive control. Immune signaling was induced by co-transfecting with an expression plasmid for the CARD domain of RIG-I. One day post transfection, firefly luciferase activity was determined and normalized to *Gaussia* luciferase activity (top panel). Data are shown as mean and s.d. of three biological replicates (n = 3), and were analyzed by two-way ANOVA with Sidak's multiple comparison test. ORF3c expression was monitored by Western blotting (bottom panel).

(D) HEK293T cells were co-transfected with expression plasmids and analyzed essentially as described in (C). The respective alanine mutations are indicated in the alignment on the left. Data are shown as mean and s.d. of two or four biological replicates (n = 2 or 4) and were analyzed by one-way ANOVA with Dunnett's multiple comparison test.

Next, we wanted to test if the function of ORF3c is also conserved within the Sarbecovirus subgenus. We therefore selected four different *ORF3c* orthologues covering the two main clusters (SARS-CoV & SARS-CoV-2), as well as different host species (i.e. humans and bats) and performed luciferase reporter assays, using increasing amounts of ORF3c expression plasmids. We observed a strong immunosuppressive effect already at low concentrations of Wuhan-Hu1 ORF3c and its orthologue in ZXC21. With increasing amounts however, all tested variants of ORF3c had an

equally strong suppressive effect on IFN-β promoter activity (Fig. 8C). Interestingly, Wuhan-Hu1 ORF3c protein was already detectable at low plasmid concentrations, while ZXC21 was only detectable at the highest concentration. Conversely, neither BANAL20-52 nor Tor2 ORF3c were detectable at any of the concentrations tested (Fig. 8C lower panel). This suggests that the activity of ORF3c orthologues is conserved within the Sarbecovirus subgenus, but does not necessarily correlate with their expression/detection levels. Given the high similarity in amino acid sequences between the different ORF3c orthologues, I investigated if a conserved amino acid motif is essential for its immunosuppressive activity. To achieve this, I performed an alanine scan, in which pairs of amino acids were exchanged for double alanines. The *IFNB1* reporter assay revealed that almost all variants tested retained their suppressive activity compared to wild-type ORF3c. Notably, however, the double mutants L2A/L3A and I6A/L7A showed significantly less suppressive capacity compared to the wild-type (Fig. 8D). The N-terminus of ORF3c therefore plays a central role in its ability to inhibit IFN-β induction.

4.3 ORF3c disrupts activation and nuclear translocation of IRF3

The transcription factor IRF3 is central to the induction of interferon-β in response to viral infection. One potential mechanism underlying the immunosuppressive activity of ORF3c could therefore lie in its ability to reduce overall IRF3 protein levels within the cell, leading to reduced IRF3-mediated gene expression. To test this, I transfected HEK293T cells with an ORF3c expression plasmid and measured endogenous IRF3 levels by flow cytometry. While the Non-structural protein 1 (NSP1) of Nebraska Calf Diarrhea Virus (NCDV), a known IRF3-degrading viral protein, was able to significantly reduce IRF3 levels, I did not observe any significant effect in the presence of any of the ORF3c concentrations tested (Fig. 9A), suggesting that ORF3c does not alter overall IRF3 protein levels. The phosphorylation of IRF3 is an essential prerequisite for its activation, irrespective of its expression levels. I therefore wanted to test the effect of ORF3c on IRF3 phosphorylation. Sendai virus stimulation of HEK293T cells transfected with an empty vector allowed immediate detection of phosphorylated IRF3 (Fig. 9B). In contrast, phosphorylation was significantly reduced in cells

transfected with ORF3c. Notably, this shift in activation was not the result of reduced total IRF3 levels, as previously also observed by flow cytometry (Fig. 9A).
Once activated, IRF3 forms homo-dimers and translocates into the nucleus to act as a transcription factor. We hypothesized that reduced IRF3 activation also leads to its reduced nuclear import in the presence of ORF3c. Using an HA-tagged ORF3c, I was able to detect its presence exclusively in the cytoplasm. Moreover, upon infection with SeV, I observed a reduced translocation of IRF3 into the nucleus in ORF3c transfected cells compared to cells transfected with empty vector control (Fig. 9C). Together, these results show that ORF3c suppresses interferon signaling within the cytoplasm and leads to reduced IRF3 phosphorylation.

4.4 ORF3c inhibits MDA5- and RIG-I mediated signaling

To identify potential cellular target(s) of ORF3c, I analysed different steps of the antiviral signaling cascade (Fig. 10A). The IFN-β promoter harbours binding sites not only for IRF3, but also NF-κB. We therefore took advantage of a reporter construct depleted of these sites to monitor the effect of ORF3c independently of NF-κB mediated activation. As expected, the induction of this modified construct was reduced compared to the wild-type promoter (Fig. 10B, right). Moreover, ORF3c was still able to suppress the activation in a dose-dependent manner (Fig. 10B, left). This indicates that ORF3c does not target NF-κB activation selectively but might be active at an earlier step within the RIG-I/MDA5 sensing pathway. I then activated the sensing cascade at different steps via over-expressing MDA5, MAVS or a constitutively active mutant of IRF3. While *IFNB1* promoter induction through MDA5 and RIG-I was suppressed to a similar extent by ORF3c, I did not observe any reduction in promoter activity after stimulation with MAVS or a constitutively active IRF3 (Fig. 10C). Together, these data suggest that SARS-CoV-2 ORF3c targets IFN signaling at the level of or upstream of MAVS.

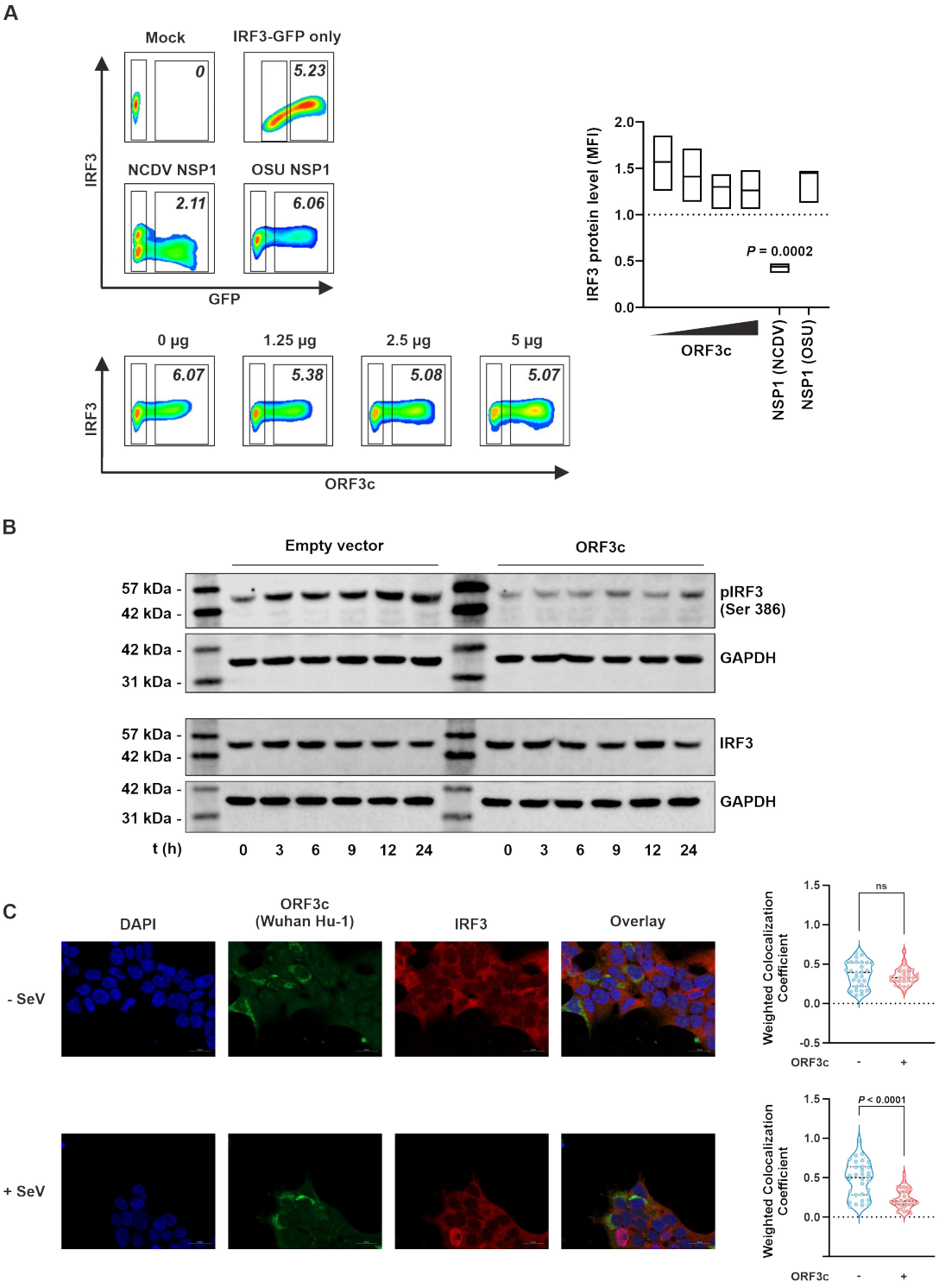

Figure 9: ORF3c suppresses phosphorylation and nuclear translocation of IRF3

(A) HEK293T cells were transfected with increasing amounts of expression plasmids for Wuhan Hu-1 ORF3c co-expressing eGFP via an IRES. Transfection with expression plasmids for NSP1 from the rotaviruses NCDV (reduces IRF3 expression) or OSU (inactive against IRF3) (both co-expressing YFP) served as controls. One day post transfection, cells were fixed, permeabilized and stained against IRF3 (AF555) before flow cytometric analysis. Numbers in gates indicate MFI of IRF3-AF555 (left). Levels of IRF3 expression are shown as MFI of AF555 in GFP positive over GFP negative cells. Data are shown as bars (min to max) with median of three biological replicates (n = 3) and were analyzed by one-way ANOVA with Dunnett's multiple comparison test.

Figure 9 continued:

(B) HEK293T cells were transfected with either Wuhan Hu-1 ORF3c or an empty vector control and stimulated with SeV 6 h.p.t. Cells were harvested at the indicated time points, and (phosphorylated) IRF3 was analyzed by western blotting. Data are representative of three biological replicates (n = 3).
(C) Representative images of HEK293T cells transfected with expression plasmids for Wuhan Hu-1 ORF3c or an empty vector control. One day post transfection, cells were treated with SeV for 6 h and subsequently stained for ORF3c (anti-HA, green), IRF3 (endogenous, red) and nuclei (DAPI, blue) (scale bar = 20 µm). Weighted colocalization coefficient of IRF3 with DAPI was determined as a marker for IRF3 translocation into the nucleus (n = 28-32 cells were analyzed per condition). Data are shown as individual cells with the median and quartiles indicated as dotted lines (right panels).

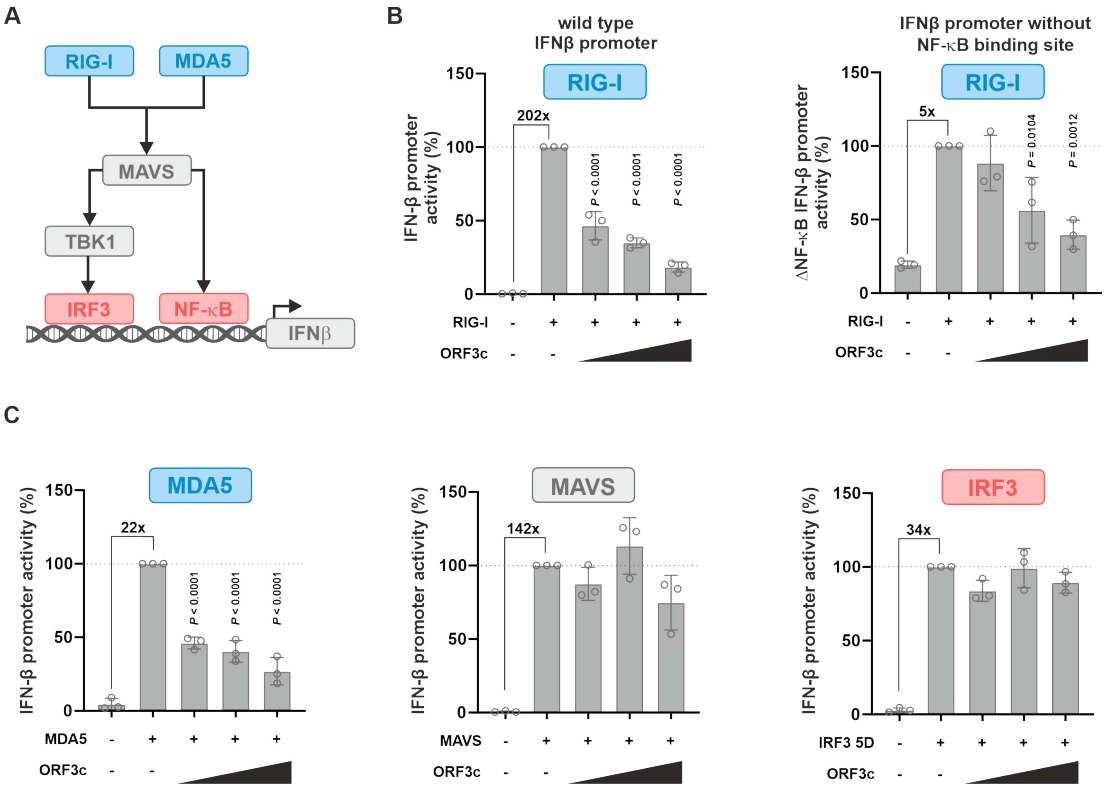

Figure 10: ORF3c inhibits innate sensing by targeting MAVS

(A) Cartoon illustrating IRF3- and NF-κB-mediated activation of the *IFNB1* promoter upon RIG-I- or MDA5-mediated sensing.
(B) HEK293T cells were co-transfected with increasing amounts of an expression plasmid for SARS-CoV-2 ORF3c, a construct expressing *Gaussia* luciferase under the control of a minimal promoter and a reporter plasmid expressing firefly luciferase under the control of the *IFNB1* promoter (left panel) or a mutant thereof lacking the NF-κB binding site (right panel). Immune signaling was induced by co-transfecting an expression plasmid for the CARD domain of RIG-I. One day post transfection, firefly luciferase activity was determined and normalized to *Gaussia* luciferase activity. Data are shown as mean and s.d. of three biological replicates (n = 3) and were analyzed by one-way ANOVA with Dunnett's multiple comparison test.
(C) HEK293T cells were transfected and analyzed essentially as described in (B). Immune signaling was induced by co-transfecting expression plasmids for MDA5 (left panel), MAVS (central panel) or a constitutively active mutant of IRF3 (right panel).

4.5 ORF3c interacts with MAVS and induces its C-terminal cleavage

While the interaction partners of MAVS, namely RIG-I, MDA5 and TBK1, can be found throughout the cytoplasm, MAVS is predominantly localized at the mitochondrial membrane [99] [112] [113]. During viral infection, mitochondria are a key compartment through which antiviral signaling is transmitted, and I hypothesized that ORF3c localizes to the mitochondria to interfere directly with antiviral signaling.

To test this, I performed confocal microscopy using a fluorescent protein targeted to the mitochondrial membrane (dsRedMito). Simultaneous labeling of overexpressed ORF3c via its HA-tag showed colocalization of both signals (Fig. 11A, upper row). Furthermore, infection with Sendai virus did not change the subcellular localization of ORF3c (Fig. 11A, lower row). These results suggest that ORF3c is located at the mitochondrial membrane during viral infection. We therefore tested if ORF3c directly interacts with MAVS and/or one of its signaling partners. Using Co-IP, we observed a weak interaction between MAVS and ORF3c. In contrast, we did not find any evidence for an interaction of ORF3c with RIG-I, MDA5 or TBK1 (Fig. 11B). This suggests that ORF3c interferes with antiviral signaling by directly binding to MAVS. Since activation of MAVS is triggered by interaction between the CARD domains of both MAVS and RIG-I or MDA5, we hypothesized that ORF3c binding sterically prevents this interaction. I therefore repeated the Co-IP experiment (Fig. 11B) with a mutant of MAVS lacking the N-terminal CARD domain. Contrary to our expectations, ORF3c also co-precipitated with this deletion mutant of MAVS, suggesting that the interaction takes place closer to the C-terminus of MAVS (Fig. 11C).

Next, I tested if the interaction between ORF3c and MAVS is conserved across the different orthologues of ORF3c characterized in Fig. 8C and D. In line with our previous results (Fig. 8C, lower panel), we detected only low levels of the different ORF3c orthologues in the input compared to ORF3c from Wuhan-Hu1. Additionally, we also tested the ORF3c alanine mutants L2A/L3A and I6A/L7A due to their reduced immunosuppressive activity (Fig. 8D). Notably, both alanine variants were detectable at levels equal to those of Wuhan-Hu1 ORF3c in the input. Following coimmunoprecipitation however, we only observed an interaction between MAVS and ORF3c

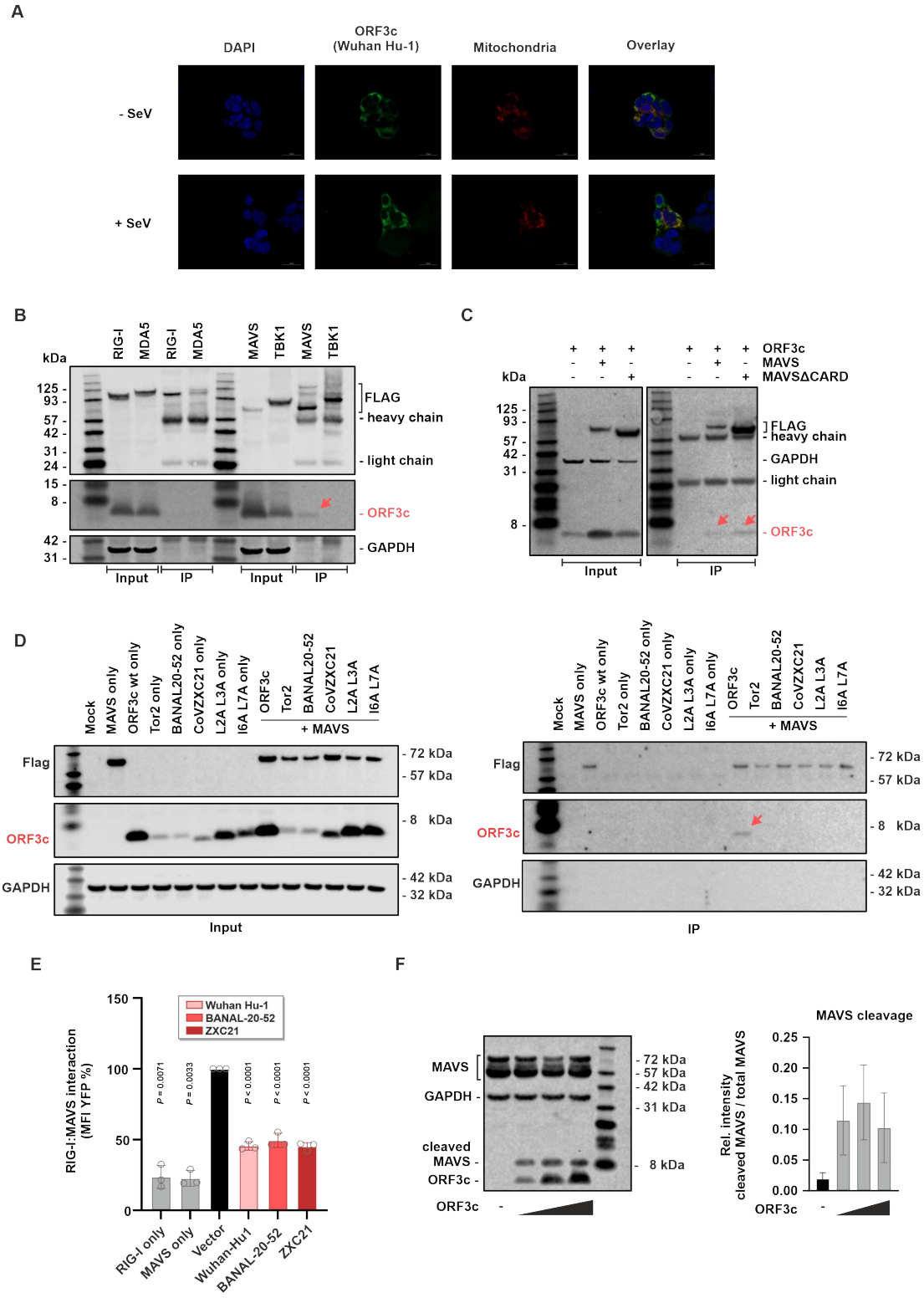

Figure 11: ORF3c binds to MAVS and suppresses RIG-I:MAVS interaction

(A) Representative images of HEK293T cells transfected with the expression plasmid dsRedMito coding for a mitochondrial marker, as well as expression plasmids for Wuhan Hu-1 ORF3c or an empty vector control. One day post transfection, cells were infected with SeV for 6 h and subsequently stained for ORF3c (anti-HA, green) and nuclei (DAPI, blue) (scale bar = 20 µm). Data are representative of two biological replicates (n = 2).

Figure 11 continued:
(B-C) HEK293T cells were co-transfected with expression plasmids for (B) Flag-tagged RIG-I, MDA5, MAVS, TBK1, (C) MAVS or a mutant thereof lacking its CARD domain (MAVSΔCARD) and an expression plasmid for HA-tagged SARS-CoV-2 ORF3c. One day post transfection, cells were lysed. Cell lysates were analyzed by Western blotting, either directly ("input") or upon pull-down using a Flag-specific antibody ("IP"). Data are representative of three biological replicates (n = 3).
(D) HEK293T cells were co-transfected with expression plasmids for Flag-tagged MAVS and expression plasmids for the indicated HA-tagged SARS-CoV-2 ORF3c variants. One day post transfection, cells were lysed and lysates were analyzed by Western blotting, either directly ("Input") or upon pull-down using a Flag-specific antibody ("IP"). Data are representative of two biological replicates (n = 2) and were analyzed byone-way ANOVA with Dunnett's multiple comparison test.
(E) HEK293T cells were transfected with plasmids expressing BFP, ORF3c, the C-terminal part of YFP fused to RIG-I and/or the N-terminal part of YFP fused to MAVS. After 24 h, cells were fixed, and YFP fluorescence was detected by flow cytometry as a reporter for MAVS:RIG-I interaction. Data are shown as mean and s.d. of three biological replicates (n = 3) and were analyzed by one-way ANOVA with Dunnett's multiple-comparison test.
(F) HEK293T cells were transfected with increasing amounts of an expression plasmid for SARS-CoV-2 ORF3c. One day post transfection, cells were lysed for Western blotting. ORF3c was detected via its HA-tag, and MAVS was detected with antiserum specific for the C-terminal part of MAVS. GAPDH served as loading control. Data are representative of three biological replicates (n = 3). MAVS bands were quantified, and the ratio of the 9 kDa fragment to total MAVS was calculated. Data are presented as mean (±SEM) of three independent experiments (n = 3) and were analyzed by one-way ANOVA with Dunnett's multiple comparison test.

from Wuhan-Hu1 (Fig. 11D). While we cannot exclude the interaction between MAVS and different ORF3c orthologues due to their low expression, the lack of interaction observed for the two alanine variants suggests that the N-terminus of ORF3c is important for direct binding to MAVS.

Even though ORF3c does not appear to directly interact with the CARD domain of MAVS, its association might still interfere with the interaction of MAVS with its upstream receptors RIG-I and MDA5. Given the similarities in sequence and IFN-suppressing activity, I tested whether the different orthologues of ORF3c are able to interfere with RIG-I : MAVS interaction. Using flow cytometry, I was able to detect ORF3c from Wuhan-Hu1, BANAL20-52 and ZXC21, but not Tor2. As this is in line with previous western blot results of Tor2 expression (Fig. 8C, lower panel, 10C), I went on to test ORF3c of Wuhan-Hu1, BANAL20-52 and ZXC21 in a BiFC-based interaction assay [99]. Here, a strong interaction signal was detectable when a modified RIG-I receptor carrying one half of the yellow fluorescent protein (YFP) was co-transfected with a modified MAVS protein tagged with the complementary half of YFP (Fig. 11E). More importantly, this signal was significantly diminished in the presence of ORF3c from Wuhan-Hu1, BANAL20-52 and ZXC21, further confirming its conserved immunosuppressive effect. I hypothesized that in addition to sterical interference overall MAVS stability might be compromised in the presence of ORF3c. Indeed, western blot analysis revealed the emergence of a 9 kDa fragment from the C-terminus of MAVS in ORF3c transfected cells (Fig. 11F). Together, these data show

that SARS-CoV-2 ORF3c directly interacts with MAVS and induces its C-terminal cleavage.

4.6 A naturally occurring R36I variant does not affect ORF3c activity

Throughout the COVID-19 pandemic, new SARS-CoV-2 variants emerged carrying defining mutations across their genome. Monitoring these novel variants, we identified a notable mutation (G25563T) within the *ORF3a* gene of the beta, eta, iota and mu strain, causing the non-synonymous mutation Q57H (Fig. 12A). More importantly, this polymorphism also introduces a non-synonymous mutation (R36I) in the predicted trans-membrane domain of ORF3c.

We hypothesized that this change might affect ORF3c structure and potentially function. Indeed, *in silico* analysies predicted that R36I might alter the 3D structure of ORF3c (Fig. 12B) and potentially stabilize its hypothetical trans-membrane domain (Fig. 11C). These data suggest differences in subcellular localization, as well as an altered function of ORF3c in infection with these variants. To test this, we performed confocal microscopy comparing wild-type ORF3c with a variant carrying the R36I mutation. Both peptides were readily detectable within the cytoplasm of transfected cells, and there was no obvious difference in subcellular between wild-type and R36I ORF3c (Fig. 12D). In line with these results, both variants were equally effective in suppressing IFN-β promoter induction (Fig. 12E). Together, this suggests that the R36I polymorphism does not alter the cellular localization of ORF3c or its ability to suppress the IFN response.

4.7 ORF3c is dispensable for SARS-CoV-2 replication

We had previously investigated the activity and mechanism of ORF3c in isolation using overexpression. Next, we wanted to investigate whether ORF3c suppresses the immune response during SARS-CoV-2 infection. Using circular polymerase extension reaction (CPER), we, together with our collaborators at the University of Tokyo, generated a SARS-CoV-2 variant harbouring a non-synonymous mutation in the start

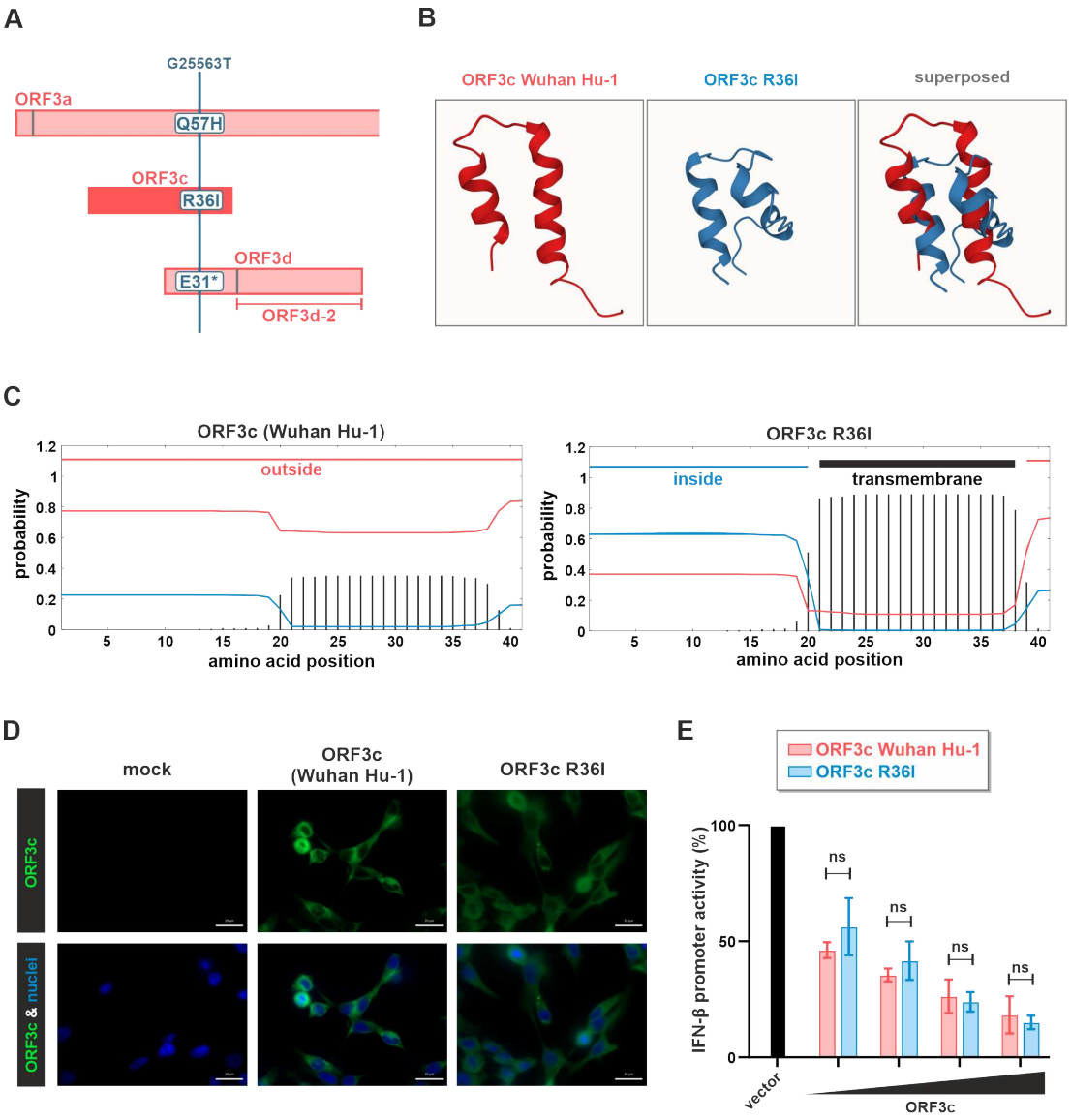

Figure 12: Characterization of a naturally occurring variant of SARS-CoV-2 ORF3c

(A) Cartoon illustrating non-synonymous changes in ORF3a, c and d as a result of the naturally occurring polymorphism G25563T.
(B) Secondary structure of Wuhan Hu-1 ORF3c (red) and the respective R36I variant thereof (blue) as predicted using PEP-FOLD3.
(C) The presence of transmembrane domains in Wuhan Hu-1 ORF3c (left panel) and the respective R36I variant thereof (right panel) was predicted using TMHMM - 2.0.
(D) Representative images of HEK293T cells transfected with expression plasmids for Wuhan Hu-1 ORF3c or ORF3c R36I. One day post transfection, cells were stained for ORF3c (anti-HA, green) and nuclei (DAPI, blue) (scale bar = 20 µm).
(E) HEK293T cells were co-transfected with increasing amounts of the indicated ORF3c expression plasmids, a reporter plasmid expressing firefly luciferase under the control of the *IFNB1* promoter and a construct expressing *Gaussia* luciferase under the control of a minimal promoter. Immune signaling was induced by co-transfecting an expression plasmid for the CARD domain of RIG-I. One day post transfection, firefly luciferase activity was determined and normalized to *Gaussia* luciferase activity. Data are shown as mean and s.d. of three biological replicates (n = 3) and were analyzed by two-way ANOVA with Sidak's multiple comparison test.

codon of ORF3c (M1T), while leaving the sequence of ORF3a unchanged (D22D) (Fig. 13A, left). After viral rescue and sequence validation, we infected CaCo-2 and CaLu-3 cells at an MOI of 0.1. Quantification of viral RNA by qPCR revealed similar replication kinetics of both viruses in either cell lines (Fig. 13A, right).

After viral rescue and sequence validation, we infected CaCo-2 and CaLu-3 cells at an MOI of 0.1. Quantification of viral RNA by qPCR revealed similar replication kinetics of both viruses in either cell lines (Fig. 13A, right). Since this mutation has not been observed in naturally circulating strains, we also generated a SARS-CoV-2 mutant carrying the above-mentioned naturally occurring stop mutant in ORF3c (Q5*) (Fig. 13B, left). As this mutation also causes a synonymous mutation in ORF3a (S26L), we additionally introduced an early stop codon in this frame (R6*) to exclude potential confounding effects by ORF3a. We observed an

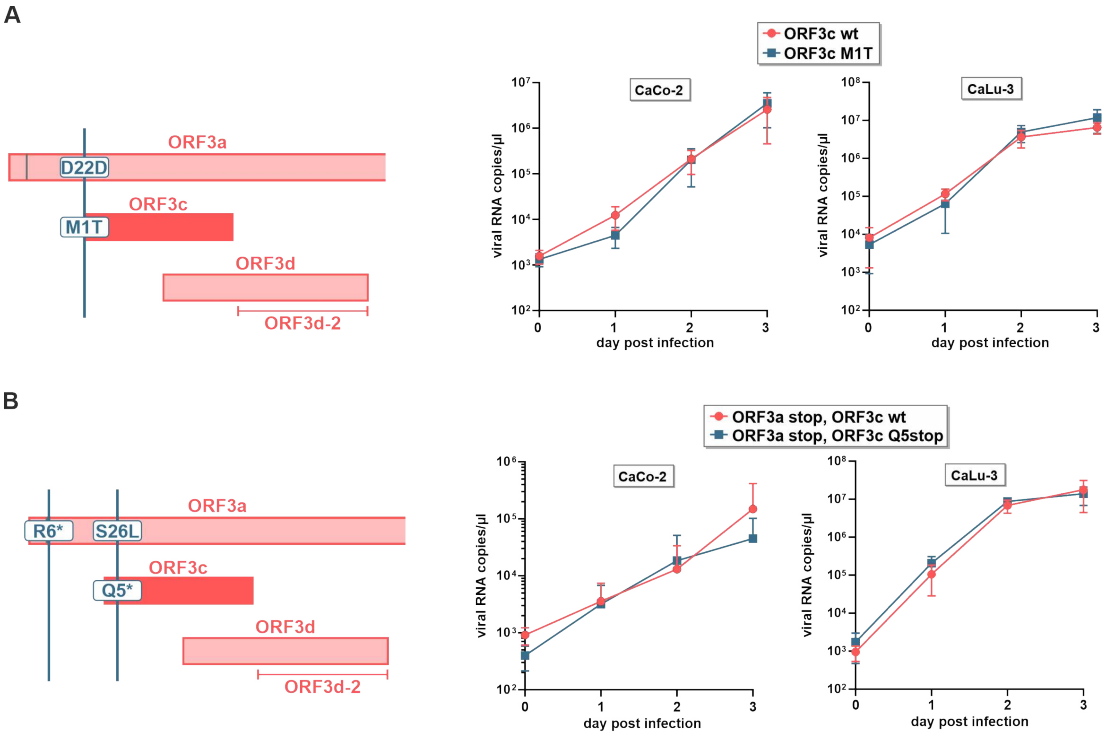

Figure 13: Disruption of ORF3c does not affect SARS-CoV-2 replication in CaCo-2 and CaLu-3 cells

(A) CPER was used to disrupt the start codon of ORF3c (M1T) in SARS-CoV-2 without affecting the amino acid sequence of ORF3a (left panel). CaCo-2 and CaLu-3 cells were infected with ORF3c wild-type (red) or ORF3c-mutated (blue) SARS-CoV-2 at an MOI of 0.1. Viral replication was monitored over 72 h by determining viral RNA copies in the culture supernatants (right panels). Data are shown as mean and s.d. of four (n = 4, CaCo-2) or eight (n = 8, CaLu-3) biological replicates.

(B) CPER was used to introduce a premature stop codon in ORF3c (Q5stop). To avoid any bias by simultaneously changing the protein sequence of ORF3a (S26L), a premature stop codon was also inserted in ORF3a (R6*) (left panel). Viral replication (right panels) was monitored in CaCo-2 and CaLu-3 cells as described in (A). Data are shown as mean and s.d. of eight (n = 8) biological replicates.

overall reduction in replicative fitness of both viruses compared to wt SARS-CoV-2 in CaCo-2, but not in CaLu-3 cells. Importantly, however, confirming our *in silico* analysis of the ORF3c Q5* mutant, we did not observe any replication disadvantage of a SARS-CoV-2 mutant carrying the ORF3c stop mutation over the wild-type in either cell line (Fig. 13B, right). Together, these replication kinetics demonstrate that ORF3c is dispensable for efficient viral replication *in vitro*.

ORF3c is not the only protein employed by SARS-CoV-2 to suppress the immune response [69], [114], [115]. While its activity might appear strong in isolation, other antagonists such as ORF6 or Nsp12 could mask its effect during infection. Using bacterial artificial chromosome (BAC) cloning, Dr. A. Herrmann (Universität Erlangen-Nürnberg) generated a SARS-CoV-2 variant encoding YFP in place of ORF6 (ΔORF6-YFP). This reporter virus allowed us to investigate the contribution of ORF3c to viral replication in the absence of another potent IFN antagonist. Furthermore, the expression of YFP enabled us to closely monitor virus spread by live cell imaging. A second variant was generated additionally carrying the previously mentioned M1T mutation to ablate ORF3c expression (Fig. 14A, left). Unexpectedly, there was no observable difference in replication between both variants, in either infected CaCo-2 or CaLu-3 cells (Fig. 14B, C). I hypothesized that other viral proteins compensate the effect of both ORF6 and ORF3c to suppress the immune response. To test this, I used the supernatants of infected CaLu-3 cells to perform a cytokine array. I did not observe differences in expression levels of IFN-β or any other of the 40 cytokines tested (Fig. 14C). Together, these results further support that ORF3c is not essential for viral replication *in vitro*.

Previous studies have suggested that some ORFs might be more relevant for virus replication in cells from the actual animal reservoir rather than in human cell culture [116]. Since bats of the genus *Rhinolophus* are considered the natural reservoir of SARS-related coronaviruses, I decided to test viral replication in a related cell culture model [117], [116], [118]. I therefore repeated the replication experiment in an immortalized cell line derived from *Rhinolophus alcyone* bats, using the YFP reporter virus (Fig. 15A). In agreement with my previous results, I did not observe any differences

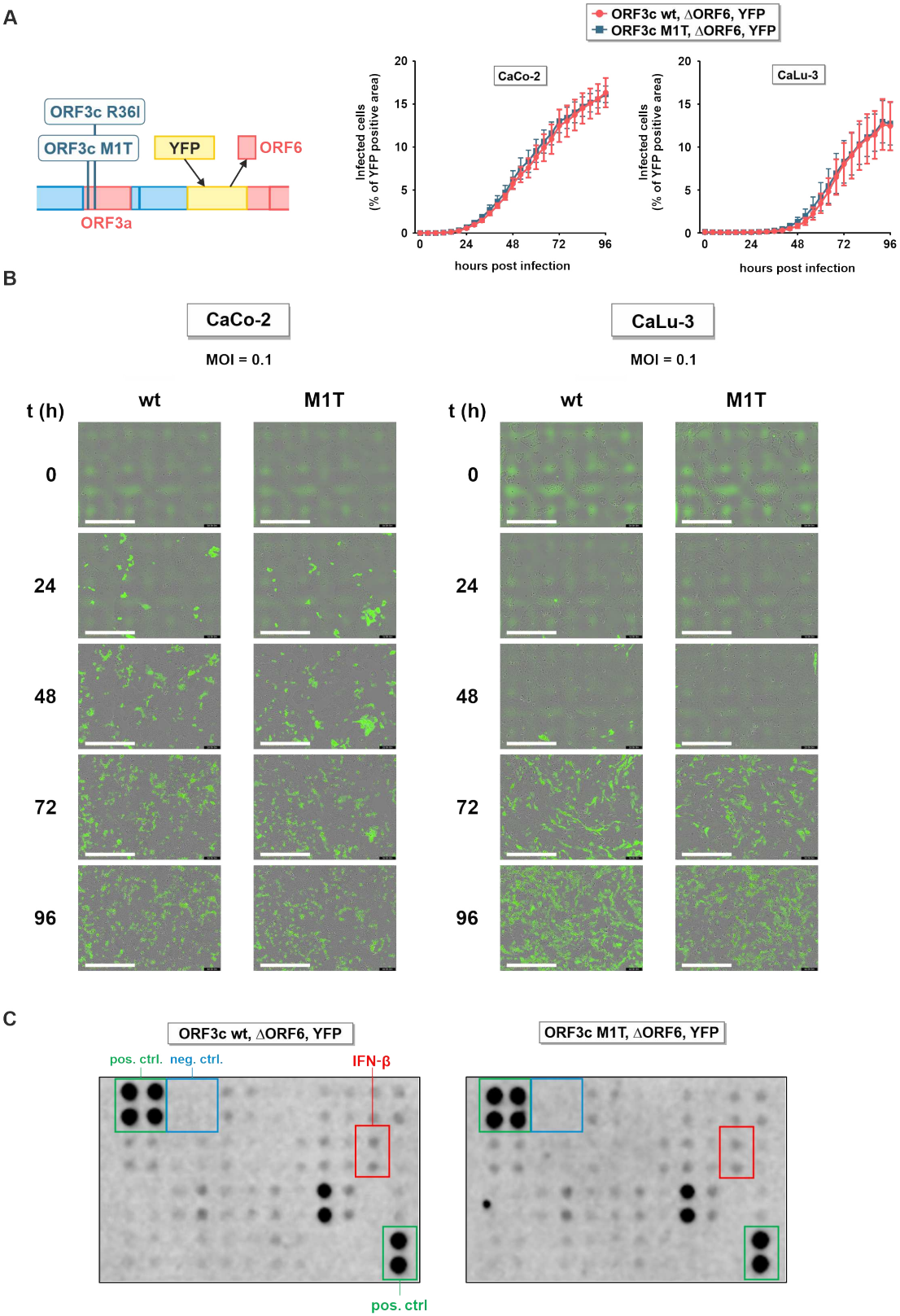

Figure 14: Depletion of ORF6 does not unmask an effect of ORF3c on SARS-CoV-2 replication or IFN-β secretion *in vitro*

(A) A SARS-CoV-2 BAC clone harbouring a disrupted *ORF3c* (M1T) and expressing YFP instead of ORF6 was generated (left panel). CaCo-2 and CaLu-3 cells were infected with SARS-CoV-2 ΔORF6-YFP (red) or SARS-CoV-2 ΔORF6-YFP ΔORF3c (blue) at an MOI of 0.1.

Figure 14 continued:
(B) Representative live cell images of replication kinetics as described in (A). Images show continuous virus spread (green) over the indicated time points from one randomly chosen well. Data are shown as mean and s.d. of three (n =3) biological replicates.
(C) 96 h post infection, supernatants of one of the CaLu-3 experiments shown in Fig. 14B were harvested and cytokine amounts were quantified using a membrane-based array. This approach enables a semi-quantitative analysis of cytokine release. The signal intensity of each dot indicates the amount of a specific cytokine in the culture supernatant (in duplicates). Positive and negative controls are highlighted in green and blue, respectively. IFN-β is highlighted in red. Data are representative of two biological replicates (n = 2).

in replication (Fig. 15B) or viral spread between the wild-type or ORF3c-deficient virus at both MOIs tested (Fig. 15C).

4.8 Some SARS-CoV-2 variants revert naturally occuring stop codons in *ORF3c*

In order to gain deeper insights into *ORF3c* in the context of viral transmission, our collaborators J. Ito & A. Strange (The University of Tokyo) conducted a comprehensive analysis of the GISAID SARS-CoV-2 sequence database [119].

We set an arbitrary threshold for PANGO (sub)lineages that contained a premature stop codon in the ORF3c gene in a minimum of 20% of the sampled isolates. Two mutations that meet these requirements were selected for further analysis. The first mutation (C25469T) results in an S26L mutation in ORF3a and leads to the emergence of a premature stop codon (Q5*) in ORF3c (Fig. 16A). This particular mutation is present in approximately 44% of B.1.617 isolates and is nearly ubiquitous in sequences belonging to the B.1.617.1 (delta) and B.1.617.2 (kappa) sublineages (Fig. 16B). The second mutation (del25498-25530) causes an in-frame deletion within ORF3a and is detected in approximately 80% of all B.1.630 isolates. This deletion leads to the removal of the initiation codon for ORF3d and introduces a premature stop codon (Y14*) in ORF3c (Fig. 16A, B).

The prevalence of premature stop codons in ORF3c within a significant portion of both B.1.617 and B.1.630 lineages suggests that ORF3c is not essential for effective viral replication *in vivo* or could potentially be compensated for by alterations elsewhere in the genome. Notably, however, the analysis of GISAID SARS-CoV-2 sequences also revealed that a subset (~3%) of B.1.617.2 viruses had acquired an

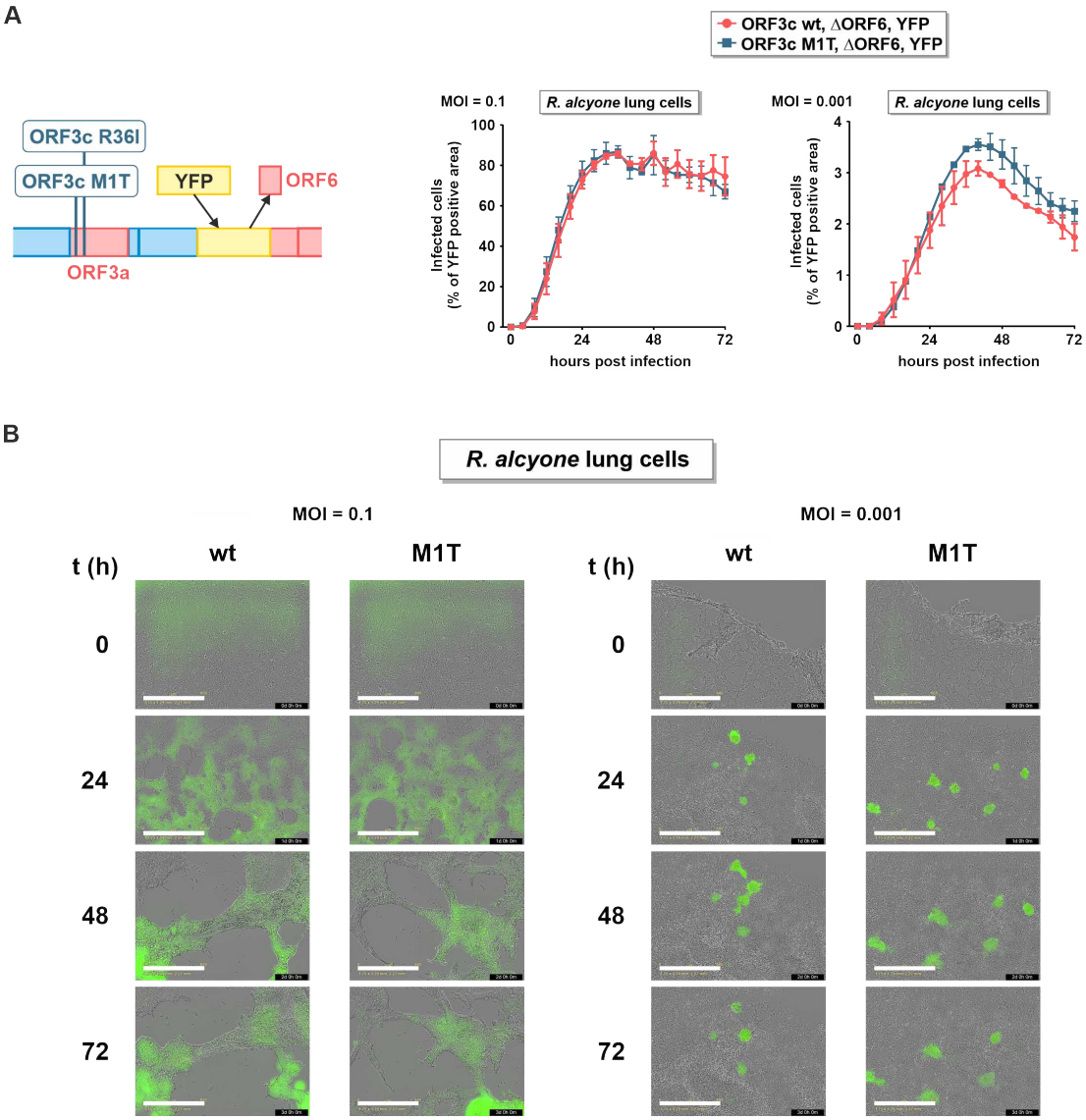

Figure 15: Disruption of ORF3c does not affect SARS-CoV-2 infection and/or replication in a bat cell line

(A) *Rhinolophus alcyone* lung cells stably expressing human ACE2 cells were infected with SARS-CoV-2 ΔORF6-YFP (red) or SARS-CoV-2 ΔORF6-YFP ΔORF3c (blue) at an MOI of 0.1 (left panel) or 0.001 (right panel). Cells were placed in a live cell imaging device and the area of YFP positive cells over the total area of cells was quantified every 4 h for 72 h. Data are shown as mean and s.d. of two (n = 2, MOI 0.001) to three (n = 3, MOI 0.1) biological replicates. **(B)** Representative live cell images of replication kinetics as described in (A). Images show continuous virus spread (green) over the indicated time points from one randomly chosen well. Data are shown as mean and s.d. of three (n =3) biological replicates.

additional point mutation that reverted the stop codon at position 5 to a tyrosine (*5Y), thereby reconstituting ORF3c at a later time point.

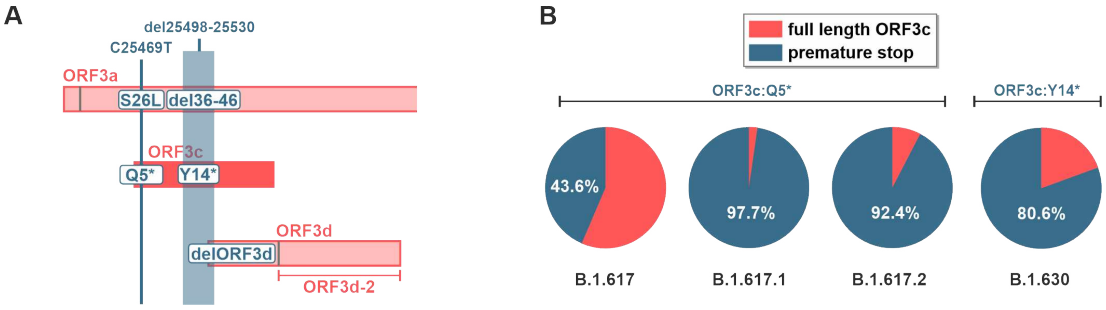

Figure 16: Naturally occurring stop codons in *ORF3c*
(A) Mutations introducing premature stop codons in ORF3c that can be found in at least 20% of the samples of at least one PANGO (sub)lineage.
(B) Frequency of the mutations shown in (A) in the PANGO (sub)lineages B.1.617.1 (delta), B.1.617.2 (kappa), B.1.617 and B.1.630.

In summary, ORF3c is an efficient suppressor of the interferon response and acts by binding to MAVS and promoting its degradation. While being conserved within the Sarbecovirus subgenus, ORF3c is not essential for SARS-CoV-2 replication *in vitro*.

5 Discussion

ORF3c is an accessory protein found in differnet Sarbecoviruses and encoded in the +1 reading frame of the ORF3a gene. It was first identified as a peptide in SARS-CoV, with which it shares a high degree of sequence homology. *In silico* analyses suggested that ORF3c is likely expressed by leaky scanning due to the strong initiation context of its ATG start codon compared to ATGs found upstream in *ORF3a* [55], [51]. Additionally, different predictive studies using ribosomal profiling [42], RNA sequencing [120] and comparative genomics [43] have concluded that ORF3c is likely expressed during SARS-CoV-2 infection. However, little was known about the function of ORF3c. While ORF3c has been proposed to act as a viroporin, its presence in infected cells and contribution to efficient viral replication have remained unclear [52].

A major challenge in the characterization of ORF3c is the lack of a commercially available antibody. During the course of this study, we and others were unable to generate an antibody against ORF3c [121]. This might be due to low immunogenicity of the peptide, also evident by the lack of detectable antibodies in our LIPS assay. However, a recent study investigating the HLA-II immunopeptidome of SARS-CoV-2 found evidence for the expression of at least one ORF3c-derived peptide (ALHFLLFFRALPKS) in infected humans, supporting its expression and immungenicity [109]. To confirm the expression of ORF3c during SARS-CoV-2 infection, I used CPER cloning to generate a SARS-CoV-2 variant harboring an HA-tagged ORF3c. Since the modification of ORF3c inadvertently changes the genomic sequence of ORF3a, I employed two different cloning strategies: First, I replaced the nucleotide sequence downstream of ORF3c with the HA-tag sequence. I was subsequently unable to rescue viable virus carrying this modification. It is tempting to speculate that replacement of ten amino acids in ORF3a is deleterious for SARS-CoV-2. However, the role of ORF3a in the viral replication cycle appears to be largely supportive in nature by promoting release or vesicle formation [122]. Furthermore, deletion of ORF3a still allows for infection and viral replication in both cell culture (Fig. 13B) and transgenic mice [123]. In a parallel approach, I therefore added the nucleotide sequence of the HA-tag down-

stream of ORF3c. This resulted in the addition of ten amino acids in ORF3a and yielded replication-competent SARS-CoV-2. Most importantly, subsequent infection of CaCo-2 cells allowed detection of ORF3c by western blot. To the best of my knowledge, this is the first time expression of the accessory protein ORF3c has been shown during SARS-CoV-2 infection.

After confirming the presence of ORF3c in SARS-CoV-2 infected cells, I investigated its role in the viral replication cycle. Many of the accessory proteins of SARS-CoV-2, including ORF6, ORF7b and ORF9b, have been shown to suppress antiviral signaling [89], [48], [49]. Interestingly, ORF3b, another peptide also encoded in *ORF3a*, had previously been identified as a potent IFN antagonist [47]. Therefore, I initially hypothesized that other cryptic ORFs encoded in *ORF3a* might show similar immune evasion activities. I subsequently tested an array of ORF3 proteins (ORF3c, ORF3d, ORF3d-2, ORF3b, ORF3b-2, ORF3e, ORF3b-3 & ORF3b-4) for their ability to suppress an *IFNB1* promoter luciferase construct and found that only ORF3c is able to interfere with its activation when stimulated with the CARD domain of RIG-I (Fig. 7B). The immunosuppressive effect of ORF3c was also observed when monitoring the levels of *IFNB1* mRNA in cells overexpressing ORF3c in the presence or absence of SeV, a known inducer of RIG-I signaling [124]. Interestingly, some of these ORFs were only weakly (ORF3b and ORF3e) or not at all detectable (ORF3b-2, ORF3b-3, ORF3b-4) by western blot (Fig. 7A). It is tempting to assume that these ORFs did not inhibit *IFNB1* promoter activation due to their low levels of expression. However, both ORF3d and ORF3d-2 also did not inhibit *IFNB1* promoter activation despite being readily detectable by western blot, indicating that only ORF3c is able to suppress the IFN response. As mentioned earlier, ORF3b had previously been identified as an IFN-antagonist [47]. Contrary to my findings, the authors observed strong suppression of an *IFNB1* promoter, as well as high detectable ORF3b protein levels. Although the experimental setup was similar, this discrepancy could be the result of codon-optimization and a different plasmid system used to express ORF3b. Nevertheless, the results of these assays need to be interpreted carefully as they rely on experimental overexpression of ORF3 peptides and therefore might not reflect the

physiological levels during viral infection. A complementary approach could be the generation of a stably transduced or inducible cell line to mimic the levels observed in infected cells.

The identification of ORF3c as a suppressor of the *IFNB1* promoter raised the question of the underlying molecular mechanism. I hypothesized that stimulation of the signaling pathway at different steps and in the presence of ORF3c can reveal its cellular target. Using overexpression of either RIG-I or MDA5 as a stimulus of the *IFNB1* promoter, I found efficient suppression by ORF3c in both conditions (Fig. 10D left, E left). Interestingly, recent studies have suggested that MDA5, rather than RIG-I, is the main driver of the IFN response during SARS-CoV-2 infection [125], [126]. However, since I observed efficient suppression using either stimulus, it is likely that the effect of ORF3c is independent of the PPR and that its target is found further downstream in the sensing cascade. In line with this, the antagonistic effect of ORF3c was absent when I overexpressed MAVS or a constitutively active mutant of IRF3 to activate the *IFNB1* promoter (Fig. 10C middle, right). This further indicated that the target of ORF3c is found upstream of, or at the level of MAVS. Indeed, when performing coimmunoprecipitation experiments, I found ORF3c to precipitate solely with MAVS, but not other components of the antiviral signaling pathway, specifically RIG-I, MDA5 and TBK1 (Fig. 11B).

Activation of MAVS by RIG-I and MDA5 is mediated through direct CARD : CARD interaction [56], [127]. I initially hypothesized that binding of ORF3c to the CARD domain of MAVS sterically obstructs its interaction with RIG-I. However, when performing coimmunoprecipitation assays of ORF3c with a MAVS mutant lacking its CARD domain, I was still able to precipitate ORF3c (Fig. 11C). While the CARD domain of MAVS is essential to induce IFN-β signaling, ORF3c might still interfere with its adaptor function by binding elsewhere on MAVS [113]. Therefore, further mutational analyses of MAVS should be performed to identify domains necessary for ORF3c : MAVS interaction.

Acting as a signal hub in antiviral signaling, MAVS is often targeted by proteins from different viruses. For example, avian Influenza A virus utilizes its PB1-F2 protein to prevent MAVS aggregation at the mitochondrial membrane [128]. Furthermore, human herpesvirus 6B, Zika virus and hepatitis C virus target MAVS for degradation by polyubiquitination [129], [130], [131]. At the time of writing this thesis, another study characterizing ORF3c had been published [121]. In line with my results, the authors identified MAVS as the target of ORF3c to disrupt IFN signaling by inducing MAVS degradation. Additionally, they suggest that this activity is mediated by the host cell protease PGAM5, which has been described to regulate the antiviral response [132], [133]. This three-way interaction can then lead to caspase activation and MAVS degradation by an unknown mechanism. Intriguingly, I observed the emergence of an approximately 9 kDa C-terminal fragment of MAVS in ORF3c overexpressing cells (Fig. 11F). This supports previous findings that ORF3c exerts its immunosuppressive function by inducing the proteolytic cleavage of MAVS. Additionally, this mode of action is not unique to ORF3c or coronaviruses in general. For example, encephalomyocarditis virus, Hepatovirus 3ABC, Coxsackievirus B3 and Rhinovirus C all express proteases directly cleaving MAVS [134], [135], [136]. The C-terminus of MAVS contains the transmembrane domain responsible for anchoring the protein in the outer mitochondrial membrane. Additionally, truncation of the C-terminal part of MAVS has been shown to result in its dissociation from mitochondria and becoming a soluble, cytosolic protein [113]. The same study also shows that ablation of the TM-domain alone is detrimental for MAVS ability to induce *IFNB1* promoter activation [113]. It is tempting to speculate that ORF3c-induced MAVS degradation leads to its dissociation from mitochondria. Importantly, confocal microscopy conducted in the study here does not exclude this possibility as I show colocalization of ORF3c with mitochondria overall and not MAVS directly. Future experiments could investigate the subcellular localization of MAVS in the presence of ORF3c by confocal microscopy to confirm its N-terminus dissociating from mitochondria.

In line with its central role in immune signaling, MAVS is also a known inducer of NF-κB signaling by activating IKKε [137]. Intriguingly, although NF-κB induces pro-inflammatory immune responses and antiviral gene expression, it remains active during SARS-CoV-2 replication [138], [139]. In line with this, ORF8 and Nsp12 have even been shown to support the induction of NF-κB signaling and drive a pro-inflammatory state [140], [141]. Although this outcome seems counterproductive for the virus, it has been suggested that at least some transcriptional targets of NF-κB are essential for virus replication [138]. When performing luciferase assays with an *IFNB1* promoter lacking all NF-κB binding sites, I observed reduced overall induction, confirming that NF-κB contributes to IFN-β induction (Fig. 10B, right pannel). Similarily, SeV can also induce TLR3 signaling, which in turn activates IRF3 and NF-κB via TRIF and TRAF6 respectively [142]. A previous study found no inhibition of TRIF-mediated IRF3 activation in the presence of SARS-CoV-2 ORF3c [121]. Since this pathway is independent of MAVS, it would be interesting to see whether or not NF-κB-mediated signaling is maintained through this route. It is tempting to speculate that ORF3c targets IRF3-mediated induction of IFN-β selectively to retain beneficial NF-κB signaling. To confirm this hypothesis, future studies could analyse the presence and abundance of NF-κB-driven transcripts in ORF3c-transfected cells.

The identification of ORF3c as a potential immune evasion factor raised the question whether or not its function is conserved in other coronaviruses or unique to SARS-CoV-2. We found a high degree of sequence homology of ORF3c orthologues within the Sarbecovirus subgenus which suggests conservation of functionality or evolutionary pressure exerted from overlapping ORFs. This is in line with a previous study where the authors compared whole genome sequences of 44 Sarbecovirus strains and found both a strong coding signature and functional conservation of ORF3c [43]. Indeed, orthologues of ORF3c from different Sarbecoviruses are all effective suppressors of the *IFNB1* promoter construct (Fig. 8C). Of note, ORF3c of SARS-CoV-2 Wuhan-Hu-1 and a closely related orthologue in bats (ZXC21) showed relatively high protein levels and IFN-antagonistic activity in transient transfection assays, even at low amounts of ORF3c, compared to orthologues from BANAL20-52

and Tor2. In contrast, protein levels of ORF3c orthologues from SARS-CoV Tor2 and SARS-CoV-2 bat-like BANAL20-52 were lower overall (Fig. 8C). Reduced activity and lower protein levels distinguishing less active BANAL20-52 ORF3c from Wuhan-Hu-1 ORF3c could be attributed to a single amino acid change (L11P) (Fig. 8B) [27]. While L11 is largely conserved in the SARS-CoV-2 cluster, most of the viruses in the SARS-CoV cluster harbor a glutamine at this position. Thus, a leucine at position 11 might contribute to the suppressive function of ORF3c. An alanine screen revealed that ORF3c function is highly resilient to changes at almost all positions. However, mutation of positions 2 and 3 (L2A/L3A) or 6 and 7 (I6A/L7A) resulted in decreased IFN-suppressive activity and loss of precipitation with MAVS (Fig. 8D, Fig. 11D), without affecting protein levles. Interestingly, these positions are highly conserved across different Sarbecovirus clusters and viral isolates from different host species. It is therefore possible that the ability to bind MAVS is a prerequisite for ORF3c to exert its function. To confirm this hypothesis, additional co-immunoprecipitation assays should be performed to see whether or not the remaining, IFN suppressive ORF3c mutants have retained their ability to co-precipitate with MAVS.

Intriguingly, ORF3c is not the only protein in SARS-CoV-2 that interferes with MAVS signaling. For example, a recent report found that in SARS-CoV-2-infected cells, ORF9b localizes to mitochondria and suppresses the antiviral IFN-I response by association with TOM70 [143], [84]. TOM70 is a known interaction partner of MAVS and can induce an IFN response by interacting with Hsp90, which results in the recruitment of TBK1 and IRF3. It has been suggested that ORF9b competes with Hsp90 for TOM70 binding on the outer mitochondrial membrane to dampen the IFN response [143]. Interestingly, this effect had already been described for ORF9b in SARS-CoV [144]. However, the authors also find interaction between ORF9b and a variant of TOM70 lacking a crucial domain for chaperon binding. Thus, the mechanism of ORF9b interference with regards to TOM70 binding remains unknown. A third approach to target MAVS-mediated signaling has been described for ORF10 [145]. This accessory protein is uniquely expressed by SARS-CoV-2 and induces MAVS degradation. Intriguingly, ORF10 also localizes to the mitochondrial membrane where it

induces mitophagy and prevents MAVS aggregation [145]. The similarities in subcellular localization between ORF9b, ORF10 and ORF3c suggests that Sarbecoviruses have evolved cooperative strategies between their accessory proteins to target mitochondria within the immune signaling pathway. This overlap might act as a fail-safe for efficient IFN suppression in the event of one of the ORFs becoming less or non-effective. At the same time, it underlines the pressure that is exerted by the IFN pathway on virus evolution.

Although the main route of infection of SARS-CoV-2 is via the respiratory tract, viral antigens have been found in gastric, rectal, and duodenal mucosa samples, suggesting the gastro-intestinal system as a potential route of transmission [146], [147]. The choice of an appropriate *in vitro* model is therefore essential to understand SARS-CoV-2 infection biology and growth kinetics. We initially decided to use two different cell lines in parallel for infection experiments. CaCo-2 cells are an established cell line and derived from a colorectal adenocarcinoma and show characteristics of small intestine enterocytes. Additionally, we used CaLu-3 cells, which are derived from a lung adenocarcinoma [148]. Notably, proteomic analysis identified 177 proteins in CaCo-2 and over 6000 in CaLu-3 cells which were differently expressed upon SARS-CoV-2 infection [149]. Interestingly, I did not observe any differences in viral replication between a wild-type or ORF3c deficient virus in either cell line (Fig. 13A). Since SARS-CoV-2 has only recently been introduced into the human population, I hypothesized that the function of ORF3c may be more relevant for replication in cells from the actual animal reservoir. Bats of the genus *Rhinolophus* are considered the *bona fide* animal reservoir for SARS-CoV-2-like viruses [27]. To reveal potential species-specific differences, we performed additional virus growth kinetic experiments in a lung cell line derived from *Rhinolophus* bats. In line with our observations in both human-derived cell lines, we did not observe any difference in SARS-CoV-2 replication in the presence or absence of ORF3c (Fig. 15). Culture models that more closely resemble the target tissue of SARS-CoV-2, such as nasal epithelial cells, primary human tracheal airway epithelial cells and human small airway epithelial cells should be considered to reveal even subtle effects of ORF3c. While these cells have a

limited lifetime and are more difficult to handle compared to immortalized cell lines, they retain their geno- and phenotypic characteristics and more closely resemble the site of natural infection and replication [150], [151]. Ultimately, an animal model can be considered the gold standard to investigate the pathogenicity and role of accessory proteins during SARS-CoV-2 infection. For example, both syrian gold hamsters, and humanised transgenic mice expressing hACE2, have already been used to investigate the role of the IFN-antagonists ORF6 and ORF7b [89], [123], [152]. While both models do not represent the natural host of SARS-CoV-2, they can potentially reveal ORF3c-dependent differences in viral pathogenicity which are not observable in tissue culture.

Deciphering the role of ORF3c is not only dependent on the host cell context, but also other viral proteins as well. ORF6 for example is a potent interferon antagonist and as such potentially able to mask the the immune regulatory activity of ORF3c during SARS-CoV-2 infection. However, using a SARS-CoV-2 mutant lacking both ORF3c and ORF6, we observed no difference in viral replication compared to a virus deficient only in ORF6 (Fig 8A). In line with this, we did not observe a difference in IFN-β mRNA levels produced by CaLu-3 cells infected with either virus. As a consequence of the overlapping activity of many different accessory genes, it is possible that yet another viral protein with anti-IFN activity (e.g. ORF7b) compensates for the activity of ORF6 and OR3c [153]. A simple approach could be the extension of the already performed replication kinetics with SARS-CoV-2 mutants deficient in other known IFN-antagonists such as ORF7b and ORF9b. Similarily, the cytokine profile of uninfected cells could be determined and compared to the ORF6 and ORF3c-deficient virus to see whether or not these viruses were still able to suppress IFN induction.

A parallel approach to the experimental investigation of ORF3c in cell culture or animal models is available through the unprecedented level of genome sequencing. Over the course of the pandemic many transmissible SARS-CoV-2 variants have emerged in humans, harboring truncations or deletions in their accessory genes. The persistence and spread of these variants can yield useful information about the accessory proteins affected. For example, a variant that emerged in early 2020 carried a 382-nucleotide deletion (Δ382) in its *ORF7* gene, resulting in its truncation and the deletion of the *ORF8* transcription start site. Patients infected with this variant showed weaker signs of inflammation and less severe disease outcome [154]. Similarly, truncations of ORF6 have been found in approximately 0.2% of all pandemic variants and result in significantly reduced anti-IFN activity [155], [156]. Interestingly, another cryptic peptide encoded within *ORF3a*, *ORF3b*, is heavily truncated in SARS-CoV-2 through the introduction of multiple stop codons. A report of two patients infected with a variant carrying a mutation that leads to the extension of the sequence by reversion of the first premature stop codon revealed an enhanced anti-IFN-I activity of ORF3b *in vitro* [47].

Similarly, mutations affecting the sequence of ORF3c have occurred throughout the pandemic. Most notable here was the emergence of the B.1.617.2 (Delta) VOC, which rapidly spread even in the absence of a functional ORF3c. Here, a mutation of position C25469T lead to the introduction of an early stop codon (Q5*) in *ORF3c* [157]. Moreover, we found that more than 80% of the sequenced genomes of B.1.617.1 (Kappa), Delta, and B.1.630 harbor premature stop codons at positions 5 (Q5*) and 14 (Y14*), respectively. Introduction of the Q5* mutation in ORF3c simultaneously results in an S26L change in ORF3a, and I hypothesized that either mutation covers a fitness advantage to the virus. However, deletion of ORF3c while maintaining or simultaneously deleting ORF3a did not affect virus replication *in vitro* (Fig. 13). Following Occam's razor, it was initially tempting to speculate that changes in ORF3c have been a side effect of other, more advantageous mutations elsewhere in the genome. However, over the course of the pandemic, it became evident that the Q5* mutation was only present in the Kappa, Delta and B.1.630 variants and has disappeared entirely since then. Moreover, even within Delta viruses, a subfraction

reverted their ORF3c stop codon at position 5 to a tyrosine (*5Y), thereby reverting to a full-length sequence. This reversion can be indicative of an overall beneficial contribution of ORF3c to viral fitness *in vivo*. A question we did not answer here is whether or not full length ORF3c, as found in SARS-CoV-2 Wuhan-Hu-1, would benefit viral replication of Delta. Since a reversion of the Q5* mutation is not possible without changing position 26L, an alternative approach could be the infection of a stably transduced, ORF3c expressing cell line with a SARS-CoV-2 variant harboring the M1T mutation. In line with this, *IFNB1* promtoer assays could be used to identify differences between ORF3c from Wuhan-Hu-1 and the *5Y revertant sporadically found in Delta.

Another interesting mutation found in SARS-CoV-2 (G25563T) showcases a rare event, in which a single nucleotide change causes non-synonymous amino acid changes in three overlapping ORFs. Besides ORF3a (Q57H) and ORF3c (R36I), this mutation also affects ORF3d (E14*), another potential IFN antagonist and potential immunogen [158], [111]. Interestingly, the Q57H mutation had previously been identified as a main characteristic of a wave of infections in Hong Kong in November 2020 [159]. While the authors acknowledge the effect of the mutation on ORF3d, their analysis did not incude possible effects on ORF3c. When we performed replication kinetics with a SARS-CoV-2 variant deficient in ORF3c and carrying the R36I mutation, we did not observe a difference compared to a virus expressing ORF3c. However, we did not exclude the effect of a truncated ORF3d in this assay. It would therefore be interesting to compare the replication efficiency of different viruses which express only one of the three sequences affected by G25563T.

When characterizing overlapping ORFs, close attention must also be paid to leaky scanning in the context of overexpression plasmids. In the case of ORF3a for example, previous studies might have inadvertently included ORF3c in their experimental setups as a byproduct of plasmid-based transfections. Similarly, earlier studies on ORF3a in SARS-CoV should be re-evaluated for the potential confounding effect of ORF3c in experiments where its expression might have been possible via leaky scanning.

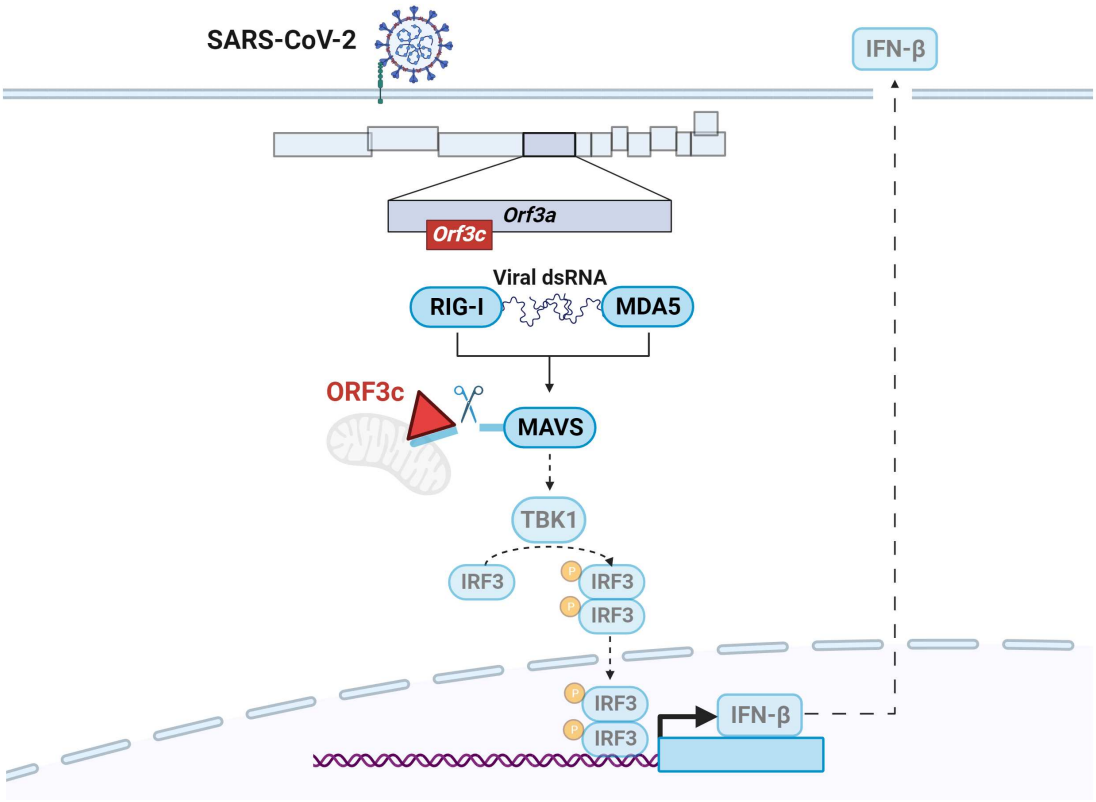

Figure 17: SARS-CoV-2 ORF3c is expressed during infection and acts as an immune evasion factor

SARS-CoV-2 ORF3c is a 41-amino-acid peptide encoded in an alternative reading frame of the viral *ORF3a* gene. Within the cell, ORF3c localizes to mitochondria, where it directly binds to the antiviral signaling protein MAVS. This interaction leads to MAVS degradation and reduced IFN-β induction. Although conserved among Sarbecoviruses, ORF3c is dispensable for virus replication *in vitro* and *in vivo*.

In summary, the results I present here show for the first time that ORF3c is expressed during SARS-CoV-2 infection. ORF3c is yet another member in a growing list of proteins encoded within an alternate reading frame and expressed by non-canonical translation. Acting as an immune evasion factor, I could demonstrate that it targets the antiviral signaling protein MAVS and induces its degradation, leading to a reduction in IFN-β expression. Furthermore, both the activity and sequence of ORF3c are highly conserved within the Sarbecovirus subgenus. While ORF3c appears to be dispensable for viral replication *in vitro*, its contribution to viral fitness and adaptation in the bat or human host remains the subject of future studies. Together, these results provide insight into a new immune evasion mechanism of SARS-CoV-2. Furthermore, they highlight the coding potential of alternative reading frames, emphasizing the need to consider this aspect in future analyses of the co-evolution of viral genes specifically with other viral genes and/or host restriction factors.

6 Summary

The respiratory virus SARS-CoV-2 is the causative agent for the COVID-19 pandemic. Transmitted by airborne droplets, once the virus reaches and infects its target cells in the respiratory tract, a battle for the cells' resources ensues. Failure to prevent or contain viral replication allows the virus to mutate and spread further. Nonetheless, throughout evolution, both virus and cell have developed mechanisms in response to each other to guarantee their individual persistence.

Coronaviruses use an intricate way to encode multiple proteins within a single RNA molecule. During translation initiation, ribosomes may not recognise the first start codon they encounter and do so at an additional start further downstream (leaky scanning). In the viral *ORF3a* gene, this mechanism can lead to the expression of ORF3c from an alternative reading frame. Both, ORF3a and ORF3c, are accessory viral proteins, which often function as antagonists of the viral defense mechanisms of the host. Specifically, cells can recognise the presence of non-self molecules, such as viral RNA, by means of pattern recognition receptors. Once activated, these receptors induce a signaling cascade which culminates in the induction of interferons and promote an antiviral state. Many proteins ins SARS-CoV-2 have been identified to interfere with the cellulars immune response, oftentimes helping to avoid recognition of viral components or by directly targeting and disrupting antiviral signaling. Although ORF3c had previously been described in SARS-CoV, its expression and function have remained unknown.

To characterize ORF3c, I generated a SARS-CoV-2 variant expressing a tagged ORF3c and was subsequently able to prove its expression during infection *in vitro*. Furthermore, ORF3c was the only accessory protein encoded in *ORF3a* capable of efficiently suppressing activity of the IFN-β promoter, hinting at its possible function. Further analysis showed that ORF3c directly interacts with the mitochondrial antiviral signaling protein (MAVS) and leads to its degradation. *In silico* analysis showed that the sequence of ORF3c is highly conserved across sarbecoviruses, which was reflected in the ability of different orthologs to also efficiently suppress IFN-β induction. Detailed analysis of naturally occurring mutations in ORF3c revealed that efficient viral

replication is maintained in the absence of ORF3c. These observation could be confirmed in two human and a bat-derived cell line.

Together, I here identified ORF3c as an IFN antagonist of SARS-CoV-2 and other sarbecoviruses. While ORF3c appears to be dispensable for efficient replication *in vitro* and *in vivo*, its high degree of conservation might be indicative of an important role in SARS-CoV-2 natural host as well as during co-evolution with other viral genes.

Zusammenfassung

SARS-CoV-2 ist der Erreger der COVID-19-Pandemie und wird durch Tröpfchen in der Luft übertragen. Sobald es seine Zielzellen in den Atemwegen erreicht und infiziert hat, beginnt ein Kampf um die Ressourcen der Zelle. Gelingt es der Zelle nicht, die Virusvermehrung zu verhindern oder einzudämmen, kann das Virus mutieren und sich weiter ausbreiten. Im Laufe der Evolution haben sowohl das Virus als auch die Zelle Mechanismen entwickelt um ihr Fortbestehen zu gewährleisten.
Coronaviren kodieren auf komplexe Weise mehrere Proteine in einem einzigen RNA-Molekül. Während der Initiierung der Translation erkennen Ribosomen teilweise nicht das erste Startcodon und beginnen die Proteinsynthese erst bei einem folgenden (*Leaky Scanning*). Im Falle des viralen Gens *ORF3a* kann dieser Mechanismus zur Expression von ORF3c in einem alternativen Leserahmen führen. Sowohl ORF3a als auch ORF3c sind akzessorische, virale Proteine, die häufig virale Abwehrmechanismen der Zelle antagonisieren. Insbesondere können Zellen das Vorhandensein fremder Moleküle, wie z. B. viraler RNA, mit Hilfe von speziellen Rezeptoren erkennen. Sobald diese Rezeptoren aktiviert sind, lösen sie eine Signalkaskade aus, die zur Induktion von Interferonen führt und einen antiviralen Zustand induzieren. Viele Proteine in SARS-CoV-2 sind in der Lage die Erkennung viraler Komponenten zu verhindern oder direkt die antivirale Signalübertragung zu stören. Obwohl ORF3c bereits bei SARS-CoV beschrieben wurde, waren seine Expression und Funktion bisher unbekannt.
Um ORF3c zu charakterisieren habe ich eine SARS-CoV-2-Variante generiert, die ein markiertes ORF3c exprimiert, und konnte anschließend dessen Expression während der Infektion *in vitro* nachweisen. Darüber hinaus war ORF3c das einzige akzessorische Protein kodiert in *ORF3a* welches in der Lage war die Aktivität des IFN-β-Promotors effizient zu unterdrücken. Weitere Analysen zeigten, dass ORF3c direkt mit dem mitochondrialen antiviralen Signalprotein MAVS interagiert und dessen Abbau induziert. *In-silico*-Analysen zeigten, dass die Sequenz von ORF3c bei allen Sarbecoviren hoch konserviert ist. Dies spiegelte sich in der Fähigkeit verschiedener ORF3c-Orthologe wieder, die IFN-β-Induktion effizient zu unterdrücken. Eine de-

taillierte Analyse natürlich vorkommender Mutationen in ORF3c ergab, dass eine effiziente virale Replikation in Abwesenheit von ORF3c aufrechterhalten wird. Diese Beobachtung konnte in zwei menschlichen und einer von Fledermäusen stammenden Zelllinie bestätigt werden.

Zusammenfassend konnte ich ORF3c als IFN-Antagonist von SARS-CoV-2 und anderen Sarbecoviren identifizieren. Obwohl ORF3c für eine effiziente Replikation *in vitro* und *in vivo* entbehrlich zu sein scheint, könnte sein hoher Erhaltungsgrad auf eine wichtige Rolle in SARS-CoV-2 im natürlichen Wirt, sowie während der Koevolution mit anderen viralen Genen hinweisen.

Acknowledgments

First and foremost, I would like to thank Prof. Dr. Daniel Sauter for giving me the chance to pursue my doctorate in his group. When I started my PhD in Ulm, I had no idea of the extent to which I would enjoy the work, the science and our discussions. I still am baffled by the zen-like patience with which you keep answering every question I have and the depth of your knowledge. Under your supervision I not only became a better scientist but also grew as a person. Thank you for being an inspiring guide and for believing in me.

I would also like to express my gratitude to my second supervisor, Prof. Dr. Thorsten Stafforst, for taking the time to provide me with valuable feedback and advice. Special thanks to Prof. Dr. Michael Schindler and Dr. Rosa Lozano-Durán for being part of my thesis committee and for the insightful discussions we had throughout the years, both within our institute and during conferences. A heartfelt thank you extends to all our collaborators for their experimental contributions, provision of reagents, and valuable feedback.

Ein großer Dank gilt meinen Eltern. Egal, welche Idee ich mir in den Kopf gesetzt habe – sei es, doch noch zu studieren, mal immer weiter weg und dann quer durchs Land zu ziehen –, ihr habt mich immer ohne zu zögern unterstützt. Danke für euer Vertrauen, ihr habt mir alle Türen geöffnet. Danke auch an Erik und Tosca. Unsere Treffen zu dritt bedeuten mir viel, und ich bin froh, euch immer hinter mir zu wissen. Danke Martin R., ohne deine Freundschaft wäre ich nicht wo ich heute bin.

A special thanks goes to all my colleagues in the lab. This tight-knit community is what made the whole PhD journey complete, and dare I say, fun. You supported me when my experiments failed and let me join the celebration of your successful ones. You made the bad days feel short and the good ones long. I will miss our BBQs in the summer and half marathons in winter. Lastly, a big thank you to my friends outside of Tübingen—be you in Canada, The Netherlands, France, or Switzerland. Thank you all for putting up with me, your friendship, and your support.

Statutory Declaration

I hereby declare that I wrote the present dissertation with the title

ORF3c is expressed in SARS-CoV-2-infected cells and inhibits innate sensing by targeting MAVS

independently and used no other aids than those cited. In each individual case, I have clearly identified the source of the passages that are taken word for word or paraphrased from other works.

I also hereby declare that I have carried out my scientific work according to the principles of good scientific practice in accordance with the current codex „Leitlinien zur Sicherung guter wissenschaftlicher Praxis“ “ [Rules of the University of Tübingen for Assuring Good Scientific Practice].

Tübingen, _____

_____

Martin Müller

References

[1] D. Hamre and J. J. Procknow, "A new virus isolated from the human respiratory tract," *Proc Soc Exp Biol Med*, vol. 121, no. 1, pp. 190–193, Jan 1966.

[2] D. A. Tyrrell and M. Fielder, *Cold Wars: The Fight against the Common Cold*. Oxford: Oxford University Press, 2002.

[3] J. D. Almeida and D. A. Tyrrell, "The morphology of three previously uncharacterized human respiratory viruses that grow in organ culture," *J Gen Virol*, vol. 1, no. 2, pp. 175–178, Apr 1967.

[4] D. A. TYRRELL and M. L. BYNOE, "CULTIVATION OF A NOVEL TYPE OF COMMON-COLD VIRUS IN ORGAN CULTURES," *Br Med J*, vol. 1, no. 5448, pp. 1467–1470, Jun 1965.

[5] J. D. Almeida, D. . M. Berry, C. H. Cunningham, D. Hamre, M. S. Hofstad, L. Mallucci, K. McIntosh, and D. A. Tyrrell, "CCoronaviruses," *Nature*, vol. 220, no. 5168, p. 650, Nov 1968.

[6] P. C. Y. Woo, R. J. de Groot, B. Haagmans, S. K. P. Lau, B. W. Neuman, S. Perlman, I. Sola, L. van der Hoek, A. C. P. Wong, and S. H. Yeh, "2023," *J Gen Virol*, vol. 104, no. 4, Apr 2023.

[7] P. C. Woo, S. K. Lau, C. S. Lam, C. C. Lau, A. K. Tsang, J. H. Lau, R. Bai, J. L. Teng, C. C. Tsang, M. Wang, B. J. Zheng, K. H. Chan, and K. Y. Yuen, "Discovery of seven novel Mammalian and avian coronaviruses in the genus deltacoronavirus supports bat coronaviruses as the gene source of alphacoronavirus and betacoronavirus and avian coronaviruses as the gene source of gammacoronavirus and deltacoronavirus," *J Virol*, vol. 86, no. 7, pp. 3995–4008, Apr 2012.

[8] S. L. Zhai, M. F. Sun, J. F. Zhang, C. Zheng, and M. Liao, "Spillover infection of common animal coronaviruses to humans," *Lancet Microbe*, vol. 3, no. 11, p. e808, Nov 2022.

[9] V. M. Corman, D. Muth, D. Niemeyer, and C. Drosten, "Hosts and Sources of Endemic Human Coronaviruses," *Adv Virus Res*, vol. 100, pp. 163–188, 2018.

[10] V. M. Corman, H. J. Baldwin, A. F. Tateno, R. M. Zerbinati, A. Annan, M. Owusu, E. E. Nkrumah, G. D. Maganga, S. Oppong, Y. Adu-Sarkodie, P. Vallo, L. V. da Silva Filho, E. M. Leroy, V. Thiel, L. van der Hoek, L. L. Poon, M. Tschapka, C. Drosten, and J. F. Drexler, "Evidence for an Ancestral Association of Human Coronavirus 229E with Bats," *J Virol*, vol. 89, no. 23, pp. 11 858–11 870, Dec 2015.

[11] F. Kong, Q. Wang, S. P. Kenney, K. Jung, A. N. Vlasova, and L. J. Saif, "Porcine Deltacoronaviruses: Origin, Evolution, Cross-Species Transmission and Zoonotic Potential," *Pathogens*, vol. 11, no. 1, Jan 2022.

[12] V. Marchenko, A. Danilenko, N. Kolosova, M. Bragina, M. Molchanova, Y. Bulanovich, V. Gorodov, S. Leonov, A. Gudymo, G. Onkhonova, S. Svyatchenko, and A. Ryzhikov, "Diversity of gammacoronaviruses and deltacoronaviruses in wild birds and poultry in Russia," *Sci Rep*, vol. 12, no. 1, p. 19412, Nov 2022.

[13] Y. Guan, B. J. Zheng, Y. Q. He, X. L. Liu, Z. X. Zhuang, C. L. Cheung, S. W. Luo, P. H. Li, L. J. Zhang, Y. J. Guan, K. M. Butt, K. L. Wong, K. W. Chan, W. Lim, K. F. Shortridge, K. Y. Yuen, J. S. Peiris, and L. L. Poon, "Isolation and characterization of viruses related to the SARS coronavirus from animals in southern China," *Science*, vol. 302, no. 5643, pp. 276–278, Oct 2003.

[14] L. F. Wang and B. T. Eaton, "Bats, civets and the emergence of SARS," *Curr Top Microbiol Immunol*, vol. 315, pp. 325–344, 2007.

[15] N. Wang, S. Y. Li, X. L. Yang, H. M. Huang, Y. J. Zhang, H. Guo, C. M. Luo, M. Miller, G. Zhu, A. A. Chmura, E. Hagan, J. H. Zhou, Y. Z. Zhang, L. F. Wang, P. Daszak, and Z. L. Shi, "Serological Evidence of Bat SARS-Related Coronavirus Infection in Humans, China," *Virol Sin*, vol. 33, no. 1, pp. 104–107, Feb 2018.

[16] H. D. Song, C. C. Tu, G. W. Zhang, S. Y. Wang, K. Zheng, L. C. Lei, Q. X. Chen, Y. W. Gao, H. Q. Zhou, H. Xiang, H. J. Zheng, S. W. Chern, F. Cheng, C. M. Pan, H. Xuan, S. J. Chen, H. M. Luo, D. H. Zhou, Y. F. Liu, J. F. He, P. Z. Qin, L. H. Li, Y. Q. Ren, W. J. Liang, Y. D. Yu, L. Anderson, M. Wang, R. H. Xu, X. W. Wu, H. Y. Zheng, J. D. Chen, G. Liang, Y. Gao, M. Liao, L. Fang, L. Y. Jiang, H. Li, F. Chen, B. Di, L. J. He, J. Y. Lin, S. Tong, X. Kong, L. Du, P. Hao, H. Tang, A. Bernini, X. J. Yu, O. Spiga, Z. M. Guo, H. Y. Pan, W. Z. He, J. C. Manuguerra, A. Fontanet, A. Danchin, N. Niccolai, Y. X. Li, C. I. Wu, and G. P. Zhao, "Cross-host evolution of severe acute respiratory syndrome coronavirus in palm civet and human," *Proc Natl Acad Sci U S A*, vol. 102, no. 7, pp. 2430–2435, Feb 2005.

[17] J. S. Peiris, Y. Guan, and K. Y. Yuen, "Severe acute respiratory syndrome," *Nat Med*, vol. 10, no. 12 Suppl, pp. 88–97, Dec 2004.

[18] B. L. Haagmans, S. H. Al Dhahiry, C. B. Reusken, V. S. Raj, M. Galiano, R. Myers, G. J. Godeke, M. Jonges, E. Farag, A. Diab, H. Ghobashy, F. Alhajri, M. Al-Thani, S. A. Al-Marri, H. E. Al Romaihi, A. Al Khal, A. Bermingham, A. D. Osterhaus, M. M. AlHajri, and M. P. Koopmans, "Middle East respiratory syndrome coronavirus in dromedary camels: an outbreak investigation," *Lancet Infect Dis*, vol. 14, no. 2, pp. 140–145, Feb 2014.

[19] H. Gao, H. Yao, S. Yang, and L. Li, "From SARS to MERS: evidence and speculation," *Front Med*, vol. 10, no. 4, pp. 377–382, Dec 2016.

[20] A. Pormohammad, S. Ghorbani, A. Khatami, R. Farzi, B. Baradaran, D. L. Turner, R. J. Turner, N. C. Bahr, and J. P. Idrovo, "Comparison of confirmed COVID-19 with SARS and MERS cases - Clinical characteristics, laboratory findings, radiographic signs and outcomes: A systematic review and meta-analysis," *Rev Med Virol*, vol. 30, no. 4, p. e2112, Jul 2020.

[21] P. Zhou, X. L. Yang, X. G. Wang, B. Hu, L. Zhang, W. Zhang, H. R. Si, Y. Zhu, B. Li, C. L. Huang, H. D. Chen, J. Chen, Y. Luo, H. Guo, R. D. Jiang, M. Q. Liu, Y. Chen, X. R. Shen, X. Wang, X. S. Zheng, K. Zhao, Q. J. Chen, F. Deng, L. L. Liu, B. Yan, F. X. Zhan, Y. Y. Wang, G. F. Xiao, and Z. L. Shi, "A pneumonia

outbreak associated with a new coronavirus of probable bat origin," *Nature*, vol. 579, no. 7798, pp. 270–273, Mar 2020.

[22] F. Wu, S. Zhao, B. Yu, Y. M. Chen, W. Wang, Z. G. Song, Y. Hu, Z. W. Tao, J. H. Tian, Y. Y. Pei, M. L. Yuan, Y. L. Zhang, F. H. Dai, Y. Liu, Q. M. Wang, J. J. Zheng, L. Xu, E. C. Holmes, and Y. Z. Zhang, "A new coronavirus associated with human respiratory disease in China," *Nature*, vol. 579, no. 7798, pp. 265–269, Mar 2020.

[23] B. Hu, H. Guo, P. Zhou, and Z. L. Shi, "Characteristics of SARS-CoV-2 and COVID-19," *Nat Rev Microbiol*, vol. 19, no. 3, pp. 141–154, Mar 2021.

[24] R. Lu, X. Zhao, J. Li, P. Niu, B. Yang, H. Wu, W. Wang, H. Song, B. Huang, N. Zhu, Y. Bi, X. Ma, F. Zhan, L. Wang, T. Hu, H. Zhou, Z. Hu, W. Zhou, L. Zhao, J. Chen, Y. Meng, J. Wang, Y. Lin, J. Yuan, Z. Xie, J. Ma, W. J. Liu, D. Wang, W. Xu, E. C. Holmes, G. F. Gao, G. Wu, W. Chen, W. Shi, and W. Tan, "Genomic characterisation and epidemiology of 2019 novel coronavirus: implications for virus origins and receptor binding," *Lancet*, vol. 395, no. 10224, pp. 565–574, Feb 2020.

[25] J. Li, S. Lai, G. F. Gao, and W. Shi, "The emergence, genomic diversity and global spread of SARS-CoV-2," *Nature*, vol. 600, no. 7889, pp. 408–418, Dec 2021.

[26] D. Paraskevis, E. G. Kostaki, G. Magiorkinis, G. Panayiotakopoulos, G. Sourvinos, and S. Tsiodras, "Full-genome evolutionary analysis of the novel corona virus (2019-nCoV) rejects the hypothesis of emergence as a result of a recent recombination event," *Infect Genet Evol*, vol. 79, p. 104212, Apr 2020.

[27] S. Temmam, K. Vongphayloth, E. Baquero, S. Munier, M. Bonomi, B. Regnault, B. Douangboubpha, Y. Karami, D. tien, D. Sanamxay, V. Xayaphet, P. Paphaphanh, V. Lacoste, S. Somlor, K. Lakeomany, N. Phommavanh, P. rot, O. Dehan, F. Amara, F. Donati, T. Bigot, M. Nilges, F. A. Rey, S. van der Werf, P. T. Brey, and M. Eloit, "Bat coronaviruses related to SARS-CoV-2 and infectious for human cells," *Nature*, vol. 604, no. 7905, pp. 330–336, Apr 2022.

[28] H. Wang, X. Li, T. Li, S. Zhang, L. Wang, X. Wu, and J. Liu, "The genetic sequence, origin, and diagnosis of SARS-CoV-2," *Eur J Clin Microbiol Infect Dis*, vol. 39, no. 9, pp. 1629–1635, Sep 2020.

[29] I. P. Trougakos, K. Stamatelopoulos, E. Terpos, O. E. Tsitsilonis, E. Aivalioti, D. Paraskevis, E. Kastritis, G. N. Pavlakis, and M. A. Dimopoulos, "Insights to SARS-CoV-2 life cycle, pathophysiology, and rationalized treatments that target COVID-19 clinical complications," *J Biomed Sci*, vol. 28, no. 1, p. 9, Jan 2021.

[30] N. Vabret, G. J. Britton, C. Gruber, S. Hegde, J. Kim, M. Kuksin, R. Levantovsky, L. Malle, A. Moreira, M. D. Park, L. Pia, E. Risson, M. Saffern, B. é, M. Esai Selvan, M. P. Spindler, J. Tan, V. van der Heide, J. K. Gregory, K. Alexandropoulos, N. Bhardwaj, B. D. Brown, B. Greenbaum, Z. H. ş, D. Homann, A. Horowitz, A. O. Kamphorst, M. A. Curotto de Lafaille, S. Mehandru, M. Merad, R. M. Samstein, M. Agrawal, M. Aleynick, M. Belabed, M. Brown, M. Casanova-Acebes, J. Catalan, M. Centa, A. Charap, A. Chan, S. T. Chen, J. Chung, C. C. Bozkus, E. Cody, F. Cossarini, E. Dalla, N. Fernandez, J. Grout, D. F. Ruan, P. Hamon, E. Humblin, D. Jha, J. Kodysh, A. Leader, M. Lin, K. Lindblad, D. Lozano-Ojalvo, G. Lubitz, A. Magen, Z. Mahmood, G. Martinez-Delgado, J. Mateus-Tique, E. Meritt, C. Moon, J. Noel, T. O'Donnell, M. Ota, T. Plitt, V. Pothula, J. Redes, I. Reyes Torres, M. Roberto, A. R. Sanchez-Paulete, J. Shang, A. S. Schanoski, M. Suprun, M. Tran, N. Vaninov, C. M. Wilk, J. Aguirre-Ghiso, D. Bogunovic, J. Cho, J. Faith, E. Grasset, P. Heeger, E. Kenigsberg, F. Krammer, and U. Laserson, "Immunology of COVID-19: Current State of the Science," *Immunity*, vol. 52, no. 6, pp. 910–941, Jun 2020.

[31] S. Beyerstedt, E. B. Casaro, and B. Rangel, "COVID-19: angiotensin-converting enzyme 2 (ACE2) expression and tissue susceptibility to SARS-CoV-2 infection," *Eur J Clin Microbiol Infect Dis*, vol. 40, no. 5, pp. 905–919, May 2021.

[32] C. B. Jackson, M. Farzan, B. Chen, and H. Choe, "Mechanisms of SARS-CoV-2 entry into cells," *Nat Rev Mol Cell Biol*, vol. 23, no. 1, pp. 3–20, Jan 2022.

[33] G. R. Whittaker, S. Daniel, and J. K. Millet, "Coronavirus entry: how we arrived at SARS-CoV-2," *Curr Opin Virol*, vol. 47, pp. 113–120, Apr 2021.

[34] P. V'kovski, A. Kratzel, S. Steiner, H. Stalder, and V. Thiel, "Coronavirus biology and replication: implications for SARS-CoV-2," *Nat Rev Microbiol*, vol. 19, no. 3, pp. 155–170, Mar 2021.

[35] B. Malone, N. Urakova, E. J. Snijder, and E. A. Campbell, "Structures and functions of coronavirus replication-transcription complexes and their relevance for SARS-CoV-2 drug design," *Nat Rev Mol Cell Biol*, vol. 23, no. 1, pp. 21–39, Jan 2022.

[36] H. Yang and Z. Rao, "Structural biology of SARS-CoV-2 and implications for therapeutic development," *Nat Rev Microbiol*, vol. 19, no. 11, pp. 685–700, Nov 2021.

[37] K. Narayanan, C. Huang, K. Lokugamage, W. Kamitani, T. Ikegami, C. T. Tseng, and S. Makino, "Severe acute respiratory syndrome coronavirus nsp1 suppresses host gene expression, including that of type I interferon, in infected cells," *J Virol*, vol. 82, no. 9, pp. 4471–4479, May 2008.

[38] R. Rungruangmaitree, S. Phoochaijaroen, A. Chimprasit, P. Saparpakorn, K. Pootanakit, and D. Tanramluk, "Structural analysis of the coronavirus main protease for the design of pan-variant inhibitors," *Sci Rep*, vol. 13, no. 1, p. 7055, Apr 2023.

[39] R. Gorkhali, P. Koirala, S. Rijal, A. Mainali, A. Baral, and H. K. Bhattarai, "Structure and Function of Major SARS-CoV-2 and SARS-CoV Proteins," *Bioinform Biol Insights*, vol. 15, p. 11779322211025876, 2021.

[40] I. Sola, F. n, S. iga, and L. Enjuanes, "Continuous and Discontinuous RNA Synthesis in Coronaviruses," *Annu Rev Virol*, vol. 2, no. 1, pp. 265–288, Nov 2015.

[41] D. Kim, J. Y. Lee, J. S. Yang, J. W. Kim, V. N. Kim, and H. Chang, "The Architecture of SARS-CoV-2 Transcriptome," *Cell*, vol. 181, no. 4, pp. 914–921, May 2020.

[42] Y. Finkel, O. Mizrahi, A. Nachshon, S. Weingarten-Gabbay, D. Morgenstern, Y. Yahalom-Ronen, H. Tamir, H. Achdout, D. Stein, O. Israeli, A. Beth-Din, S. Melamed, S. Weiss, T. Israely, N. Paran, M. Schwartz, and N. Stern-Ginossar, "The coding capacity of SARS-CoV-2," *Nature*, vol. 589, no. 7840, pp. 125–130, Jan 2021.

[43] I. Jungreis, R. Sealfon, and M. Kellis, "SARS-CoV-2 gene content and COVID-19 mutation impact by comparing 44 Sarbecovirus genomes," *Nat Commun*, vol. 12, no. 1, p. 2642, May 2021.

[44] W. Chen, P. A. Calvo, D. Malide, J. Gibbs, U. Schubert, I. Bacik, S. Basta, R. O'Neill, J. Schickli, P. Palese, P. Henklein, J. R. Bennink, and J. W. Yewdell, "A novel influenza A virus mitochondrial protein that induces cell death," *Nat Med*, vol. 7, no. 12, pp. 1306–1312, Dec 2001.

[45] N. M. Mattion, D. B. Mitchell, G. W. Both, and M. K. Estes, "Expression of rotavirus proteins encoded by alternative open reading frames of genome segment 11," *Virology*, vol. 181, no. 1, pp. 295–304, Mar 1991.

[46] S. D. Senanayake, M. A. Hofmann, J. L. Maki, and D. A. Brian, "The nucleocapsid protein gene of bovine coronavirus is bicistronic," *J Virol*, vol. 66, no. 9, pp. 5277–5283, Sep 1992.

[47] Y. Konno, I. Kimura, K. Uriu, M. Fukushi, T. Irie, Y. Koyanagi, D. Sauter, R. J. Gifford, S. Nakagawa, and K. Sato, "SARS-CoV-2 ORF3b Is a Potent Interferon Antagonist Whose Activity Is Increased by a Naturally Occurring Elongation Variant," *Cell Rep*, vol. 32, no. 12, p. 108185, Sep 2020.

[48] S. R. Schaecher, J. M. Mackenzie, and A. Pekosz, "The ORF7b protein of severe acute respiratory syndrome coronavirus (SARS-CoV) is expressed in virus-

infected cells and incorporated into SARS-CoV particles," *J Virol*, vol. 81, no. 2, pp. 718–731, Jan 2007.

[49] C. Meier, A. R. Aricescu, R. Assenberg, R. T. Aplin, R. J. Gilbert, J. M. Grimes, and D. I. Stuart, "The crystal structure of ORF-9b, a lipid binding protein from the SARS coronavirus," *Structure*, vol. 14, no. 7, pp. 1157–1165, Jul 2006.

[50] A. C. Gleason, G. Ghadge, J. Chen, Y. Sonobe, and R. P. Roos, "Machine learning predicts translation initiation sites in neurologic diseases with nucleotide repeat expansions," *PLoS One*, vol. 17, no. 6, p. e0256411, 2022.

[51] A. E. Firth, "A putative new SARS-CoV protein, 3c, encoded in an ORF overlapping ORF3a," *J Gen Virol*, vol. 101, no. 10, pp. 1085–1089, Oct 2020.

[52] R. Cagliani, D. Forni, M. Clerici, and M. Sironi, "Coding potential and sequence conservation of SARS-CoV-2 and related animal viruses," *Infect Genet Evol*, vol. 83, p. 104353, Sep 2020.

[53] A. Pavesi, "New insights into the evolutionary features of viral overlapping genes by discriminant analysis," *Virology*, vol. 546, pp. 51–66, Jul 2020.

[54] I. Jungreis, C. W. Nelson, Z. Ardern, Y. Finkel, N. J. Krogan, K. Sato, J. Ziebuhr, N. Stern-Ginossar, A. Pavesi, A. E. Firth, A. E. Gorbalenya, and M. Kellis, "Conflicting and ambiguous names of overlapping ORFs in the SARS-CoV-2 genome: A homology-based resolution," *Virology*, vol. 558, pp. 145–151, Jun 2021.

[55] M. Kozak, "Point mutations define a sequence flanking the AUG initiator codon that modulates translation by eukaryotic ribosomes," *Cell*, vol. 44, no. 2, pp. 283–292, Jan 1986.

[56] J. Rehwinkel and M. U. Gack, "RIG-I-like receptors: their regulation and roles in RNA sensing," *Nat Rev Immunol*, vol. 20, no. 9, pp. 537–551, Sep 2020.

[57] D. Goubau, M. Schlee, S. Deddouche, A. J. Pruijssers, T. Zillinger, M. Goldeck, C. Schuberth, A. G. Van der Veen, T. Fujimura, J. Rehwinkel, J. A.

Iskarpatyoti, W. Barchet, J. Ludwig, T. S. Dermody, G. Hartmann, and C. Reis e Sousa, "Antiviral immunity via RIG-I-mediated recognition of RNA bearing 5'-diphosphates," *Nature*, vol. 514, no. 7522, pp. 372–375, Oct 2014.

[58] Y. Kasuga, B. Zhu, K. J. Jang, and J. S. Yoo, "Innate immune sensing of coronavirus and viral evasion strategies," *Exp Mol Med*, vol. 53, no. 5, pp. 723–736, May 2021.

[59] H. Kato, O. Takeuchi, E. Mikamo-Satoh, R. Hirai, T. Kawai, K. Matsushita, A. Hiiragi, T. S. Dermody, T. Fujita, and S. Akira, "Length-dependent recognition of double-stranded ribonucleic acids by retinoic acid-inducible gene-I and melanoma differentiation-associated gene 5," *J Exp Med*, vol. 205, no. 7, pp. 1601–1610, Jul 2008.

[60] J. T. Marques, T. Devosse, D. Wang, M. Zamanian-Daryoush, P. Serbinowski, R. Hartmann, T. Fujita, M. A. Behlke, and B. R. Williams, "A structural basis for discriminating between self and nonself double-stranded RNAs in mammalian cells," *Nat Biotechnol*, vol. 24, no. 5, pp. 559–565, May 2006.

[61] I. Duic, H. Tadakuma, Y. Harada, R. Yamaue, K. Deguchi, Y. Suzuki, S. H. Yoshimura, H. Kato, K. Takeyasu, and T. Fujita, "Viral RNA recognition by LGP2 and MDA5, and activation of signaling through step-by-step conformational changes," *Nucleic Acids Res*, vol. 48, no. 20, pp. 11 664–11 674, Nov 2020.

[62] H. Xu, X. He, H. Zheng, L. J. Huang, F. Hou, Z. Yu, M. J. de la Cruz, B. Borkowski, X. Zhang, Z. J. Chen, and Q. X. Jiang, "Structural basis for the prion-like MAVS filaments in antiviral innate immunity," *Elife*, vol. 3, p. e01489, Jan 2014.

[63] D. Thoresen, W. Wang, D. Galls, R. Guo, L. Xu, and A. M. Pyle, "The molecular mechanism of RIG-I activation and signaling," *Immunol Rev*, vol. 304, no. 1, pp. 154–168, Nov 2021.

[64] L. C. Platanias, "Mechanisms of type-I- and type-II-interferon-mediated signalling," *Nat Rev Immunol*, vol. 5, no. 5, pp. 375–386, May 2005.

[65] A. Bayati, R. Kumar, V. Francis, and P. S. McPherson, "SARS-CoV-2 infects cells after viral entry via clathrin-mediated endocytosis," *J Biol Chem*, vol. 296, p. 100306, 2021.

[66] J. M. Meyers, M. Ramanathan, R. L. Shanderson, A. Beck, L. Donohue, I. Ferguson, M. G. Guo, D. S. Rao, W. Miao, D. Reynolds, X. Yang, Y. Zhao, Y. Y. Yang, C. Blish, Y. Wang, and P. A. Khavari, "The proximal proteome of 17 SARS-CoV-2 proteins links to disrupted antiviral signaling and host translation," *PLoS Pathog*, vol. 17, no. 10, p. e1009412, Oct 2021.

[67] D. E. Gordon, J. Hiatt, M. Bouhaddou, V. V. Rezelj, S. Ulferts, H. Braberg, A. S. Jureka, K. Obernier, J. Z. Guo, J. Batra, R. M. Kaake, A. R. Weckstein, T. W. Owens, M. Gupta, S. Pourmal, E. W. Titus, M. Cakir, M. Soucheray, M. McGregor, Z. Cakir, G. Jang, M. J. O'Meara, T. A. Tummino, Z. Zhang, H. Foussard, A. Rojc, Y. Zhou, D. Kuchenov, R. ttenhain, J. Xu, M. Eckhardt, D. L. Swaney, J. M. Fabius, M. Ummadi, B. Tutuncuoglu, U. Rathore, M. Modak, P. Haas, K. M. Haas, Z. Z. C. Naing, E. H. Pulido, Y. Shi, I. Barrio-Hernandez, D. Memon, E. Petsalaki, A. Dunham, M. C. Marrero, D. Burke, C. Koh, T. Vallet, J. A. Silvas, C. M. Azumaya, C. lle, A. F. Brilot, M. G. Campbell, A. Diallo, M. S. Dickinson, D. Diwanji, N. Herrera, N. Hoppe, H. T. Kratochvil, Y. Liu, G. E. Merz, M. Moritz, H. C. Nguyen, C. Nowotny, C. Puchades, A. N. Rizo, U. Schulze-Gahmen, A. M. Smith, M. Sun, I. D. Young, J. Zhao, D. Asarnow, J. Biel, A. Bowen, J. R. Braxton, J. Chen, C. M. Chio, U. S. Chio, I. Deshpande, L. Doan, B. Faust, S. Flores, M. Jin, K. Kim, V. L. Lam, F. Li, J. Li, Y. L. Li, Y. Li, X. Liu, M. Lo, K. E. Lopez, A. A. Melo, F. R. Moss, P. Nguyen, J. Paulino, K. I. Pawar, J. K. Peters, T. H. Pospiech, M. Safari, S. Sangwan, K. Schaefer, P. V. Thomas, A. C. Thwin, R. Trenker, E. Tse, T. K. M. Tsui, F. Wang, N. Whitis, Z. Yu, K. Zhang, Y. Zhang, F. Zhou, D. Saltzberg, A. J. Hodder, A. S. Shun-Shion, D. M. Williams, K. M. White, R. Rosales, T. Kehrer, L. Miorin, E. Moreno, A. H. Patel, S. Rihn, M. M. Khalid, A. Vallejo-Gracia, P. Fozouni, C. R. Simoneau, T. L. Roth, D. Wu, M. A. Karim, M. Ghoussaini, I. Dunham, F. Berardi, S. Weigang, M. Chazal, J. Park, J. Logue, M. McGrath, S. Weston, R. Haupt, C. J. Hastie,

M. Elliott, F. Brown, K. A. Burness, E. Reid, M. Dorward, C. Johnson, S. G. Wilkinson, A. Geyer, D. M. Giesel, C. Baillie, S. Raggett, H. Leech, R. Toth, N. Goodman, K. C. Keough, A. L. Lind, R. J. Klesh, K. R. Hemphill, J. Carlson-Stevermer, J. Oki, K. Holden, T. Maures, K. S. Pollard, A. Sali, D. A. Agard, Y. Cheng, J. S. Fraser, A. Frost, N. Jura, T. Kortemme, A. Manglik, D. R. Southworth, R. M. Stroud, D. R. Alessi, P. Davies, M. B. Frieman, T. Ideker, C. Abate, N. Jouvenet, G. Kochs, B. Shoichet, M. Ott, M. Palmarini, K. M. Shokat, A. a Sastre, J. A. Rassen, R. Grosse, O. S. Rosenberg, K. A. Verba, C. F. Basler, M. Vignuzzi, A. A. Peden, P. Beltrao, N. J. Krogan, T. W. Owens, M. Gupta, S. Pourmal, E. W. Titus, C. M. Azumaya, C. lle, A. F. Brilot, M. G. Campbell, A. Diallo, M. S. Dickinson, D. Diwanji, N. Herrera, N. Hoppe, H. T. Kratochvil, Y. Liu, G. E. Merz, M. Moritz, H. C. Nguyen, C. Nowotny, C. Puchades, A. N. Rizo, U. Schulze-Gahmen, A. M. Smith, M. Sun, I. D. Young, J. Zhao, D. Asarnow, J. Biel, A. Bowen, J. R. Braxton, J. Chen, C. M. Chio, U. S. Chio, I. Deshpande, L. Doan, B. Faust, S. Flores, M. Jin, K. Kim, V. L. Lam, F. Li, J. Li, Y. L. Li, Y. Li, X. Liu, M. Lo, K. E. Lopez, A. A. Melo, F. R. Moss, P. Nguyen, J. Paulino, K. I. Pawar, J. K. Peters, T. H. Pospiech, M. Safari, S. Sangwan, K. Schaefer, P. V. Thomas, A. C. Thwin, R. Trenker, E. Tse, T. K. M. Tsui, F. Wang, N. Whitis, Z. Yu, K. Zhang, Y. Zhang, F. Zhou, D. Trinidad, D. A. Agard, Y. Cheng, J. S. Fraser, A. Frost, N. Jura, T. Kortemme, A. Manglik, D. R. Southworth, R. M. Stroud, O. S. Rosenberg, K. A. Verba, J. Damas, G. M. Hughes, K. C. Keough, C. A. Painter, N. S. Persky, M. Corbo, B. Kirilenko, M. Hiller, K. P. Koepfli, I. Kaplow, M. Wirthlin, A. R. Pfenning, H. Zhao, D. P. Genereux, R. Swofford, A. Lind, K. S. Pollard, O. A. Ryderq, M. T. Nweeia, J. Meadows, M. Dong, O. Wallerman, V. Marinescu, K. Lindblad-Toh, D. A. Ray, S. Power, E. C. Teeling, G. Chauhan, S. X. Li, E. K. Karlsson, and H. A. Lewin, "Comparative host-coronavirus protein interaction networks reveal pan-viral disease mechanisms," *Science*, vol. 370, no. 6521, Dec 2020.

[68] D. Bojkova, K. Klann, B. Koch, M. Widera, D. Krause, S. Ciesek, J. Cinatl, and C. nch, "Proteomics of SARS-CoV-2-infected host cells reveals therapy targets,"

Nature, vol. 583, no. 7816, pp. 469–472, Jul 2020.

[69] J. M. Minkoff and B. tenOever, "Innate immune evasion strategies of SARS-CoV-2," *Nat Rev Microbiol*, vol. 21, no. 3, pp. 178–194, Mar 2023.

[70] A. P. Walker, H. Fan, J. R. Keown, M. L. Knight, J. M. Grimes, and E. Fodor, "The SARS-CoV-2 RNA polymerase is a viral RNA capping enzyme," *Nucleic Acids Res*, vol. 49, no. 22, pp. 13 019–13 030, Dec 2021.

[71] K. A. Ivanov, V. Thiel, J. C. Dobbe, Y. van der Meer, E. J. Snijder, and J. Ziebuhr, "Multiple enzymatic activities associated with severe acute respiratory syndrome coronavirus helicase," *J Virol*, vol. 78, no. 11, pp. 5619–5632, Jun 2004.

[72] Y. Chen, H. Cai, J. Pan, N. Xiang, P. Tien, T. Ahola, and D. Guo, "Functional screen reveals SARS coronavirus nonstructural protein nsp14 as a novel cap N7 methyltransferase," *Proc Natl Acad Sci U S A*, vol. 106, no. 9, pp. 3484–3489, Mar 2009.

[73] M. Bouvet, C. Debarnot, I. Imbert, B. Selisko, E. J. Snijder, B. Canard, and E. Decroly, "In vitro reconstitution of SARS-coronavirus mRNA cap methylation," *PLoS Pathog*, vol. 6, no. 4, p. e1000863, Apr 2010.

[74] L. Yan, J. Ge, L. Zheng, Y. Zhang, Y. Gao, T. Wang, Y. Huang, Y. Yang, S. Gao, M. Li, Z. Liu, H. Wang, Y. Li, Y. Chen, L. W. Guddat, Q. Wang, Z. Rao, and Z. Lou, "Cryo-EM Structure of an Extended SARS-CoV-2 Replication and Transcription Complex Reveals an Intermediate State in Cap Synthesis," *Cell*, vol. 184, no. 1, pp. 184–193, Jan 2021.

[75] M. N. Frazier, L. B. Dillard, J. M. Krahn, L. Perera, J. G. Williams, I. M. Wilson, Z. D. Stewart, M. C. Pillon, L. J. Deterding, M. J. Borgnia, and R. E. Stanley, "Characterization of SARS2 Nsp15 nuclease activity reveals it's mad about U," *Nucleic Acids Res*, vol. 49, no. 17, pp. 10 136–10 149, Sep 2021.

[76] M. M. Angelini, M. Akhlaghpour, B. W. Neuman, and M. J. Buchmeier, "Severe acute respiratory syndrome coronavirus nonstructural proteins 3, 4, and 6 induce double-membrane vesicles," *mBio*, vol. 4, no. 4, Aug 2013.

[77] S. Ricciardi, A. M. Guarino, L. Giaquinto, E. V. Polishchuk, M. Santoro, G. Di Tullio, C. Wilson, F. Panariello, V. C. Soares, S. S. G. Dias, J. C. Santos, T. M. L. Souza, G. Fusco, M. Viscardi, S. Brandi, P. T. Bozza, R. S. Polishchuk, R. Venditti, and M. A. De Matteis, "The role of NSP6 in the biogenesis of the SARS-CoV-2 replication organelle," *Nature*, vol. 606, no. 7915, pp. 761–768, Jun 2022.

[78] T. Kouwaki, T. Nishimura, G. Wang, and H. Oshiumi, "RIG-I-Like Receptor-Mediated Recognition of Viral Genomic RNA of Severe Acute Respiratory Syndrome Coronavirus-2 and Viral Escape From the Host Innate Immune Responses," *Front Immunol*, vol. 12, p. 700926, 2021.

[79] G. Liu, J. H. Lee, Z. M. Parker, D. Acharya, J. J. Chiang, M. van Gent, W. Riedl, M. E. Davis-Gardner, E. Wies, C. Chiang, and M. U. Gack, "ISG15-dependent activation of the sensor MDA5 is antagonized by the SARS-CoV-2 papain-like protease to evade host innate immunity," *Nat Microbiol*, vol. 6, no. 4, pp. 467–478, Apr 2021.

[80] A. Stukalov, V. Girault, V. Grass, O. Karayel, V. Bergant, C. Urban, D. A. Haas, Y. Huang, L. Oubraham, A. Wang, M. S. Hamad, A. Piras, F. M. Hansen, M. C. Tanzer, I. Paron, L. Zinzula, T. Engleitner, M. Reinecke, T. M. Lavacca, R. Ehmann, R. lfel, J. Jores, B. Kuster, U. Protzer, R. Rad, J. Ziebuhr, V. Thiel, P. Scaturro, M. Mann, and A. Pichlmair, "Multilevel proteomics reveals host perturbations by SARS-CoV-2 and SARS-CoV," *Nature*, vol. 594, no. 7862, pp. 246–252, Jun 2021.

[81] X. Gao, K. Zhu, B. Qin, V. Olieric, M. Wang, and S. Cui, "Crystal structure of SARS-CoV-2 Orf9b in complex with human TOM70 suggests unusual virus-host interactions," *Nat Commun*, vol. 12, no. 1, p. 2843, May 2021.

[82] Y. Liu, C. Qin, Y. Rao, C. Ngo, J. J. Feng, J. Zhao, S. Zhang, T. Y. Wang, J. Carriere, A. C. Savas, M. Zarinfar, S. Rice, H. Yang, W. Yuan, J. A. Camarero, J. Yu, X. S. Chen, C. Zhang, and P. Feng, "SARS-CoV-2 Nsp5 Demonstrates Two Dis-

tinct Mechanisms Targeting RIG-I and MAVS To Evade the Innate Immune Response," *mBio*, vol. 12, no. 5, p. e0233521, Oct 2021.

[83] F. Yu-Zhi, W. Su-Yun, Z. Zhou-Qin, H. Yi, L. Wei-Wei, X. Zhi-Sheng, and W. Yan-Yi, "SARS-CoV-2 membrane glycoprotein Membrane (M) antagonizes the MAVS-mediated innate antiviral response," *Cellular and Molecular Immunology*, vol. 18, pp. 613–620, 2021.

[84] L. Han, M. W. Zhuang, J. Deng, Y. Zheng, J. Zhang, M. L. Nan, X. J. Zhang, C. Gao, and P. H. Wang, "SARS-CoV-2 ORF9b antagonizes type I and III interferons by targeting multiple components of the RIG-I/MDA-5-MAVS, TLR3-TRIF, and cGAS-STING signaling pathways," *J Med Virol*, vol. 93, no. 9, pp. 5376–5389, Sep 2021.

[85] L. Sui, Y. Zhao, W. Wang, P. Wu, Z. Wang, Y. Yu, Z. Hou, G. Tan, and Q. Liu, "SARS-CoV-2 Membrane Protein Inhibits Type I Interferon Production Through Ubiquitin-Mediated Degradation of TBK1," *Front Immunol*, vol. 12, p. 662989, 2021.

[86] R. S. Freitas, T. F. Crum, and K. Parvatiyar, "SARS-CoV-2 Spike Antagonizes Innate Antiviral Immunity by Targeting Interferon Regulatory Factor 3," *Front Cell Infect Microbiol*, vol. 11, p. 789462, 2021.

[87] M. Moustaqil, E. Ollivier, H. P. Chiu, S. Van Tol, P. Rudolffi-Soto, C. Stevens, A. Bhumkar, D. J. B. Hunter, A. N. Freiberg, D. Jacques, B. Lee, E. Sierecki, and Y. Gambin, "SARS-CoV-2 proteases PLpro and 3CLpro cleave IRF3 and critical modulators of inflammatory pathways (NLRP12 and TAB1): implications for disease presentation across species," *Emerg Microbes Infect*, vol. 10, no. 1, pp. 178–195, Dec 2021.

[88] W. Zhang, Z. Ma, Y. Wu, X. Shi, Y. Zhang, M. Zhang, M. Zhang, L. Wang, and W. Liu, "SARS-CoV-2 3C-like protease antagonizes interferon-beta production by facilitating the degradation of IRF3," *Cytokine*, vol. 148, p. 155697, Dec 2021.

[89] Y. Miyamoto, Y. Itoh, T. Suzuki, T. Tanaka, Y. Sakai, M. Koido, C. Hata, C. X. Wang, M. Otani, K. Moriishi, T. Tachibana, Y. Kamatani, Y. Yoneda, T. Okamoto, and M. Oka, "SARS-CoV-2 ORF6 disrupts nucleocytoplasmic trafficking to advance viral replication," *Commun Biol*, vol. 5, no. 1, p. 483, May 2022.

[90] H. Xia, Z. Cao, X. Xie, X. Zhang, J. Y. Chen, H. Wang, V. D. Menachery, R. Rajsbaum, and P. Y. Shi, "Evasion of Type I Interferon by SARS-CoV-2," *Cell Rep*, vol. 33, no. 1, p. 108234, Oct 2020.

[91] Q. Zhang, Z. Chen, C. Huang, J. Sun, M. Xue, T. Feng, W. Pan, K. Wang, and J. Dai, "Severe Acute Respiratory Syndrome Coronavirus 2 (SARS-CoV-2) Membrane (M) and Spike (S) Proteins Antagonize Host Type I Interferon Response," *Front Cell Infect Microbiol*, vol. 11, p. 766922, 2021.

[92] S. Y. Fung, K. L. Siu, H. Lin, M. L. Yeung, and D. Y. Jin, "SARS-CoV-2 main protease suppresses type I interferon production by preventing nuclear translocation of phosphorylated IRF3," *Int J Biol Sci*, vol. 17, no. 6, pp. 1547–1554, 2021.

[93] W. Wang, Z. Zhou, X. Xiao, Z. Tian, X. Dong, C. Wang, L. Li, L. Ren, X. Lei, Z. Xiang, and J. Wang, "SARS-CoV-2 nsp12 attenuates type I interferon production by inhibiting IRF3 nuclear translocation," *Cell Mol Immunol*, vol. 18, no. 4, pp. 945–953, Apr 2021.

[94] D. Muth, V. M. Corman, H. Roth, T. Binger, R. Dijkman, L. T. Gottula, F. Gloza-Rausch, A. Balboni, M. Battilani, D. č, I. Toplak, R. S. Ameneiros, A. Pfeifer, V. Thiel, J. F. Drexler, M. A. ller, and C. Drosten, "Attenuation of replication by a 29 nucleotide deletion in SARS-coronavirus acquired during the early stages of human-to-human transmission," *Sci Rep*, vol. 8, no. 1, p. 15177, Oct 2018.

[95] B. P. Doehle, K. Chang, A. Rustagi, J. McNevin, M. J. McElrath, and M. Gale, "Vpu mediates depletion of interferon regulatory factor 3 during HIV infection by a lysosome-dependent mechanism," *J Virol*, vol. 86, no. 16, pp. 8367–8374, Aug 2012.

[96] D. Sauter, D. Hotter, B. Van Driessche, C. M. rzel, S. F. Kluge, S. Wildum, H. Yu, B. Baumann, T. Wirth, J. C. Plantier, M. Leoz, B. H. Hahn, C. Van Lint, and F. Kirchhoff, "B-mediated proviral and antiviral host gene expression by primate lentiviral Nef and Vpu proteins," *Cell Rep*, vol. 10, no. 4, pp. 586–599, Feb 2015.

[97] A. Sen, N. Feng, K. Ettayebi, M. E. Hardy, and H. B. Greenberg, "IRF3 inhibition by rotavirus NSP1 is host cell and virus strain dependent but independent of NSP1 proteasomal degradation," *J Virol*, vol. 83, no. 20, pp. 10 322–10 335, Oct 2009.

[98] P. D. Burbelo, K. H. Ching, C. M. Klimavicz, and M. J. Iadarola, "Antibody profiling by Luciferase Immunoprecipitation Systems (LIPS)," *J Vis Exp*, no. 32, Oct 2009.

[99] M. T. Sanchez-Aparicio, J. Ayllon, A. Leo-Macias, T. Wolff, and A. Garcia-Sastre, "Subcellular Localizations of RIG-I, TRIM25, and MAVS Complexes," *J Virol*, vol. 91, no. 2, Jan 2017.

[100] A. C. Camproux, R. Gautier, and P. ry, "A hidden markov model derived structural alphabet for proteins," *J Mol Biol*, vol. 339, no. 3, pp. 591–605, Jun 2004.

[101] A. Krogh, B. Larsson, G. von Heijne, and E. L. Sonnhammer, "Predicting transmembrane protein topology with a hidden Markov model: application to complete genomes," *J Mol Biol*, vol. 305, no. 3, pp. 567–580, Jan 2001.

[102] L. J. Reed and H. Muench, "A simple method of estimating fifty per cent endpoints," *American journal of epidemiology*, vol. 27, no. 3, pp. 493–497, 1938.

[103] A. Herrmann, D. Jungnickl, A. Cordsmeier, A. S. Peter, K. berla, and A. Ensser, "Cloning of a Passage-Free SARS-CoV-2 Genome and Mutagenesis Using Red Recombination," *Int J Mol Sci*, vol. 22, no. 19, Sep 2021.

[104] B. K. Tischer, J. von Einem, B. Kaufer, and N. Osterrieder, "Two-step red-mediated recombination for versatile high-efficiency markerless DNA manipulation in Escherichia coli," *Biotechniques*, vol. 40, no. 2, pp. 191–197, Feb 2006.

[105] S. Torii, C. Ono, R. Suzuki, Y. Morioka, I. Anzai, Y. Fauzyah, Y. Maeda, W. Kamitani, T. Fukuhara, and Y. Matsuura, "Establishment of a reverse genetics system for SARS-CoV-2 using circular polymerase extension reaction," *Cell Rep*, vol. 35, no. 3, p. 109014, Apr 2021.

[106] S. Matsuyama, N. Nao, K. Shirato, M. Kawase, S. Saito, I. Takayama, N. Nagata, T. Sekizuka, H. Katoh, F. Kato, M. Sakata, M. Tahara, S. Kutsuna, N. Ohmagari, M. Kuroda, T. Suzuki, T. Kageyama, and M. Takeda, "Enhanced isolation of SARS-CoV-2 by TMPRSS2-expressing cells," *Proc Natl Acad Sci U S A*, vol. 117, no. 13, pp. 7001–7003, Mar 2020.

[107] I. Kimura, D. Yamasoba, T. Tamura, N. Nao, T. Suzuki, Y. Oda, S. Mitoma, J. Ito, H. Nasser, J. Zahradnik, K. Uriu, S. Fujita, Y. Kosugi, L. Wang, M. Tsuda, M. Kishimoto, H. Ito, R. Suzuki, R. Shimizu, M. M. Begum, K. Yoshimatsu, K. T. Kimura, J. Sasaki, K. Sasaki-Tabata, Y. Yamamoto, T. Nagamoto, J. Kanamune, K. Kobiyama, H. Asakura, M. Nagashima, K. Sadamasu, K. Yoshimura, K. Shirakawa, A. Takaori-Kondo, J. Kuramochi, G. Schreiber, K. J. Ishii, T. Hashiguchi, T. Ikeda, A. Saito, T. Fukuhara, S. Tanaka, K. Matsuno, and K. Sato, "Virological characteristics of the SARS-CoV-2 Omicron BA.2 subvariants, including BA.4 and BA.5," *Cell*, vol. 185, no. 21, pp. 3992–4007, Oct 2022.

[108] A. E. Firth and I. Brierley, "Non-canonical translation in RNA viruses," *J Gen Virol*, vol. 93, no. Pt 7, pp. 1385–1409, Jul 2012.

[109] S. Weingarten-Gabbay, D. Y. Chen, S. Sarkizova, H. B. Taylor, M. Gentili, G. M. Hernandez, L. R. Pearlman, M. R. Bauer, C. M. Rice, K. R. Clauser, N. Hacohen, S. A. Carr, J. G. Abelin, M. Saeed, and P. C. Sabeti, "The HLA-II immunopeptidome of SARS-CoV-2," *Cell Rep*, vol. 43, no. 1, p. 113596, Dec 2023.

[110] L. Strahle, D. Garcin, and D. Kolakofsky, "Sendai virus defective-interfering genomes and the activation of interferon-beta," *Virology*, vol. 351, no. 1, pp. 101–111, Jul 2006.

[111] A. Hachim, N. Kavian, C. A. Cohen, A. W. H. Chin, D. K. W. Chu, C. K. P. Mok, O. T. Y. Tsang, Y. C. Yeung, R. A. P. M. Perera, L. L. M. Poon, J. S. M. Peiris,

and S. A. Valkenburg, "ORF8 and ORF3b antibodies are accurate serological markers of early and late SARS-CoV-2 infection," *Nat Immunol*, vol. 21, no. 10, pp. 1293–1301, Oct 2020.

[112] D. C. Kang, R. V. Gopalkrishnan, Q. Wu, E. Jankowsky, A. M. Pyle, and P. B. Fisher, "mda-5: An interferon-inducible putative RNA helicase with double-stranded RNA-dependent ATPase activity and melanoma growth-suppressive properties," *Proc Natl Acad Sci U S A*, vol. 99, no. 2, pp. 637–642, Jan 2002.

[113] R. B. Seth, L. Sun, C. K. Ea, and Z. J. Chen, "Identification and characterization of MAVS, a mitochondrial antiviral signaling protein that activates NF-kappaB and IRF 3," *Cell*, vol. 122, no. 5, pp. 669–682, Sep 2005.

[114] A. Sacchi, F. Giannessi, A. Sabatini, Z. A. Percario, and E. Affabris, "SARS-CoV-2 Evasion of the Interferon System: Can We Restore Its Effectiveness?" *Int J Mol Sci*, vol. 24, no. 11, May 2023.

[115] S. Zhang, L. Wang, and G. Cheng, "The battle between host and SARS-CoV-2: Innate immunity and viral evasion strategies," *Mol Ther*, vol. 30, no. 5, pp. 1869–1884, May 2022.

[116] S. Perlman and J. Netland, "Coronaviruses post-SARS: update on replication and pathogenesis," *Nat Rev Microbiol*, vol. 7, no. 6, pp. 439–450, Jun 2009.

[117] W. Li, Z. Shi, M. Yu, W. Ren, C. Smith, J. H. Epstein, H. Wang, G. Crameri, Z. Hu, H. Zhang, J. Zhang, J. McEachern, H. Field, P. Daszak, B. T. Eaton, S. Zhang, and L. F. Wang, "Bats are natural reservoirs of SARS-like coronaviruses," *Science*, vol. 310, no. 5748, pp. 676–679, Oct 2005.

[118] J. F. Drexler, V. M. Corman, and C. Drosten, "Ecology, evolution and classification of bat coronaviruses in the aftermath of SARS," *Antiviral Res*, vol. 101, pp. 45–56, Jan 2014.

[119] S. Khare, C. Gurry, L. Freitas, M. B. Schultz, G. Bach, A. Diallo, N. Akite, J. Ho, R. T. Lee, W. Yeo, G. C. Curation Team, and S. Maurer-Stroh, "GISAID's Role in Pandemic Response," *China CDC Wkly*, vol. 3, no. 49, pp. 1049–1051, Dec 2021.

[120] J. Nomburg, M. Meyerson, and J. A. DeCaprio, "Pervasive generation of non-canonical subgenomic RNAs by SARS-CoV-2," *Genome Med*, vol. 12, no. 1, p. 108, Dec 2020.

[121] H. Stewart, Y. Lu, S. O'Keefe, A. Valpadashi, L. D. Cruz-Zaragoza, H. A. Michel, S. K. Nguyen, G. W. Carnell, N. Lukhovitskaya, R. Milligan, Y. Adewusi, I. Jungreis, V. Lulla, D. A. Matthews, S. High, P. Rehling, E. Emmott, J. L. Heeney, A. D. Davidson, J. R. Edgar, G. L. Smith, and A. E. Firth, "The SARS-CoV-2 protein ORF3c is a mitochondrial modulator of innate immunity," *iScience*, vol. 26, no. 11, p. 108080, Nov 2023.

[122] J. Zhang, A. Ejikemeuwa, V. Gerzanich, M. Nasr, Q. Tang, J. M. Simard, and R. Y. Zhao, "Understanding the Role of SARS-CoV-2 ORF3a in Viral Pathogenesis and COVID-19," *Front Microbiol*, vol. 13, p. 854567, 2022.

[123] J. A. Silvas, D. M. Vasquez, J. G. Park, K. Chiem, A. Guardia, A. Garcia-Vilanova, R. N. Platt, L. Miorin, T. Kehrer, A. Cupic, A. S. Gonzalez-Reiche, H. V. Bakel, A. a Sastre, T. Anderson, J. B. Torrelles, C. Ye, and L. Martinez-Sobrido, "Contribution of SARS-CoV-2 Accessory Proteins to Viral Pathogenicity in K18 Human ACE2 Transgenic Mice," *J Virol*, vol. 95, no. 17, p. e0040221, Aug 2021.

[124] A. Baum, R. Sachidanandam, and A. a Sastre, "Preference of RIG-I for short viral RNA molecules in infected cells revealed by next-generation sequencing," *Proc Natl Acad Sci U S A*, vol. 107, no. 37, pp. 16 303–16 308, Sep 2010.

[125] X. Yin, L. Riva, Y. Pu, L. Martin-Sancho, J. Kanamune, Y. Yamamoto, K. Sakai, S. Gotoh, L. Miorin, P. D. De Jesus, C. C. Yang, K. M. Herbert, S. Yoh, J. F. Hultquist, A. Garcia-Sastre, and S. K. Chanda, "MDA5 Governs the Innate Immune Response to SARS-CoV-2 in Lung Epithelial Cells," *Cell Rep*, vol. 34, no. 2, p. 108628, Jan 2021.

[126] A. Rebendenne, A. L. C. o, M. Tauziet, G. Maarifi, B. Bonaventure, J. McKellar, R. s, S. Nisole, M. Arnaud-Arnould, O. é, and C. Goujon, "SARS-CoV-2 triggers

an MDA-5-dependent interferon response which is unable to control replication in lung epithelial cells," *J Virol*, vol. 95, no. 8, Mar 2021.

[127] K. Onomoto, K. Onoguchi, and M. Yoneyama, "Regulation of RIG-I-like receptor-mediated signaling: interaction between host and viral factors," *Cell Mol Immunol*, vol. 18, no. 3, pp. 539–555, Mar 2021.

[128] P. H. Cheung, T. T. Lee, C. Kew, H. Chen, K. Y. Yuen, C. P. Chan, and D. Y. Jin, "Virus subtype-specific suppression of MAVS aggregation and activation by PB1-F2 protein of influenza A (H7N9) virus," *PLoS Pathog*, vol. 16, no. 6, p. e1008611, Jun 2020.

[129] Q. Ding, J. M. Gaska, F. Douam, L. Wei, D. Kim, M. Balev, B. Heller, and A. Ploss, "Species-specific disruption of STING-dependent antiviral cellular defenses by the Zika virus NS2B3 protease," *Proc Natl Acad Sci U S A*, vol. 115, no. 27, pp. E6310–E6318, Jul 2018.

[130] C. Wei, C. Ni, T. Song, Y. Liu, X. Yang, Z. Zheng, Y. Jia, Y. Yuan, K. Guan, Y. Xu, X. Cheng, Y. Zhang, X. Yang, Y. Wang, C. Wen, Q. Wu, W. Shi, and H. Zhong, "The hepatitis B virus X protein disrupts innate immunity by downregulating mitochondrial antiviral signaling protein," *J Immunol*, vol. 185, no. 2, pp. 1158–1168, Jul 2010.

[131] S. Z. Li, Q. P. Shu, Y. Song, H. H. Zhang, Y. Liu, B. X. Jin, T. Z. Liuyu, C. Li, X. C. Huang, R. L. Du, W. Song, B. Zhong, and X. D. Zhang, "Phosphorylation of MAVS/VISA by Nemo-like kinase (NLK) for degradation regulates the antiviral innate immune response," *Nat Commun*, vol. 10, no. 1, p. 3233, Jul 2019.

[132] Y. Q. Yu, M. Zielinska, W. Li, D. B. Bernkopf, C. S. Heilingloh, M. F. Neurath, and C. Becker, "PGAM5-MAVS interaction regulates TBK1/ IRF3 dependent antiviral responses," *Sci Rep*, vol. 10, no. 1, p. 8323, May 2020.

[133] Z. Yang, H. Zheng, H. Li, Y. Chen, D. Hou, Q. Fan, J. Song, L. Guo, and L. Liu, "is suppressed by the viral 3D polymerase via its impact on PGAM5 expression during enterovirus D68 infection," *Virus Res*, vol. 304, p. 198549, Oct 2021.

[134] L. J. Visser, C. Aloise, K. N. Swatek, G. N. Medina, K. M. Olek, H. H. Rabouw, R. J. de Groot, M. A. Langereis, T. de Los Santos, D. Komander, T. Skern, and F. J. M. van Kuppeveld, "Dissecting distinct proteolytic activities of FMDV Lpro implicates cleavage and degradation of RLR signaling proteins, not its deISGylase/DUB activity, in type I interferon suppression," *PLoS Pathog*, vol. 16, no. 7, p. e1008702, Jul 2020.

[135] H. Feng, A. L. Sander, A. Moreira-Soto, D. Yamane, J. F. Drexler, and S. M. Lemon, "Hepatovirus 3ABC proteases and evolution of mitochondrial antiviral signaling protein (MAVS)," *J Hepatol*, vol. 71, no. 1, pp. 25–34, Jul 2019.

[136] L. L. Pang, X. H. Yuan, C. S. Shao, M. Z. Li, Y. Wang, H. M. Wang, G. C. Xie, Z. P. Xie, Y. Yuan, D. M. Zhou, X. M. Sun, Q. Zhang, Y. Xin, D. D. Li, and Z. J. Duan, "The suppression of innate immune response by human rhinovirus C," *Biochem Biophys Res Commun*, vol. 490, no. 1, pp. 22–28, Aug 2017.

[137] A. P. West, G. S. Shadel, and S. Ghosh, "Mitochondria in innate immune responses," *Nat Rev Immunol*, vol. 11, no. 6, pp. 389–402, Jun 2011.

[138] B. E. Nilsson-Payant, S. Uhl, A. Grimont, A. S. Doane, P. Cohen, R. S. Patel, C. A. Higgins, J. A. Acklin, Y. Bram, V. Chandar, D. Blanco-Melo, M. Panis, J. K. Lim, O. Elemento, R. E. Schwartz, B. R. Rosenberg, R. Chandwani, and B. R. tenOever, "B Transcriptional Footprint Is Essential for SARS-CoV-2 Replication," *J Virol*, vol. 95, no. 23, p. e0125721, Nov 2021.

[139] D. Blanco-Melo, B. E. Nilsson-Payant, W. C. Liu, S. Uhl, D. Hoagland, R. ller, T. X. Jordan, K. Oishi, M. Panis, D. Sachs, T. T. Wang, R. E. Schwartz, J. K. Lim, R. A. Albrecht, and B. R. tenOever, "Imbalanced Host Response to SARS-CoV-2 Drives Development of COVID-19," *Cell*, vol. 181, no. 5, pp. 1036–1045, May 2020.

[140] X. Wu, T. Xia, W. J. Shin, K. M. Yu, W. Jung, A. Herrmann, S. S. Foo, W. Chen, P. Zhang, J. S. Lee, H. Poo, S. A. A. Comhair, L. Jehi, Y. K. Choi, A. Ensser, and J. U. Jung, "Viral Mimicry of Interleukin-17A by SARS-CoV-2 ORF8," *mBio*, vol. 13, no. 2, p. e0040222, Apr 2022.

[141] L. Peng, Y. Hu, M. C. Mankowski, P. Ren, R. E. Chen, J. Wei, M. Zhao, T. Li, T. Tripler, L. Ye, R. D. Chow, Z. Fang, C. Wu, M. B. Dong, M. Cook, G. Wang, P. Clark, B. Nelson, D. Klein, R. Sutton, M. S. Diamond, C. B. Wilen, Y. Xiong, and S. Chen, "Monospecific and bispecific monoclonal SARS-CoV-2 neutralizing antibodies that maintain potency against B.1.617," *bioRxiv*, Dec 2021.

[142] S. Akira and K. Takeda, "Toll-like receptor signalling," *Nat Rev Immunol*, vol. 4, no. 7, pp. 499–511, Jul 2004.

[143] H. W. Jiang, H. N. Zhang, Q. F. Meng, J. Xie, Y. Li, H. Chen, Y. X. Zheng, X. N. Wang, H. Qi, J. Zhang, P. H. Wang, Z. G. Han, and S. C. Tao, "SARS-CoV-2 Orf9b suppresses type I interferon responses by targeting TOM70," *Cell Mol Immunol*, vol. 17, no. 9, pp. 998–1000, Sep 2020.

[144] C. S. Shi, H. Y. Qi, C. Boularan, N. N. Huang, M. Abu-Asab, J. H. Shelhamer, and J. H. Kehrl, "SARS-coronavirus open reading frame-9b suppresses innate immunity by targeting mitochondria and the MAVS/TRAF3/TRAF6 signalosome," *J Immunol*, vol. 193, no. 6, pp. 3080–3089, Sep 2014.

[145] X. Li, P. Hou, W. Ma, X. Wang, H. Wang, Z. Yu, H. Chang, T. Wang, S. Jin, X. Wang, W. Wang, Y. Zhao, Y. Zhao, C. Xu, X. Ma, Y. Gao, and H. He, "SARS-CoV-2 ORF10 suppresses the antiviral innate immune response by degrading MAVS through mitophagy," *Cell Mol Immunol*, vol. 19, no. 1, pp. 67–78, Jan 2022.

[146] M. Arslan, B. Xu, and M. Gamal El-Din, "Transmission of SARS-CoV-2 via fecal-oral and aerosols-borne routes: Environmental dynamics and implications for wastewater management in underprivileged societies," *Sci Total Environ*, vol. 743, p. 140709, Nov 2020.

[147] K. S. Cheung, I. F. N. Hung, P. P. Y. Chan, K. C. Lung, E. Tso, R. Liu, Y. Y. Ng, M. Y. Chu, T. W. H. Chung, A. R. Tam, C. C. Y. Yip, K. H. Leung, A. Y. Fung, R. R. Zhang, Y. Lin, H. M. Cheng, A. J. X. Zhang, K. K. W. To, K. H. Chan, K. Y. Yuen, and W. K. Leung, "Gastrointestinal Manifestations of SARS-CoV-2 Infection and Virus Load in Fecal Samples From a Hong Kong Cohort: Systematic Review and Meta-analysis," *Gastroenterology*, vol. 159, no. 1, pp. 81–95, Jul 2020.

[148] J. Fogh, J. M. Fogh, and T. Orfeo, "One hundred and twenty-seven cultured human tumor cell lines producing tumors in nude mice," *J Natl Cancer Inst*, vol. 59, no. 1, pp. 221–226, Jul 1977.

[149] E. Saccon, X. Chen, F. Mikaeloff, J. E. Rodriguez, L. Szekely, B. S. Vinhas, S. Krishnan, S. N. Byrareddy, T. Frisan, A. ri, A. Mirazimi, U. Neogi, and S. Gupta, "Cell-type-resolved quantitative proteomics map of interferon response against SARS-CoV-2," *iScience*, vol. 24, no. 5, p. 102420, May 2021.

[150] A. M. Gamage, K. S. Tan, W. O. Y. Chan, J. Liu, C. W. Tan, Y. K. Ong, M. Thong, A. K. Andiappan, D. E. Anderson, Y. Wang, and L. F. Wang, "Infection of human Nasal Epithelial Cells with SARS-CoV-2 and a 382-nt deletion isolate lacking ORF8 reveals similar viral kinetics and host transcriptional profiles," *PLoS Pathog*, vol. 16, no. 12, p. e1009130, Dec 2020.

[151] T. N. D. Do, K. Donckers, L. Vangeel, A. K. Chatterjee, P. A. Gallay, M. D. Bobardt, J. P. Bilello, T. Cihlar, S. De Jonghe, J. Neyts, and D. Jochmans, "A robust SARS-CoV-2 replication model in primary human epithelial cells at the air liquid interface to assess antiviral agents," *Antiviral Res*, vol. 192, p. 105122, Aug 2021.

[152] S. R. Schaecher, J. Stabenow, C. Oberle, J. Schriewer, R. M. Buller, J. E. Sagartz, and A. Pekosz, "An immunosuppressed Syrian golden hamster model for SARS-CoV infection," *Virology*, vol. 380, no. 2, pp. 312–321, Oct 2008.

[153] M. Li, K. Ayyanathan, M. Dittmar, J. Miller, I. Tapescu, J. S. Lee, M. E. McGrath, Y. Xue, S. Vashee, D. C. Schultz, M. B. Frieman, and S. Cherry, "SARS-CoV-2

ORF6 protein does not antagonize interferon signaling in respiratory epithelial Calu-3 cells during infection," *mBio*, vol. 14, no. 4, p. e0119423, Aug 2023.

[154] B. E. Young, S. W. Fong, Y. H. Chan, T. M. Mak, L. W. Ang, D. E. Anderson, C. Y. Lee, S. N. Amrun, B. Lee, Y. S. Goh, Y. C. F. Su, W. E. Wei, S. Kalimuddin, L. Y. A. Chai, S. Pada, S. Y. Tan, L. Sun, P. Parthasarathy, Y. Y. C. Chen, T. Barkham, R. T. P. Lin, S. Maurer-Stroh, Y. S. Leo, L. F. Wang, L. Renia, V. J. Lee, G. J. D. Smith, D. C. Lye, and L. F. P. Ng, "Effects of a major deletion in the SARS-CoV-2 genome on the severity of infection and the inflammatory response: an observational cohort study," *Lancet*, vol. 396, no. 10251, pp. 603–611, Aug 2020.

[155] I. Kimura, Y. Konno, K. Uriu, K. Hopfensperger, D. Sauter, S. Nakagawa, and K. Sato, "Sarbecovirus ORF6 proteins hamper induction of interferon signaling," *Cell Rep*, vol. 34, no. 13, p. 108916, Mar 2021.

[156] T. Kehrer, A. Cupic, C. Ye, S. Yildiz, M. Bouhaddou, N. A. Crossland, E. A. Barrall, P. Cohen, A. Tseng, T. atay, R. Rathnasinghe, D. Flores, S. Jangra, F. Alam, I. Mena, S. Aslam, A. Saqi, M. Rutkowska, M. R. Ummadi, G. Pisanelli, R. B. Richardson, E. C. Veit, J. M. Fabius, M. Soucheray, B. J. Polacco, B. Ak, A. Marin, M. J. Evans, D. L. Swaney, A. S. Gonzalez-Reiche, E. M. Sordillo, H. van Bakel, V. Simon, L. Zuliani-Alvarez, B. M. A. Fontoura, B. R. Rosenberg, N. J. Krogan, L. Martinez-Sobrido, A. a Sastre, and L. Miorin, "Impact of SARS-CoV-2 ORF6 and its variant polymorphisms on host responses and viral pathogenesis," *Cell Host Microbe*, vol. 31, no. 10, pp. 1668–1684, Oct 2023.

[157] M. Dhawan, A. Sharma, N. Priyanka, T. Thakur, O. Rajkhowa, and Choudhary, "Delta variant (B.1.617.2) of SARS-CoV-2: Mutations, impact, challenges and possible solutions." *Hum Vaccin Immunotherapeutics*, vol. 18, no. 5, pp. 1–12, May 2022.

[158] J. Y. Lam, C. K. Yuen, J. D. Ip, W. M. Wong, K. K. To, K. Y. Yuen, and K. H. Kok, "Loss of orf3b in the circulating SARS-CoV-2 strains," *Emerg Microbes Infect*, vol. 9, no. 1, pp. 2685–2696, Dec 2020.

[159] D. K. W. Chu, K. P. Y. Hui, H. Gu, R. L. W. Ko, P. Krishnan, D. Y. M. Ng, G. Y. Z. Liu, C. K. C. Wan, M. C. Cheung, K. C. Ng, J. M. Nicholls, D. N. C. Tsang, M. Peiris, M. C. W. Chan, and L. L. M. Poon, "Introduction of ORF3a-Q57H SARS-CoV-2 Variant Causing Fourth Epidemic Wave of COVID-19, Hong Kong, China," *Emerg Infect Dis*, vol. 27, no. 5, pp. 1492–1495, May 2021.